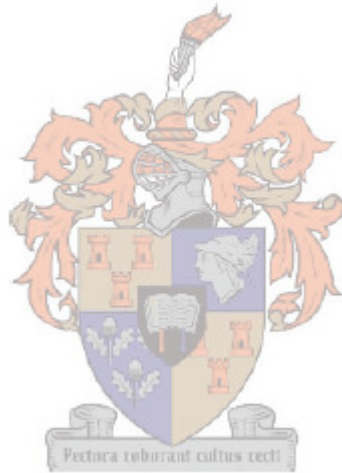


DESIGN AND IMPLEMENTATION OF A LOW  
COST GRID-CONNECTED 10 KW HYDRO  
POWER SYSTEM

Adriaan Cornelius Johannes Lombard

**Thesis presented in partial fulfilment of the requirements for the  
degree of Master of Science in Engineering at  
Stellenbosch University**



Supervisor: Professor Maarten J. Kamper

March 2010

## **Declaration**

By submitting this dissertation electronically, I declare that the entirety of the work contained therein is my own, original work, that I am the owner of the copyright thereof (unless to the extent explicitly otherwise stated) and that I have not previously in its entirety or in part submitted it for obtaining any qualification.

March 2010

Copyright © 2010 Stellenbosch University

All rights reserved

## **Abstract**

The world is increasingly being faced with the challenge of effectively exploiting available renewable energy resources, not only to meet an ever growing energy demand, but also to preserve the available amount of fossil fuels and to reduce the amount of carbon dioxide emissions released into the atmosphere by fossil fuelled power stations. Hence, every available renewable energy resource, even small rivers has a contribution to make in the attempt to reduce the amount of fossil fuel generated electricity. The focus of this study is the design and installation of a low cost grid-connected 10 kW micro hydro power system (MHPS).

The process to determine the potential of the available water resource is first to be presented. The environmental aspects of these systems, based on the study that is undertaken for the implementation of the landmark example, are discussed. The complete design of a micro hydro power system for a specific site is presented. This design is based on using commercially available components and equipment in an attempt to minimise the total cost of a micro hydro power system. The designed micro hydro power system is installed in-field and the predicted performance of the designed system is verified with measured results of the implemented system. Based on the results of the micro hydro power system landmark example, it is shown through a complete economic study, that this investment is very worthwhile.

## **Opsomming**

Die wêreld word daagliks meer en meer uitgedaag om beskikbare alternatiewe energiebronne effektief te benut, nie net om in die groeiende elektrisiteits aanvraag te voorsien nie, maar ook om die beskikbare fossiel brandstowwe te beskerm en ook om die hoeveelheid koolstofdiksied gasse wat deur fossiel brandstof kragstasies vrygestel word, te verminder. Dus het elke beskikbare alternatiewe energiebron, selfs klein riviertjies, 'n bydrae om te lewer tot die poging om die hoeveelheid elektrisiteit wat deur fossiel brandstowwe opgewek word, te verminder. Die fokus van hierdie studie is op die ontwerp en implementering van 'n lae koste netwerk gekoppelde 10 kW mikro hidro kragstelsel.

Eerstens word die proses om die potensiaal van die beskikbare waterbron te bepaal, bespreek. Al die omgewings aspekte van hierdie mikro hidro kragstelsels word dan bespreek. Dit is ten volle gebaseer op die studies wat gedoen is vir die implementering van hierdie landmerk voorbeeld. Die volledige ontwerp van 'n mikro hidro kragstelsel, vir 'n spesifieke terrein, word bespreek. Hierdie ontwerp is hoofsaaklik gebaseer op die gebruik van kommersieel beskikbare komponente met die doel om die totale koste van die stelsel te minimeer. Die stelsel wat ontwerp is, is geïnstalleer op die terrein en die verwagte prestasie van die stelsel is toe geverifieer met gemete resultate van die geïnstalleerde stelsel. 'n Volledige ekonomiese studie wat gebaseer is op die resultate van die geïnstalleerde stelsel, word dan bespreek en daar is gevind dat hierdie stelsel werklik finansieel die moeite werd is.

## **Acknowledgements**

I would like to express a sincere vote of thanks to:

- My heavenly Father and Saviour, for his endless love and blessings.
- My study leader, Prof. M.J. Kamper, for his guidance, support and patience during the duration of this project.
- My family for all their love, encouragement and understanding.
- The Jordaan family from Waterval and Laatson for their hospitality, friendliness and support during the time that the Micro Hydro Power System was installed.
- All the employees at Waterval that helped with the installation of the Micro Hydro Power System.
- The technical personnel of the US electrical engineering workshop for their help and advice, specifically Mr. P. Petzer, Mr. A Swart, Mr J. Poole and Mr. M. Jumat.
- Mrs. Suretha van Rooyen from the Department of Environmental Affairs and Development Planning for all her time and effort with the Environmental Impact Assessment.
- Mr. Jaco van Deventer from CapeNature in Porterville for all his time and help.
- All my friends and also my colleagues at the EMLab for their friendship and support.
- The Centre for Renewable and Sustainable Energy Studies at the University of Stellenbosch, SANERI and THRIP for funding this project.

## Contents

Declaration	i
Abstract	ii
Opsomming	iii
Acknowledgements	iv
List of Figures	viii
List of Tables	xii
List of Symbols and Abbreviations	xiii
1. Introduction	1
1.1 Micro Hydro Power in South Africa	1
1.2 Micro Hydro Power System Technology	3
1.3 Motivation for and Objectives of the Study	7
1.4 Format of Study	8
2. Preliminary Site Studies	10
2.1 Topographic and Geological Information	10
2.2 Hydrologic Information	12
2.3 MHP Design Parameters	12
2.3.1 Height Measurement	12
2.3.2 Water Flow Rate Measurement	13
2.4 Load Electrical System and Potential Power that can be Generated	16
3. Environmental Aspects of Micro Hydro Power Systems	20
3.1 Reserve Flow of the River	20
3.2 The EIA Process	21
3.2.1 Screening	21
3.2.2 Impact Prediction	23
3.2.3 Impact Mitigation Measures	26
3.2.4 Public Participation Process	26
3.2.5 Review and Decision Making	27
4. Mechanical and Civil Design	28
4.1 Water Diversion Structures	28
4.2 Powerhouse	32

## Contents

---

4.3	Pipeline	33
4.3.1	Design	33
4.3.2	Water Hammer	43
4.4	Hydraulic Turbine	45
4.4.1	Centrifugal Pump as Turbine Principle	46
4.4.2	Selecting a PAT and Predicting its Performance	50
4.4.3	Cavitation	58
4.5	Hydraulic Control System	60
4.6	Drive System between the PAT and the Generator	62
5.	Electrical Design	65
5.1	Generator	65
5.2	Transmission Cable	68
5.3	Interconnection with the Grid and Switchgear	69
5.3.1	General Interconnection Requirements	69
5.3.2	Operating Requirements	70
5.3.3	Switchgear Requirements	71
6.	Field Implementation and Testing	76
6.1	Pre-Construction Phase	76
6.2	Construction Phase	76
6.3	Operational Phase	77
7.	Economics of MHP Systems in South Africa	89
7.1	MHPS Costs and Savings	89
7.1.1	Costs	89
7.1.2	MHPS Savings	91
7.2	Economic Viability of a MHPS	91
7.2.1	Payback Period	92
7.2.2	Net Present Value	92
7.2.3	Internal Rate of Return	94
7.2.4	Cost of Energy	94
7.3	Sensitivity Analysis	95
8.	Conclusion and Recommendations	96

## Contents

---

References	98	
Appendix A	Preliminary Site Studies and Environmental Aspects	100
Appendix B	Pipeline Design	103
Appendix C	Turbine Design	106
Appendix D	Electrical Design	117
Appendix E	Test Results	119
Appendix F	Economic Study of the MHPS	122
Appendix G	Photographic Journey through Time	126

---

## List of Figures

Figure 1: Rainfall Distribution in South Africa [1].	2
Figure 2: Layout of a typical MHPS.	4
Figure 3: Application ranges of different types of turbines [British Hydro Association, 2004].	5
Figure 4: Illustration of reaction and impulse turbines.	5
Figure 5: A 1:50 000 topographic map, showing the location of the farm Waterval. The Olifant's River Mountain can be seen on the right hand side of the map.	11
Figure 6: Two of the 22 waterfalls along the river. The strong presence of unspoilt indigenous vegetation on the terrain can also be seen.	11
Figure 7: Schematic layout of using a weir plate to calculate the flow rate in a river.	14
Figure 8: Experimental setup for using a float to calculate the flow rate of a river.	15
Figure 9: Active energy consumption of Waterval during two consecutive years and potential energy that can be generated.	17
Figure 10: Power consumption of Waterval for the month of March 2008.	18
Figure 11: Shape coefficient of different bars to be used in a trash rack [17].	30
Figure 12: Submergence depth of the intake.	31
Figure 13: Energy line of the pipeline of a MHPS.	34
Figure 14: Head available from the main pipeline for various pipe diameters.	37
Figure 15: Lowest cost solution of the main pipeline.	38
Figure 16: A spigot and socket joint with saddles on each side of the joint	39
Figure 17: Layout of the hydraulic system in the powerhouse.	40
Figure 18: A typical draft tube [23].	42
Figure 19: Final system curve of the whole pipeline.	43
Figure 20: Range of application of different PAT types [23].	45
Figure 21: Basic flow path of water in a PAT.	47
Figure 22: Characteristic curves of a pump and a PAT for both ideal and non-ideal conditions [23, 24].	47
Figure 23: Velocity and pressure distribution in the impeller of a pump [23, 24].	49
Figure 24: Possible operating range of a PAT [23].	54
Figure 25: Predicted performance of the selected PAT.	57
Figure 26: Predicted power output and efficiency of the selected PAT.	57

Figure 27: Hydraulics at the outlet side of a PAT [23].	59
Figure 28: Final runaway conditions after the pressure sustaining valve has throttled to the preset pressure.	61
Figure 29: Reactive power consumption and voltage of the load.	72
Figure 30: Single line diagram of the induction generator that is connected to the grid at Waterval.	73
Figure 31: Construction activities with the number of days it took to complete each.	77
Figure 32: Measured and calculated net head at the end of the main pipeline.	79
Figure 33: Predicted and measured no-load and load performance of the PAT.	80
Figure 34: Predicted and measured performance of the PAT under load.	81
Figure 35: Combined efficiency curves and measured electrical power output for different operating points.	83
Figure 36: Waterval MHPS power generating profile.	85
Figure 37: Active power profile at the PCC.	87
Figure 38: Electrical energy and power details for Waterval from the 12/03/09 – 31/09/09.	87
Figure 39: NPV of the MHPS over its lifetime.	93
Figure 40: NPV of the MHPS at the end of its lifetime with varying the time dependent variables.	95
Figure A.1: Flow chart of a Basic Assessment Process and the minimum time the process takes.	102
Figure B.1: Diagram of the iterative process used for selecting the appropriate PAT and generator.	103
Figure C.1: Maximum pump-mode efficiency as a function of pump-mode specific speed and flow rate [23].	106
Figure C.2: Head conversion factor [23].	107
Figure C.3: Flow rate conversion factor [23].	107
Figure C.4: Head correction factor for PAT performance away from the BEP [23].	108
Figure C.5: Power output correction factor for PAT performance away from the BEP [23].	109
Figure C.6: Pump runaway flow rate at rated pump head [23].	110
Figure C.7: Runaway pump speed at rated pump head [23].	111
Figure C.8: Pump performance curve of the KSB ETA 50-200 pump.	112

---

Figure C.9: Pump mode performance diagram of the selected pump (KSB ETA 50-160 pump).	113
Figure C.10: Thoma number used to analyse cavitation on pumps and PATs [23].	114
Figure C.11: Atmospheric pressure variation with height above sea level [23].	114
Figure D.1: Electrical wiring diagram of the distribution board at Waterval.	117
Figure D.2: Electrical wiring diagram of the distribution board in the powerhouse.	118
Figure E.1: MHPS layout at Waterval.	119
Table F.1: Summary of the O&M costs of the MHPS at Waterval.	122
Figure F.1: Inflation and the electricity tariff increases since 1988 [35].	123
Figure F.2: Index of inflation and electricity tariffs.	124
Figure G.1: Notice of the Public Participation Process that was placed in the newspaper.	126
Figure G.2: Notice of the Public Participation Process that was placed at the entrance to the farm Waterval.	127
Figure G.3: The diversion weir just after construction.	127
Figure G.4: The powerhouse during construction (on the left) and finished (on the right).	128
Figure G.5: The powerhouse from the front where the main pipeline enters.	128
Figure G.6: The underground part of the main pipeline during construction.	129
Figure G.7: Part of the above-ground pipeline during construction.	129
Figure G.8: Part of the above-ground pipeline and also showing the saddles holding the pipes to the concrete blocks.	129
Figure G.9: Part of the above ground pipeline with the constructions that holds the pipes to the boulders.	130
Figure G.10: The isolation valve and pipeline constructed into the diversion weir, with the trash rack located behind the diversion weir.	130
Figure G.11: Power cable trench with the cable lying in it.	131
Figure G.12: Inside the powerhouse and showing hydraulic equipment.	131
Figure G.13: Inside the powerhouse and showing the electric equipment.	132
Figure G.14: Tailrace dam with the bypass line in the lower right corner and the draft tube in the middle.	132
Figure G.15: Outlet where water is released back into the Assegaaibos River.	133
Figure G.16: Main distribution board where the MHPS is connected to the load and grid.	133

Figure G.17: The underground part of the pipeline, just after it was buried (on the left) and after a year (on the right). 134

Figure G.18: The above-ground part of the pipeline, just after installation (on the left) and after a year (on the right) 134

**List of Tables**

Table 1: Correction factors to obtain the mean velocity of the flow rate in a river [12, 13].	15
Table 2: Correction factors when $\Phi > 0^\circ$ , $S/b = 0.599$ and $\varphi = 90^\circ$ [17].	30
Table 3: Characteristics of common pipe materials.	36
Table 4: Turbine and pump mode operating conditions considered at Waterval.	56
Table 5: Actual PAT load test measurements.	81
Table 6: Runaway test results.	84
Table 7: Installation Costs of the MHPS.	90
Table A.1: Flow rate measurements using the thin-plate weir method.	100
Table A.2: Flow rate measurements using the velocity-area method.	101
Table B.1: Values of the Hazen Williams coefficient [21].	104
Table B.2: uPVC pipe sizes and costs [Petzetakis, 2009].	104
Table B.3: Loss coefficients for fittings used in the whole pipeline [10, 20 - 22].	105
Table C.1: Analytical results of the PAT selection process for the MHPS at Waterval.	115
Table C.2: Vapour pressure variation with temperature [23].	116
Table D.1: Voltage drop of multicore PVC insulated cables [SANS 10142-1:2003].	117
Table E.1: PAT No-load Test Results.	119
Table E.2: PAT Load Test Results.	120
Table F.2: Financial related data used for the calculation of the economic performance indicators.	124
Table F.3: Calculated NPV of the MHPS.	125
Table F.4: Calculated NPV of the MHPS with varying time dependent variables.	125

## List of Symbols and Abbreviations

### *Engineering Symbols*

$A$	Cross-sectional area [m <sup>2</sup> ]
$A_{dt}$	Cross-sectional area of the draft tube outlet [m <sup>2</sup> ]
$A_{te}$	Cross-sectional area of the turbine outlet exit [m <sup>2</sup> ]
$a$	Velocity of the pressure wave in the pipeline [m/s]
$B_{sc}$	Shape coefficient of the bars in the trash rack
$\Delta B$	Width between two successive depth and velocity measuring points [m]
$b$	Opening between two successive trash rack bars [m]
$C$	Capacitance [ $\mu$ F]
$C_{af}$	Approach coefficient of the flow
$C_{cf}$	Capacity factor [%]
$C_D$	Discharge Coefficient
$C_h$	Head conversion factor
$C_{hs}$	Head conversion factor of the selected pump
$C_{HW}$	Hazen-Williams coefficient of friction
$C_p$	Heat capacity of water [J/kg <sup>o</sup> C]
$C_q$	Flow conversion factor
$C_{qp}$	Flow conversion factor of the selected pump
$C_v$	Voltage drop of a specific conductor size [mV/A/m]
$D_{intake}$	Height of the intake mouth [m]
$D_{pipe}$	Inner diameter of the pipe [m]
$D_{te}$	Diameter of the turbine exit [m]
$D_i$	Depth of water in the river at a certain measuring point [m]
$E_a$	Active energy that can be generated [kWh]
$E_{pipe}$	Modulus of elasticity of the pipe material [Pa]
$E_{water}$	Modulus of elasticity of the water in the pipe [Pa]
$f$	Frequency [Hz]
$g$	Gravitational acceleration [m/s <sup>2</sup> ]
$h_{depth}$	Minimum submergence depth of the intake mouth [m]

## List of Symbols and Abbreviations

---

$h_{dt}$	Head loss in the draft tube [m]
$h_f$	Wall shear frictional losses in the pipeline [m]
$h_g$	Gross head [m]
$h_l$	Total head loss in the whole pipeline [m]
$h_m$	Minor losses in the pipeline [m]
$h_p$	Pump mode head [m]
$h_{ps}$	Rated Best Efficient Point head of the selected pump [m]
$h_s$	Elevation of the blades of the impeller above the tailrace water level [m]
$h_t$	Net head available for power generation [m]
$h_{tr}$	Trash rack head loss [m]
$h_{ts\_BEP}$	Best Efficient Point head of the selected Pump as Turbine [m]
$h_{ts\_max}$	Maximum Best Efficient Point head of the Pump as Turbine [m]
$h_{ts\_min}$	Minimum Best Efficient Point head of the Pump as Turbine [m]
$h_{tsr}$	Runaway head of the Pump as Turbine [m]
$h_{w\_crest}$	Height of the water flowing over the crest of the thin-plate weir [m]
$I$	Rated current of the induction generator [A]
$i$	Specific depth and velocity measuring point
$K$	Loss coefficient of a fitting
$K_{tr}$	Trash rack head loss coefficient
$l$	Length of the pipeline [m]
$l_{cable}$	Length of cable [m]
$l_{dt}$	Draft tube length [m]
$l_{initial}$	Initial length [m]
$\Delta l_{thermal}$	Change in length due to thermal expansion and contraction [m]
$N$	Number of measuring points
$NPSH_A$	Available Net Positive Suction Head [m]
$NPSH_R$	Required Net Positive Suction Head [m]
$n_{qp}$	Pump specific speed [rpm]
$n_{qps}$	Pump mode specific speed of the selected pump
$n_{qt}$	Turbine mode specific speed
$n_p$	Rated pump mode speed of the pump [rpm]

## List of Symbols and Abbreviations

---

$n_s$	Synchronous speed of the rotating field in the induction machine [rpm]
$n_t$	Required turbine shaft speed [rpm]
$n_{tsr}$	Runaway shaft speed of the Pump as Turbine [rpm]
$P_{IG}$	Rated active power of the induction machine [kW]
$P_{pot}$	Potential power that can be generated [kW]
$P_{ts\_max}$	Maximum predicted mechanical power output of the Pump as Turbine [kW]
$P_{ts\_min}$	Minimum predicted mechanical power output of the Pump as Turbine [kW]
$\Delta P_{loss}$	Power loss in the pipeline due to friction [J/s]
$p_1$	Pressure of the water at the intake [ $\text{N/m}^2$ ]
$p_2$	Pressure of the water in the tailrace [ $\text{N/m}^2$ ]
$p_{atm}$	Atmospheric pressure [ $\text{N/m}^2$ ]
$p_{IM}$	Number of poles of the induction machine
$p_v$	Vapour pressure [ $\text{N/m}^2$ ]
$\Delta p$	Change in water pressure [Pa]
$Q$	Reactive power [kvar]
$Q_p$	Pump mode flow [ $\text{m}^3/\text{s}$ ]
$Q_{pipe}$	Flow in the pipeline [ $\text{m}^3/\text{s}$ ]
$Q_{ps}$	Rated Best Efficient Point flow of the selected pump [ $\text{m}^3/\text{s}$ ]
$Q_{river}$	Flow in the river [ $\text{m}^3/\text{s}$ ]
$Q_t$	Required flow through the turbine [ $\text{m}^3/\text{s}$ ]
$Q_{ts\_BEP}$	Best Efficient Point flow of the selected Pump as Turbine [ $\text{m}^3/\text{s}$ ]
$Q_{ts\_max}$	Maximum Best Efficient Point flow of the Pump as Turbine [ $\text{m}^3/\text{s}$ ]
$Q_{ts\_min}$	Minimum Best Efficient Point flow of the Pump as Turbine [ $\text{m}^3/\text{s}$ ]
$Q_{tsr}$	Runaway flow of the Pump as Turbine [ $\text{m}^3/\text{s}$ ]
$R$	Resistance coefficient of a pipeline
$S$	Apparent power [kVA]
$s$	Thickness of trash rack bars [m]
$\Delta T$	Difference between day and night temperatures [ $^{\circ}\text{C}$ ]
$\Delta T_w$	Change in water temperature [ $^{\circ}\text{C}$ ]
$t$	Wall thickness of the pipe [m]
$t_p$	Period in time [Hours]

## List of Symbols and Abbreviations

---

$t_r$	Reflection time [s]
$V_d$	Voltage drop over a length of cable [V]
$V_L$	Rated line voltage of the induction generator [V]
$v_{mean}$	Mean velocity of the flow in the river [m/s]
$v_{af}$	Velocity of the flow approaching the intake [m/s]
$v_{df}$	Velocity of the diverted flow [m/s]
$v_{dt}$	Velocity of the water in the draft tube [m/s]
$v_{te}$	Velocity of the outlet of the turbine [m/s]
$\Delta v$	Change of the velocity of the water in the pipeline [m/s]
$X_c$	Capacitive reactance per phase [ $\Omega$ ]
$z_1$	Elevation of the water level at the intake above a certain reference level [m]
$z_2$	Elevation of the water level in the tailrace above a certain reference level [m]

### ***Greek Engineering Symbols***

$\alpha_{1/2}$	Kinetic energy correction factor
$\alpha_t$	Thermal expansion coefficient [ $^{\circ}\text{C}^{-1}$ ]
$\beta$	Impeller blade angle [ $^{\circ}$ ]
$\beta'$	Angle at which the relative velocity vector of the water leaves the impeller [ $^{\circ}$ ]
$\varepsilon$	Runaway shaft speed correction factor
$\eta_{sys}$	Micro Hydro Power System efficiency [%]
$\gamma$	Specific weight of water [ $\text{N}/\text{m}^3$ ]
$\kappa$	Runaway flow correction factor
$\varphi$	Angle of the trash rack bars with the horizontal [ $^{\circ}$ ]
$\Phi$	Angle of the approaching flow with the trash rack [ $^{\circ}$ ]
$\rho_w$	Density of water [ $\text{kg}/\text{m}^3$ ]
$\sigma_T$	Thoma number
$\theta$	Notch angle of the thin plate measuring weir [ $^{\circ}$ ]
$\Theta$	Angle at which the walls of the draft tube diverge [ $^{\circ}$ ]

### ***Financial Symbols***

$COE$	Cost of electrical energy [ZAR/kWh]
-------	-------------------------------------

## List of Symbols and Abbreviations

---

<i>CI</i>	Capital investment [ZAR]
<i>IRR</i>	Internal rate of return [%]
<i>i</i>	Relative year
<i>LCC</i>	Life cycle cost [ZAR]
<i>N</i>	Investment Period [Years]
<i>NPV</i>	Net present value [ZAR]
<i>OM</i>	Operation and maintenance cost [ZAR]
<i>PP</i>	Payback period [Years]
<i>r</i>	Real interest rate [%]
<i>S</i>	Cost of the annual energy savings [ZAR]
<i>PV</i>	Present value [ZAR]
<i>ZAR</i>	South African Rand [Rand]

### ***Abbreviations***

<b>AC</b>	Alternating Current
<b>AMSL</b>	Above Mean Sea Level
<b>BAP</b>	Basic Assessment Process
<b>BEP</b>	Best Efficient Point
<b>CD</b>	Compact Disk
<b>CPI</b>	Consumer Price Index
<b>DEA&amp;DP</b>	Department of Environmental Affairs and Development Planning
<b>DWAF</b>	Department of Water Affairs and Forestry
<b>EIA</b>	Environmental Impact Assessment
<b>EMP</b>	Environmental Management Plan
<b>GPS</b>	Global Positioning System
<b>HDPE</b>	High-Density Polyethylene
<b>I&amp;AP</b>	Interested and Affected Party
<b>MAR</b>	Mean Annual Runoff
<b>MHP</b>	Micro Hydro Power
<b>MHPS</b>	Micro Hydro Power System
<b>NEMA</b>	National Environmental Management Act

## List of Symbols and Abbreviations

---

<b>NMD</b>	Notified Maximum Demand
<b>NWA</b>	National Water Act
<b>O&amp;M</b>	Operation and Maintenance
<b>PAT</b>	Pump as Turbine
<b>PCC</b>	Point of Common Coupling
<b>PPA</b>	Power Purchase Agreement
<b>uPVC</b>	Unplasticised Poly Vinyl Chloride

## **1. Introduction**

### **1.1 Micro Hydro Power in South Africa**

Electrical energy plays a vital role in the development of any country and for sustainable development more and more electrical energy is required. To continue to meet an increasing electrical energy demand the renewable energy resources of the earth need to be harnessed. However growth in the demand is not the only reason for considering the use of these resources. It is commonly known that South Africa has an extensive dependence on the burning of coal to produce electricity. Although there still is a vast availability of this resource, the reliance on fossil fuels for energy supply needs to be reduced, in order to conserve it for future use in all the other applications where it is needed. As coal is burned to produce energy, huge amounts of carbon dioxide are produced, polluting the atmosphere and enhancing the global climate change process [2, 3]. Thus both large and small scale sustainable energy supply options need to be investigated and if justified economically, need to be developed.

Despite the fact that South Africa has a good potential of solar, wind, biomass and micro hydro resources, less than 1 % of the total energy that is generated comes from these renewable sources. In the White Paper on Renewable Energy, published by the Department of Minerals and Energy in 2003, the government set a target that the contribution of these renewable energy sources to the final energy consumption in 2013 must be 10 000 GWh [3]. Hence the development of Micro Hydro Power Systems has a role to play in reaching energy generation targets and in reducing CO<sub>2</sub> emissions that are released into the atmosphere.

In order to generate hydro power, enough flow of water is needed; hence there must be sufficient rainfall. The rainfall in South Africa is very unevenly distributed as can be seen on the rainfall map in Figure 1. From this chart it can be deduced that the areas receiving rain during the late and very late summer season do not provide any significant options for generating hydro power. The eastern, southern and south-western regions provide the most suitable hydro power options as these areas have a very high rainfall, which results in high and perennial river flows [1]. The White Paper on Renewable Energy [3] and a study undertaken by RAPS Consulting Pty Ltd [2] reveal that between 3500 and 5000 potential sites exist in these regions for generating hydro power.

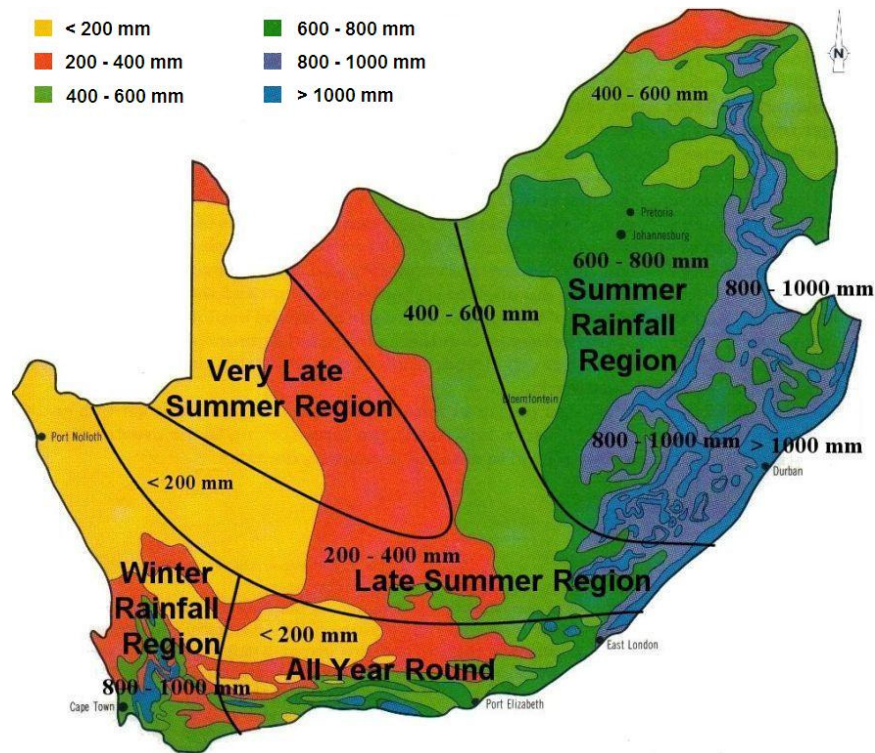


**Figure 1: Rainfall Distribution in South Africa [1].**

South Africa currently has various hydro power stations of various sizes installed that all contribute to the current installed hydro power capacity of 687 MW. Large hydro power stations (> 10 MW) contribute to 95 % of this installed capacity, 3.7 % comes from systems with a size of between 1 MW to 10 MW, also known as small hydro power systems and 1.2 % is produced by systems with a capacity of between 100 kW and 1 MW (Mini Hydro Power Systems). The other 0.1 % is produced by systems with a capacity of below 100 kW (Micro Hydro Power Systems). However the potential of Micro Hydro Power (MHP) that still needs to be exploited is estimated to be about 65 MW [2, 3].

The reason why these available MHP resources have not yet been exploited is probably the known disadvantage of MHP systems; they require high capital investment [4]. However, when comparing them to other renewable energy technologies, one of their numerous advantages is that the cost of operating and maintaining these systems is very low. Other advantages include:

- No large complicated and expensive civil works are required and these systems can be constructed in relatively short periods.
- Depending on the technology that is used, spare parts are readily available.
- They have minimal environmental impacts.

- Depending on the available water and electricity needs, electrical energy can be supplied continuously.
- They can be connected to the distribution grid or it can be stand-alone.
- These systems are very reliable and usually have long life spans.
- The capacity factor of these systems is 90 %, compared to wind energy that has a capacity factor of about 20 - 30 %.

It is believed that the economic issue of MHP development in South Africa has changed since the electricity tariffs have increased tremendously over the past two years and further electricity tariff hikes are still to come in the next two or three years [35]. Hence the incurred electricity cost savings are much higher and payback periods are shorter, which raises the hope that these available resources will be exploited in the near future.

### **1.2 Micro Hydro Power System Technology**

In a hydro system, the available potential energy of flowing water is converted to rotational mechanical energy. This mechanical energy can then be used either directly to turn mechanical equipment such as mills etc. or to turn a generator to convert the energy into electrical energy. Systems where electricity is generated can then either be stand-alone, charging batteries or powering isolated grids or they can be connected to the large distribution grid.

The concept of hydro power dates back to approximately 200 B.C. when the ancient wooden waterwheel was used for milling purposes [5]. Waterwheel technology advanced as the years passed with later waterwheels achieving operating efficiencies of up to 70 %. The growing need for smaller and faster turbines led to the first design of a hydro turbine by a French engineer in 1827 [6]. Since then turbine technology has improved a lot with the first turbine being used for generating hydro electric power in 1882. Since this date more and more hydro power stations have been developed and currently these systems provide about 20 % of the world's electricity [4].

MHP systems utilise water from small perennial water streams or rivers for power generation and are mostly of the “run-of-river” type, meaning that water is directly diverted from a river and that the structures used for diverting the water are small, hence no or little water is stored [6]. The layout of a typical Micro Hydro Power System (MHPS) is illustrated in Figure 2.

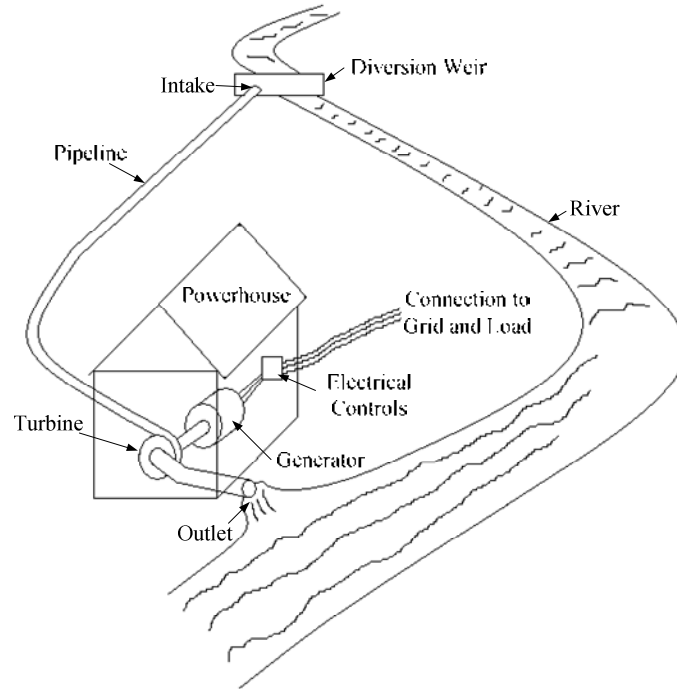


**Figure 2: Layout of a typical MHPS.**

Water is diverted from the river by means of constructing a barrier, which incorporates an intake, across the river. A constant and continuous diverted flow is thus maintained. The diverted water is pressurized by conveying it in a pipeline from a certain high level to a certain lower level, where the turbine is located. The turbine and the generator with all the necessary control equipment are situated in a small building known as the powerhouse. The generated electricity is then sent to the point of use via a transmission line. All the diverted water is then released back into the river through the tailrace upon exiting the turbine, and thus no water is consumed within this system.

The most important components in a MHPS are the turbine and the generator. The type of turbine that is used in a hydro power generation system is mainly being determined by the site characteristics, i.e. the available head and flow rate. Other considerations are the desired shaft speed and the question of whether the turbine will be required to operate at part flow conditions and if so, then to what extent, since certain turbines operate at higher efficiencies at part flow conditions than others [6]. An example of the range of head, flow rate and power that is applicable to different turbine types is shown in Figure 3, but it must be noted that this might differ among different manufacturers. Turbines are also classified either as impulse turbines or as reaction turbines and an example of each of these is presented in Figure 4.

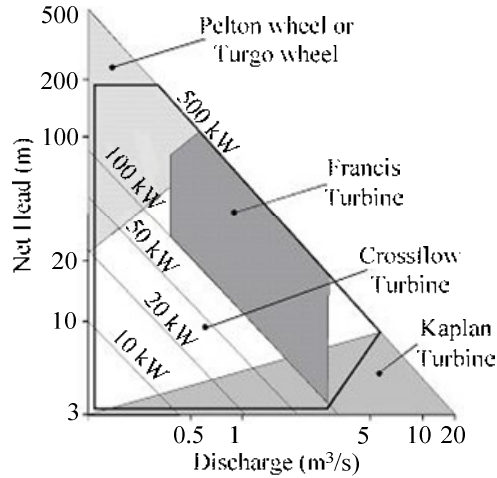


**Figure 3: Application ranges of different types of turbines [British Hydro Association, 2004].**

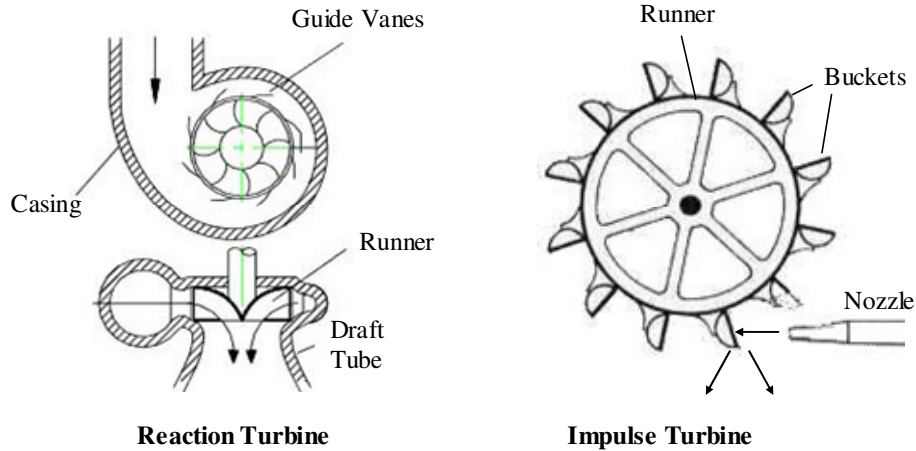


**Figure 4: Illustration of reaction and impulse turbines.**

The runner of an impulse turbine basically consists of a wheel with a series of buckets placed around its circumference. One or more jets of water then strikes these buckets, which causes the runner to turn. After making contact with the runner, the water is deflected and it falls in the discharge channel that is located below the runner. A needle is mounted inside the nozzle and is able to move back and forth to vary the flow rate through the turbine, while keeping the rotational speed constant. Impulse turbines are divided into three types:

- i. The Pelton wheel,
- ii. The Turgo turbine,
- iii. The Crossflow turbine.

As can be seen from Figure 3, each of these three impulse turbines has a certain range in which it operates. The main differences between these types are the angle at which the jets of water are oriented relative to the runner and also the shape of the propelling buckets on the runner [6].

A reaction turbine operates with its runner being fully immersed in water and enclosed by a pressure casing. The profiles of the blades / vanes of the runner are such that forces on them initiate from the pressure drop across them as water pass through them, which propel the runner to turn. Reaction turbines also usually feature a device known as a draft tube at the outlet of the turbine, which basically restores the pressure of the discharging water to the pressure of the water in the tailrace. Reaction turbines are mainly classified either as radial (Francis) turbines or as axial (Kaplan) turbines. The difference between these two turbines is that in a Francis turbine, water moves radially inwards through runner vanes, then turns 90° and leaves the runner in an axial direction. In a Kaplan turbine, the water approaches, moves through and leaves the runner in an axial direction only. Reaction turbines are fitted with adjustable guide vanes on the casing (Figure 4), and the flow rate through reaction turbines is controlled by adjusting the position of these guide vanes, while the speed of the runner remains the same. In the case of Kaplan turbines flow rate can also be controlled by varying the blade angle of the runner [6, 25]. Since both impulse and reaction turbines incorporate hydraulic flow control devices very little other hydraulic control of the water through a MHPS is necessary.

These conventional turbines tend to have efficiencies of up to 90 % when they are operated in the range of their best efficiency, but as they are custom designed and custom built for each and every application, they are very expensive [6]. A more cost justified option is to use a standard centrifugal pump that operates in reverse as a turbine [25]. This Pump as Turbine (PAT) works on the same principle as a Francis turbine, with the main difference being that a PAT does not have adjustable guide vanes for flow control. Hence, when varying the flow rate through the PAT, the speed of the runner does not remain constant. Although these machines are very robust, it is difficult to fit a PAT to a certain required operating point exactly, since the turbine mode performance curves of a pump usually do not exist. The operation and selection of a PAT, and the accompanying necessary hydraulic control devices are discussed in great detail later on in this study.

Two types of Alternating Current (AC) generators that can be used in hydro power systems exist and they are known as synchronous generators and asynchronous (induction) generators. Synchronous generators can be operated in parallel with the grid and are ideally suited for stand alone systems, since they do not require any excitation from the load or grid to which they are connected. Despite the fact that these machines operate at high efficiencies and power factors, they are not recommended to be used in MHP applications due to the fact that they are expensive and depending on the specific application, they might require extensive electrical controls. An induction generator needs to be used in conjunction with the grid, other generators or capacitors that can supply the generator with the necessary excitation. Although they operate at a slightly lower efficiency and power factor than a synchronous machine, they are preferred for use in small renewable energy systems, mainly due to their cost advantage [7]. The application of this machine in MHP systems is discussed further in Chapter 5.

### **1.3 Motivation for and Objectives of the Study**

As MHP systems use water from small streams and rivers to generate power, it is believed that many of the potential sites for MHP systems are on farms and remote areas. Farmers and people living in these remote areas do not have the knowledge to develop these systems and they require expert engineering advice to harness the available resources effectively. The high capital investment required to develop such a system is thus increased by these engineering costs, hence raising the costs to values beyond the financial ability of these people. The required investment is also increased by factors such as:

- Appointing independent environmental assessment practitioners to do the necessary environmental impact assessments.
- Custom made components that are commonly used in hydro power systems.

By equipping people with the basic knowledge to develop these systems the above mentioned costs can be reduced, which results in a MHPS investment becoming more desirable. Furthermore, the development of these systems will make a significant contribution towards reaching targets of renewable energy contribution to final energy consumption.

As abundant resources exist for the development of MHP systems, the main objective in this thesis is to become familiar with the aspects in developing a MHPS. Environmental, technical and economic aspects needed to be addressed based on a practical implemented landmark example on a farm near Porterville in the Western Cape. To increase economic viability, the exclusive goal is to implement a low cost system with high energy conversion efficiency. It should be noted that the design part of this study only focuses on the system and components of the implemented landmark example and that other options are not discussed.

### **1.4 Format of Study**

This thesis is divided into eight chapters in which MHPS development aspects and results of an implemented system are discussed. The first chapter is an introduction to MHP and its potential in South Africa. MHPS technology is discussed and the objectives of this project are also given.

Chapter 2 describes all the preliminary assessments that need to be completed for a proposed site, in order to determine its hydro power potential. These assessments include site surveys, height measurements, river flow rate measurements, matching the power that can be generated with the demand of the load, etc. All of these are described with reference to the landmark example of an actual MHPS that has been developed.

In order to ensure a sustaining environment, there are certain environmental constraints that are applicable to the development of MHP systems and due to this environmental legislation, MHPS developments need to be authorised by environmental authorities. The possible thresholds listed in legislation that may be applicable to the proposed MHPS development are discussed in Chapter 3. The necessary processes that must be followed to obtain environmental authorisation for a MHPS development are also discussed.

In Chapter 4 firstly the design of all the civil structures encountered in a MHPS is discussed. The design of the whole hydraulic system is then dealt with and guidelines to the selection and installation of components are also given. Possible troubleshooting with some of the components is also discussed.

The electrical design of a MHPS is discussed in Chapter 5. Firstly the selection of a proper generator that operates according to the turbine output conditions is discussed. This

chapter is then concluded with a complete discussion regarding the interconnecting of a MHPS to the distribution network.

In Chapter 6 the implementation of the landmark MHPS example is dealt with. All relevant results and information of the pre-construction and construction phases are discussed after which the full test and operating results of the designed and implemented system are discussed.

Certainly the biggest uncertainty and concern of MHP systems is their financial viability. An economic assessment that is based on actual results of the implemented system is made and the economic feasibility of MHP systems is discussed in Chapter 7.

Lastly the thesis is concluded in Chapter 8 with the main findings and results of this project. Possible further work for the landmark example and MHP systems in general is also addressed.

## 2. Preliminary Site Studies

The very first step in the development of a MHPS is to gather certain information about the specific site. This basically entails the assessment of where the different components will be located, since this is extremely important in determining the potential of the hydro power that can be generated and is also necessary for obtaining environmental authorisation for the project. The information given in this chapter is based on the site of the landmark example that is described. The method used to determine the hydro power that can be generated from a resource is also discussed in this chapter.

### 2.1 Topographic and Geological Information

The project site is located on a farm, just north of the town Porterville in the Western Cape, as is presented in Figure 5. Its geographical coordinates are as follows:

Longitude: 32°59'1.26" S

Latitude: 19°01'47.7" E

Altitude: 260 m AMSL

The Assegaaibos River rises in the Olifant's River Mountain, on the farm, Waterval, which is located against the mountain. It flows from the source in a west south west direction through Waterval. In the foothill zone, it enters intensive agricultural land, and then eventually joins the Kromriver before its confluence with the Berg River. This mountain is relatively steep and has a vertical height of about 800 m. Some 22 waterfalls exist in the mountain area where the river flows, of which two are shown in Figure 6. The site and particularly the location of the proposed MHPS are unspoiled and there is indigenous vegetation. The vegetation on the terrain is mainly composed of:

- i. Winterhoek Sandstone Fynbos.
- ii. Swartland Shale Renosterveld.
- iii. Wild Olive trees.
- iv. Natal Mahogany trees.
- v. River Willow trees.
- vi. Wild Almond trees.

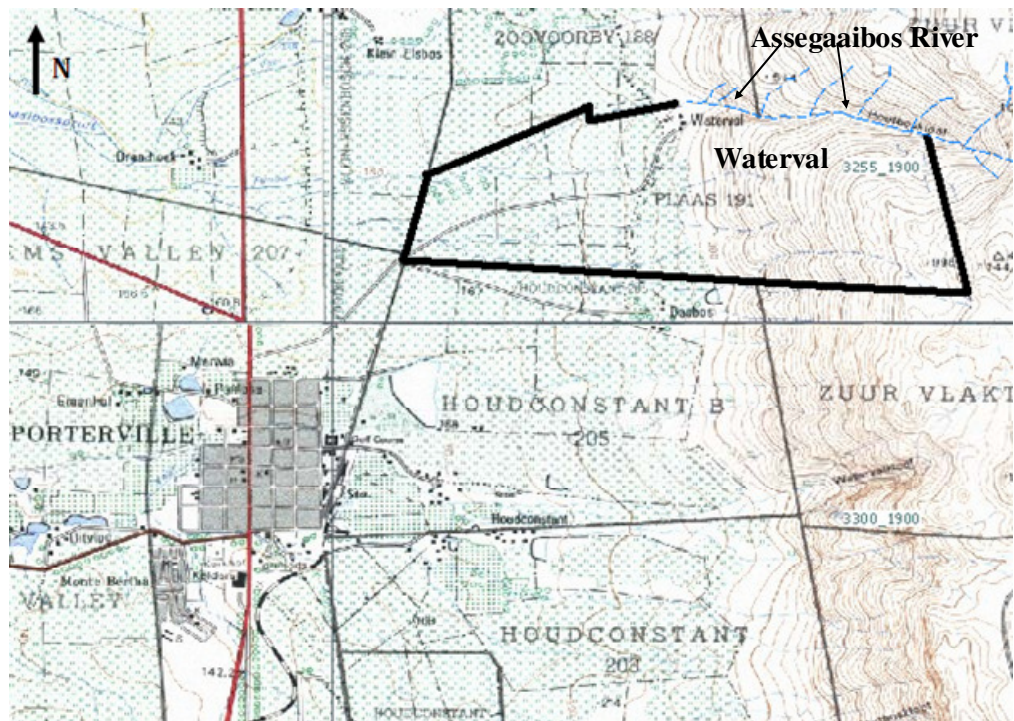


**Figure 5:** A 1:50 000 topographic map, showing the location of the farm Waterval. The Olifant's River Mountain can be seen on the right hand side of the map.

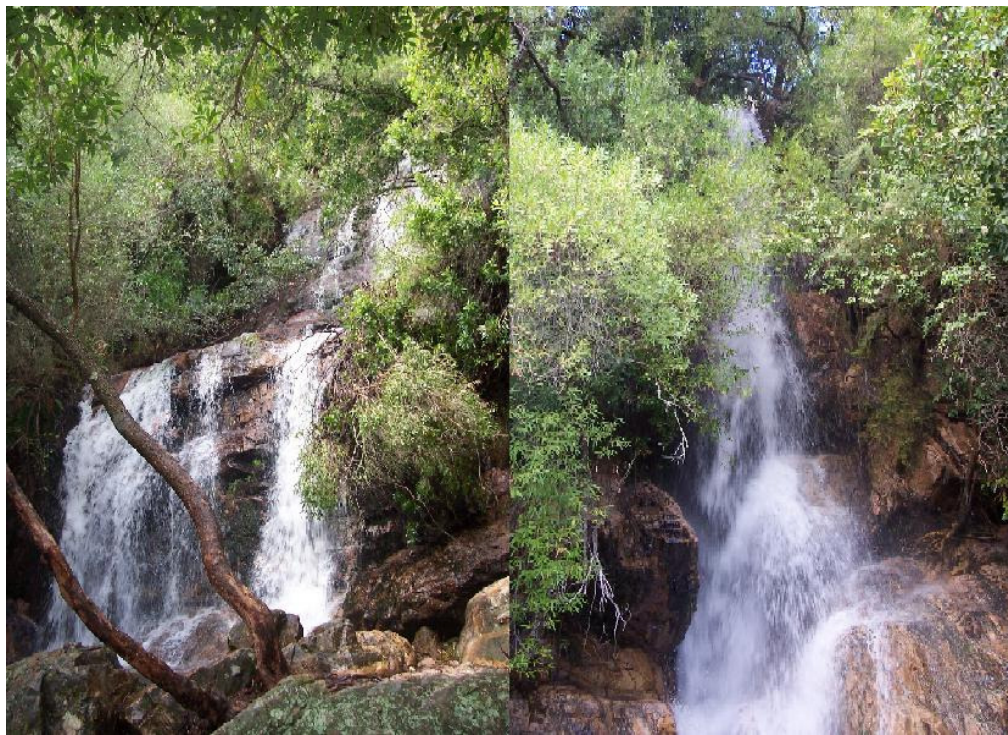


**Figure 6:** Two of the 22 waterfalls along the river. The strong presence of unspoilt indigenous vegetation on the terrain can also be seen.

Part of the land along the river has been transformed into a camping area, with various beautiful sightseeing hiking trails, extending from the foothills up to the top of the mountain. These trails follow the river.

## **2.2 Hydrologic Information**

The project area has a Mediterranean-type climate, with warm dry summers and cool wet winters and has an annual rainfall of 300 to 500 mm [36]. No detailed hydrological assessment of the river has yet been undertaken and thus very little hydrological data of the river exists. However, once off flow measurements in the past indicated that the minimum flow rate of the river is around 50 l/s [37]. The river has a perennial flow throughout the year, with about 75 % of the Mean Annual Runoff (MAR) occurring between the months of April and September [8].

The depth of the water table adjacent to the river differs along the length of the river, but it is less than 1.5 m at some locations and also becomes deeper as one moves away from the river banks. The water quality is very good and the river provides the farm with water for domestic and agricultural purposes. The water of this river is also being channelled into a pipeline downstream of Waterval to supply neighbouring farmers with water for domestic and agricultural purposes.

## **2.3 MHP Design Parameters**

### **2.3.1 Height Measurement**

The potential energy used for power generation is the height difference between the location where the water enters the pipeline and the location of the powerhouse. These two locations need to be identified, paying special attention to the geotechnical properties of the immediately surrounding soils. If the stability of the soil adjacent to the diversion weir is not sufficient, flood conditions of the river can cause the foundations of the diversion weir to erode, hence weakening its structural strength. The powerhouse location must also be well above any known flood line of the river to prevent flood damage. Shallow water tables and seasonally wet soils can result in ground sinkage, causing foundations and civil structures to weaken. These two locations also need to be identified keeping in mind that the possible environmental impacts during the constructional and operational phases of the project should be kept to minimum.

Various methods can be used to measure the height difference between these two locations, with the most common one to date, being the use of a dumpy level and staff. This method is very time consuming and since clear unobstructed views between the dumpy level and the calibrated staff is required, this method is not preferred for a woody site. The accuracy of Global Positioning Systems (GPS's) has recently become increasingly high, and for this reason a GPS is used to measure the difference in height between the identified locations for the diversion weir and the powerhouse. The GPS measured the following altitudes at Waterval:

- 318 m AMSL for the diversion weir,
- 239 m AMSL for the powerhouse.

Another method is to identify these two exact locations on a 1:10 000 ortho map of the site. The contour lines on this map can then be used to calculate the difference in height, also known as the available head, for hydro power generation. Both the GPS and the ortho map revealed that a gross head ( $h_g$ ) of 79 m is available for power generation.

### **2.3.2 Water Flow Rate Measurement**

As the flow rate of any river varies during a year, it is preferred to have a full hydrological record of the river, in order to determine a base flow rate that can be used for hydro power generation. If such information is not available, the flow rate should be measured directly for at least a year. A once off instantaneous flow rate measurement is usually of little use, since nothing is known on the variation of the flow rate during the rest of the year.

The historical flow data of the river at Waterval are very limited; hence the flow rate was measured in March 2007 in order to compare the result with existing data. Various methods exist that can be used to measure the flow rate of a river, but only the methods discussed below were used for Waterval.

#### ***Thin-Plate Weir Method***

A thin-plate weir is a temporary or permanent barrier constructed across the river. This weir has a notch in it through which all the water in the river flows, and is very suitable for measuring the flow rate of small streams. If used correctly it provides the most accurate measurements of flow in open channels [9]. The principle of this method is that the flow rate is directly related to the height of the water flowing through the notch of the weir. These weirs are

available in different forms, and the form and geometry of the weir depend purely on the application [10]. In order to obtain accurate measurements, various standards regarding the selection of the site, the installation of the weir, the weir itself and the approach channel exist. All of these are thoroughly discussed in [11].

A 90° V-notch weir plate is used for the flow rate measurements at Waterval. In comparison with other types of weirs, this weir has the advantage that it can measure a wider range of flows with a higher accuracy. A schematic of this plate is shown in Figure 7, and the flow rate through this weir is calculated from

$$Q_{river} = C_D \left( \frac{8}{15} \right) (\sqrt{2g}) h_{w\_crest}^{\frac{5}{2}} \tan \left( \frac{\theta}{2} \right) \quad (2.1)$$

where  $Q_{river}$  is the flow rate in the river,  $C_D$  is the discharge coefficient for a certain notch angle  $\theta$ ,  $g$  is the gravitational acceleration constant and  $h_{w\_crest}$  is the height of the water flowing over the crest. The discharge coefficient, for a notch angle of 90°, is 0.578 [11]. Values of the discharge coefficient that correspond with different notch angles can be found in the BS ISO 1438:2008.

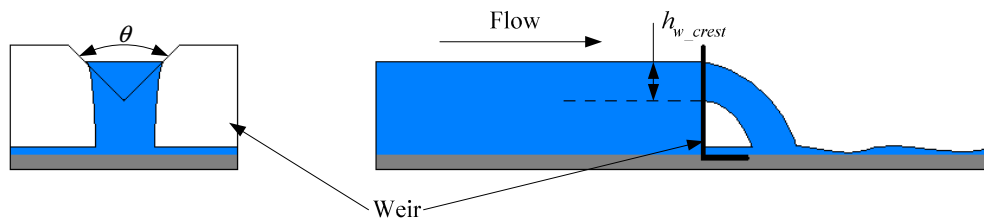


**Figure 7: Schematic layout of using a weir plate to calculate the flow rate in a river.**

### ***Velocity-Area Method***

To calculate the flow rate using this method, the velocity of the water in the river and the cross-sectional area of the river at the point where the flow rate is being measured need to be calculated. The flow rate of the river is then calculated from:

$$Q_{river} = v_{mean} A \quad (2.2)$$

where  $v_{mean}$  is the mean velocity of the flow and  $A$  the cross-sectional area of the river. All the requirements for site selection, velocity and cross-sectional area measurements are set out in great detail in the BS EN ISO 748:2007 [12].

The easiest way to measure the velocity of the water, is the timing of a float, preferably a piece of wood, over a certain measured length of the river as illustrated in Figure 8. As can be

seen from this illustration, due to surface friction, the velocity profile of the moving water is not constant. It is therefore necessary to make velocity measurements at various points across the width of the river, average these measurements and then multiply the result by a certain correction factor, to obtain the mean velocity of the flow, based on the surface velocity of the float [12, 13]. Various correction factors are given in Table 1.

The cross-sectional area of the river can be calculated once the shape of the riverbed has been established. To establish this shape, the depth of the water must be measured at various points over the width of the river. These water depth measurement points should preferably be at the same successive points where velocity measurements were made. The cross-sectional area is then calculated from

$$A = \sum_{i=0}^N D_i \Delta B \tag{2.3}$$

where  $D_i$  is the water depth at a measuring point,  $i$  is a specific measuring point,  $N$  is the number of measuring points and  $\Delta B$  is the difference in width between two successive measuring points. In order to obtain a good accuracy of the flow rate, the number of vertical segments where the velocity and water depth are measured, should be a maximum.

**Table 1: Correction factors to obtain the mean velocity of the flow rate in a river [12, 13].**

River Type	Correction Factor
Smooth, rectangular concrete channel	0.85
Large, slow clear stream ( $A > 10 \text{ m}^2$ )	0.75
Small, slow clear stream ( $A < 10 \text{ m}^2$ )	0.65
Shallow turbulent stream (Depth $< 0.5 \text{ m}$ )	0.25 – 0.45

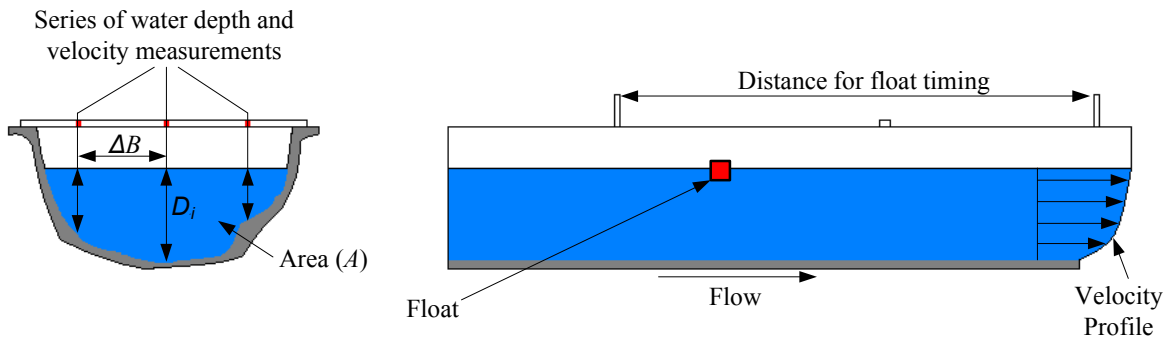


**Figure 8: Experimental setup for using a float to calculate the flow rate of a river.**

All the results of the flow rate measurements at Waterval are given in Appendix A.1. The average flow rate for the measuring period in March 2007 is about 40 l/s. This is assumed to be the lowest flow rate that exists in the river as it is measured during late summer.

A reserve flow needs to remain in the river at all times and this is discussed in Chapter 3.1. The turbine used at Waterval preferably needs a fixed flow rate as it does not operate well at part flow conditions (Chapter 4.4), hence in order to provide that this system generates hydro power all year round, the constant flow rate diverted from the river needs to be less than the minimum flow rate in the river. The flow rate used to generate hydro power is discussed in the following section.

## **2.4 Load Electrical System and Potential Power that can be Generated**

For all further reference in this study, “the distributor” refers to the company that owns the electricity distribution network to which a power generation system connects, i.e. Eskom. Eskom supplies Waterval with electricity through a 3-phase, 11 kV connection point. A 50 kVA, 11 kV / 400 V transformer then feeds the distribution board, which is fitted with three 240 V, 80 A main circuit breakers, one for each of the three phases A, B and C. The active power consumption of each phase is measured separately with “Schlumberger” rotating-disk power meters. The distribution board is also fitted with two secondary 3-phase, 240 V, 60 A circuit breakers, which is used to divide the 3-phase connection. A complete wiring diagram of this distribution board is included in Appendix D.2. This connection supplies electricity to:

- The farmhouse.
- An office.
- A large shed with heavy duty machinery.
- The camping area and eight self-catering cottages.
- A nursery.

Eskom charges electricity consumption at Waterval according to the “Landrate 2” tariff. This is an electricity tariff for rural three phase loads with a Notified Maximum Demand (NMD) of 50 kVA and 80 A per phase. This tariff is further characterised by:

- A single c/kWh active energy charge,
- An R/day network charge,

- An R/day service charge,
- A c/kWh tax that may be introduced during a financial year.

Energy consumption at Waterval differs for each year and each month as can be seen in Figure 9. Also shown in this figure is the potential energy that can be generated, but this is discussed later. The trend of energy consumption for the two years correlates fairly well and it can be seen that more energy is consumed during the summer months than during the winter months. This is because of (i) a borehole pump that is used for irrigation of guava orchards and (ii) more visitors that stay in the camping grounds and chalets on the farm. The total annual active energy consumed for the 2006 - 2007 and the 2007 - 2008 year periods is 53 783 kWh and 55 887 kWh respectively.

In order to get a better picture of the energy consumed by the load, the load profile for March 2008 is presented in Figure 10. The demand of the load varies a lot and it can clearly be seen that much more power is consumed over weekends when people are visiting the farm. For this month (March 2008) the average power consumption during the weeks is about 6.2 kW and the average over the weekends is about 13.5 kW. The potential power that can be generated, which is discussed hereafter, is also shown in this figure.

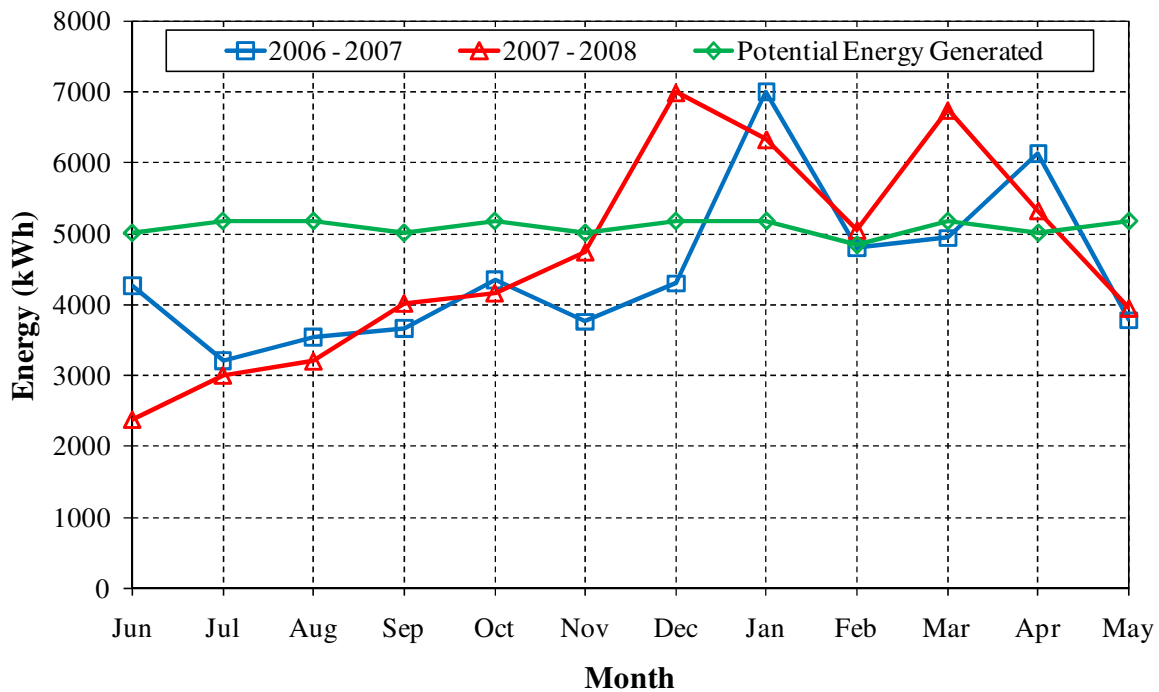


**Figure 9: Active energy consumption of Waterval during two consecutive years and potential energy that can be generated.**

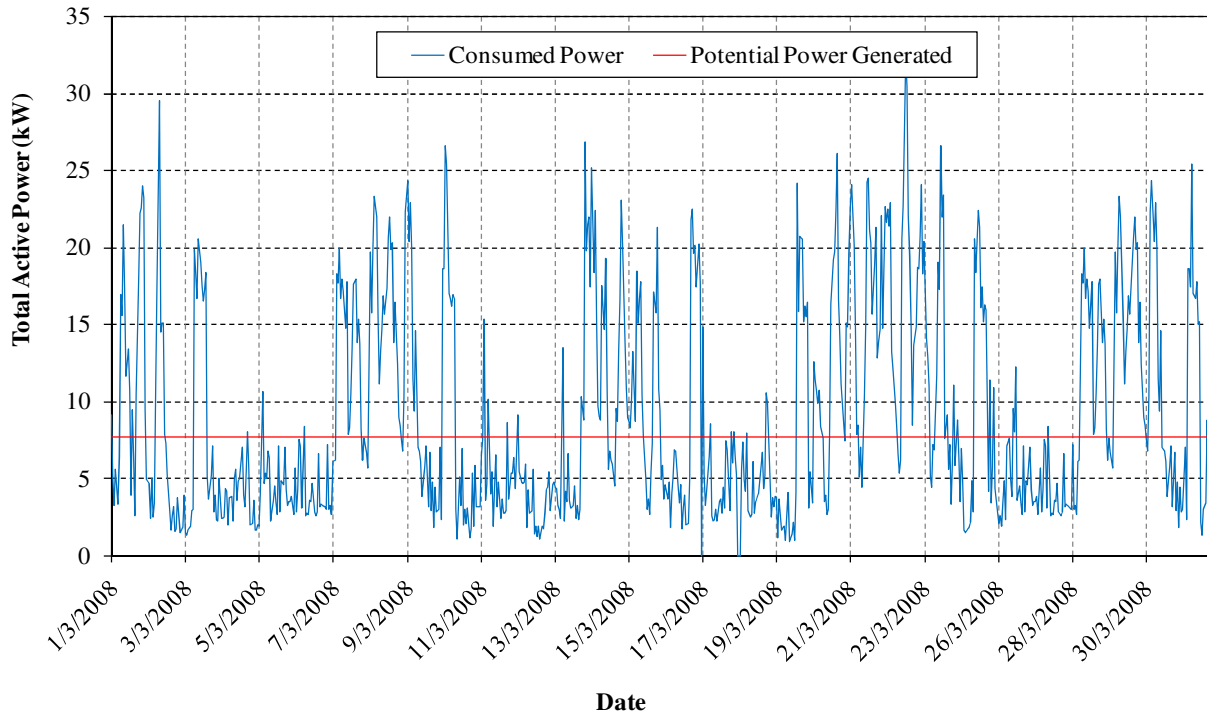


**Figure 10: Power consumption of Waterval for the month of March 2008.**

If the renewable energy source at Waterval is harnessed and the generated energy delivered to the farm, the demand from Eskom will be reduced significantly and hence the farmer can save on his electricity consumption. Hydro power that can be generated is calculated from

$$P_{pot} = \frac{\eta_{sys} \rho_w g h_g Q_{pipe}}{1000} \quad (2.4)$$

where  $P_{pot}$  is the potential power that can be generated,  $\eta_{sys}$  is the overall system efficiency,  $\rho_w$  is the density of water,  $h_g$  is the measured gross head that is available and  $Q_{pipe}$  is the flow rate in the pipeline. The system efficiency is a collective value for the pipeline efficiency, the turbine efficiency and the generator efficiency. The amount of active energy that can be generated over a certain period of time is calculated from

$$E_a = C_{cf} P_{pot} t_p \quad (2.5)$$

where  $E_a$  is the active energy,  $C_{cf}$  is the capacity factor and  $t_p$  is the time period. For all calculations, it is assumed that:

- i. The density of water is  $998.2 \text{ kg/m}^3$  at a temperature of  $20 \text{ }^\circ\text{C}$  (Table C.2).
- ii. The gravitational acceleration is  $9.81 \text{ m/s}^2$ .

For a first estimation, a flow rate of 20 l/s is considered. By using this in Equation 2.4, together with a gross head of 79 m and an estimated system efficiency of 50 %, it is calculated that 7.74 kW can be generated continuously. From Figure 10, it can be seen that the demand of the load mostly exceeds the potential power capacity that can be generated over weekends, but during the weeks the average demand is lower than the capacity that can be generated. This potential MHPS will be grid-connected, hence the grid is used as a virtual storage medium if sufficient net-metering is available, i.e. excess power that is generated is exported to the grid and any power needed in excess of the capacity that can be generated is imported from the grid. The point where the MHPS is connected to the load and the grid is known as the Point of Common Coupling (PCC). Very accurate power measurement will be required at the PCC in order to determine whether the load is a net exporter or importer of active energy at the end of each billing period, i.e. a month. Currently the distributor does not compensate for MHP that is delivered to the grid. However for the purpose of this study it is assumed that credits are obtained for energy being delivered to the grid as it is very likely that this will happen in the near future [35]. This issue of receiving compensation for energy (being a net exporter of energy) is discussed further in Chapter 5.3.

If a continuous flow rate of 20 l/s is diverted from the river and one allow for maintenance times, the potential MHPS will have a capacity factor of about 90 %. Equation 2.5 is used to calculate the total monthly amount of active energy that can be generated and these amounts are shown in Figure 9. When this is compared to the two annual demand profiles, it is deduced that excess energy will be generated during the winter months, which can be stored in the grid to be used in the summer months. The calculated monthly totals displayed on the graph, show that an annual amount of 61 022 kWh energy can be generated. If it is assumed that the future annual energy consumption remains at about 55 900 kWh, an annual estimated amount of 5 122 kWh of hydro energy will be exported to the grid, leaving the farmer with credits that can be used either in future years or for another connection point where energy is consumed from the distributor. Therefore by implementing the MHPS and diverting a flow of 20 l/s, the farmer will save his annual energy consumption expense apart from the compulsory monthly network and service charges from the distributor.

### **3. Environmental Aspects of Micro Hydro Power Systems**

When it comes to carbon footprints, hydro power is seen as a clean source of energy but despite this, it certainly has environmental and socioeconomic impacts, which can in some cases be detrimental. However, if these impacts are compared to those of large hydro power systems, these impacts of MHP systems are seen to be much smaller [4]. According to regulatory frameworks, it is still necessary that prior to the development of a MHP project, it must be known in what way the development is likely to affect the environment and the people, and that the necessary measures to mitigate these impacts must be in place. This impact prediction process is commonly known as an Environmental Impact Assessment (EIA) [14]. Before a certain project can be developed, this EIA first needs to be authorised by the Department of Environmental Affairs and Development Planning (DEA&DP). In this chapter a general discussion on the EIA and the possible impacts associated with a MHPS are presented, with reference to the Waterval site.

#### **3.1 Reserve Flow of the River**

Water resources are one of the most critically important elements of nature, since water serves as a medium through which humans, fauna and flora absorb nutrient. Without this resource no life on earth would have been possible. The National Water Act (No. 36 of 1998) (NWA) has been enacted to manage and protect the water resources of South Africa. The diversion of water for MHP generation is not a consumptive use of water as it is placed back into the river once it has passed through the turbine. As the stretch of river between the intake and the point where the water is released back into the river will experience a lower flow than usual, the reserve flow that must remain in this stretch of river to sustain the ecological function of the river needs to be determined. The NWA requires that before water can be extracted from any resource, a reserve for the resource needs to be determined and only water in excess of this reserve will be available for diversion. According to [15], this reserve consists of two parts:

- (i) The human needs reserve, refers to the water needed for any individuals that are provided for by this specific water resource.
- (ii) The ecological reserve, refers to the water needed for:
  - The protection of the aquatic ecosystem of the specific water resource.

- The wildlife.
- The protection of the biodiversity of the surrounding environment.

It is usually a long process to determine this reserve and it requires input from a variety of experts like aquatic scientists, social scientists, hydrologists and engineers. The competent authority that is directly associated with any river in South Africa and that needs to authorise the amount of water that will be diverted from a specific river, is the Department of Water Affairs and Forestry (DWAF).

DWAF allowed water diversion from the Assegaibos River on the condition that the reserve must at all times remain in the river and as soon as the flow in the river becomes equal to or less than the amount needed for hydro power generation, the diverting activities should be stopped and all the water should be allowed to remain in the river. Authorising documents are attached on a compact disk (CD) that is included at the back of this thesis.

## **3.2 The EIA Process**

Doing all the necessary environmental assessments and getting the necessary authorisation prior to developing a MHPS can be a very long process that lasts a minimum of 115 days. The EIA of a MHPS can be completed by oneself, but it must be approved by the DEA&DP. Firstly a document must be submitted to the DEA&DP whereby they are notified that an EIA for a specific development is going to be submitted and wherein exemption from appointing an independent environmental assessment practitioner to do the EIA is also applied for. Once feedback is received from the DEA&DP, the EIA process can start. A diagram of the whole EIA process and the minimum time required to obtain environmental authorisation for the development of a MHPS is attached in Appendix A.2. The processes involved in the conduction of an EIA are described hereafter.

### **3.2.1 Screening**

Screening involves the decision of whether or not a certain proposed development requires an EIA and if it is required, what type of assessment is required. The extent of activities associated with a certain development determines which of the following two processes should be undertaken:

- (i) The Basic Assessment Process applies to all activities listed in Regulation 386 of the National Environmental Management Act (NEMA, No. 107 of 1998). These are normally smaller scale activities of which the predicted impacts are usually known and can be managed easily [14].
- (ii) The Scoping Process is a more thorough assessment process and applies to all activities listed in Regulation 387 of the NEMA. These activities are usually of higher risk and the possible impacts cannot be predicted easily [14].

Usually only a basic assessment process is necessary for the development of a MHPS, since the following activities that are listed in Reg. 386 of the NEMA, may be applicable:

- *1 (k) – The construction of facilities or infrastructure, including associated structures or infrastructure, for the bulk transportation of sewage and water, including storm water, in pipelines with (i) an internal diameter of 0.36 metres or more; or (ii) a peak throughput of 120 litres per second or more.*
- *1 (m) - The construction of facilities or infrastructure, including associated structures or infrastructure, for any purpose in the one in ten year flood line of a river or stream, or within 32 metres from the bank of a river or stream where the flood line is unknown excluding purposes associated with existing residential use, but including (i) canals; (ii) channels; (iii) bridges; (iv) dams; and (v) weirs.*
- *12 – The transformation or removal of indigenous vegetation of 3 hectares or more or of any size where the transformation or removal would occur within a critically endangered or an endangered ecosystem listed in terms of section 52 of the National Environmental Management: Biodiversity Act, 2004 (Act No. 10 of 2004).*

All the necessary procedures that must be followed for an EIA are stipulated in Regulation 385 of the NEMA. This regulation also includes information on specific requirements for certain assessment processes, as well as the necessary contents of reports that must be submitted to the DEA&DP, etc.

### **3.2.2 Impact Prediction**

All the possible environmental and socio-economic impacts (positive and negative) which are likely to occur, as a result of a certain activity during any of the 3 phases of the life cycle of the project (Constructional, Operational and Decommissioning Phase) have to be predicted. All these impacts then need to be assessed for significance with the following taken into consideration:

- The extent of the impact.
- The duration of the impact.
- The intensity of the impact.
- The probability of the impact.

The most important predicted impacts for the MHPS at Waterval are summarised below and the complete EIA is included on a CD that is included at the back of this thesis. The convention used to rate the significance of the identified impacts are also included on the CD.

#### ***Noise***

Noise levels generally increase as a result of construction activities of the development. The increase in noise levels during the construction phase depends on the size of the development and topography of the site since these determine to what extent construction vehicles and equipment will be used for the development. Noise levels caused by generating equipment during the operational phase can be of a disturbance, but it is the responsibility of the developer to ensure that noise levels outside the powerhouse are within acceptable limits. At Waterval no problems with noise levels were identified.

#### ***Visual***

The aesthetic impacts of a MHPS development are determined by the characteristics of a site and its location. At Waterval, the loss of vegetation, the presence of building material and equipment and the presence of MHPS system equipment during the construction phase of the project were identified as potential impacts. The significance of these impacts are however considered as low since most of the components of the MHPS are located where the environment

has already been disturbed or where there is little access for visitors. The areas where a loss of vegetation will be experienced were kept to a minimum.

Only a small part of the pipeline is located where it is visible to people on the farm and to hikers in the mountain. Measures do exist and are implemented to make the visible components blend into the adjacent environment in order to minimise the aesthetic impacts of the permanent fixtures, hence the significance of this impact is considered as low.

### ***Water Quality***

This is certainly the most important aspect that was considered as the water in the river is used for domestic and agricultural purposes and also ensures sustainable ecological functioning of the environment. Water quality is only to be affected downstream of the point from where the water is diverted. Impacts such as the spillage of chemicals and generated waste into the river during the construction phase could have had detrimental impacts, but their significance was considered as medium since few chemicals were used and little waste was generated. Most of the construction also took place at a distance further than 7 m from the river banks. The flow in the river at the location of the diversion weir, was diverted along another route for a safe period of 30 days after the diversion weir was constructed, hence the chances of spilling concrete into the river was low.

The MHPS is a closed system whereby nothing can be added to the water that passes through the system. A concern is also the induced temperature rise of the flowing water in the pipeline as a result of friction. Assuming a constant surface temperature of the pipeline, the temperature rise of the water passing through the system is calculated from:

$$\Delta T_w = \frac{\Delta P_{loss}}{\rho_w Q_{pipe} C_p} \quad (3.1)$$

where  $\Delta T_w$  is the change in temperature of the water,  $\Delta P_{loss}$  is the energy loss in the pipeline at maximum flow and  $C_p$  is the heat capacity of water. The heat capacity of water at 20 °C is 4 182 J/kg°C. The power loss in the pipeline is discussed in Chapter 4.3, but it is calculated as 1.427 kW for a flow of 20 l/s. By using this information, the temperature change of the water in the pipeline of the MHPS at Waterval, is calculated as 0.016 °C. Hence there is no change in the water quality or temperature that passes through the MHPS.

### ***Soil***

Construction activities can have serious impacts on the soil, especially where the environment is previously undisturbed. The loss of top soil or a change in the gradient of the soil can result in serious erosion problems. Waste generation and chemicals can cause soil contamination. At Waterval the extent of the construction activities is low and no soil gradients changed, few chemicals were used and almost no waste was generated, hence the significance of these impacts is considered as low.

The possibility exists that the pipeline can be damaged in some or other way during the operational phase of the MHPS which can cause leakages to occur. Leaks at the joints may also initiate as a result of thermal expansion and contraction. These leakages can result in serious erosion problems, hence the significance of this is considered as medium.

### ***Aquatic Ecosystem***

The aquatic ecosystem will be negatively influenced if any waste or chemicals are spilled into the river during the construction period, but as already discussed, the chances of this happening are low. If the predetermined reserve does not remain in the river the aquatic ecosystem will be disturbed, but since the owner of the MHPS has entered into a legal agreement that he will ensure that the reserve will at all times remain in the river the chances of the river running dry are low. Despite the fact that no fish exist in the river, an adequate screen exists at the intake to the pipeline which will prevent any animal life from entering the pipeline.

### ***Fauna***

Some wildlife species have been identified at Waterval. The duration of the construction activities will only be about three months and the extent of any activities during the construction and operation phases are not such that these species will be harmed in any manner.

### ***Flora***

Some locations on the MHPS site had been disturbed before. Nevertheless some components of the MHPS could cause damage to vegetation. Failure to revegetate these areas can be detrimental as effects such as erosion are likely to occur and therefore the significance of this impact is considered as medium.

If the reserve flow is not maintained in the river during operation of the MHPS, or leaks occur in the pipeline resulting in erosion, the vegetation will be damaged. As discussed, minimum water levels need to be maintained in the river, but leaks can cause serious damage in the long term and therefore the significance of this impact is considered as medium.

### ***Socio-Economic***

None of the employees lives on the farm and no additional jobs were created by the construction activities of the proposed development at Waterval, since the current employees of the farmer were used. During the operational phase of the MHPS, electricity will be saved which will result in electricity cost savings. These savings can then be invested into the farm where the farmer may extend some of his farming activities. This can have a positive impact, since it is likely that more jobs on the farm will then be created.

### **3.2.3 Impact Mitigation Measures**

These measures are proposed to avoid or reduce all the predicted impacts that may result from a certain activity that is associated with a proposed MHPS development. These mitigation measures are stipulated in the Environmental Management Plan (EMP) of a development. The EMP must also be authorised by the DEA&DP and must be submitted with the EIA. The complete EMP for Waterval is attached on a CD that is included at the back of this thesis.

### **3.2.4 Public Participation Process**

Provision is made for the public who may be positively or negatively affected by certain activities of a proposed development or who are concerned with a specific proposed development, its activities and its consequences. During this process that extends over a minimum period of 30 days, they are given the opportunity to give their input regarding the activities of a proposed development. It is the responsibility of the person that conducts the EIA to ensure that notice of the proposed development is given to all potential interested and affected parties (I&AP). Notices include advertising the proposed MHPS development in local newspapers and the erection of a notice board on the site. Requirements for these notices are stipulated in guidelines that are available from the DEA&DP.

I&APs at Waterval include the DWAF, Eskom, the local municipality and the farmers downstream of Waterval that hold water rights for the river. Their concerns with the solutions are included in the public participation document that also accompanies the EIA. This document is attached on the CD that is attached at the back of this thesis and pictures of the notices for the MHPS at Waterval are shown in Appendix G.

### **3.2.5 Review and Decision Making**

After the EIA has been submitted, it is thoroughly reviewed by the DEA&DP for a maximum period of 44 days. During this period the DEA&DP may conduct a site visit and additional information regarding the development may also be requested. Based on all the information, the DEA&DP then either grants or rejects the environmental clearance to the proposed project.

Once the outcome of the application is known, the proposed development is not yet to commence, since an appeal period of 10 days exists, during which any I&AP or the applicant himself may lodge an appeal against the outcome of the application. All appeals must then first be reviewed after which a next decision regarding environmental clearance of the project is made. Activities of the development are to commence at the earliest 7 days after final environmental clearance has been obtained.

## **4. Mechanical and Civil Design**

To design a low cost MHPS, custom designed components need to be replaced with commercially available components. As the operating point of the MHPS needs to be matched to that of standard available components it is often necessary to vary the available head and flow until the operating point of the MHPS and that of standard available components match. This results in the iterative design process of which a diagram is attached in Appendix B.1.

In this chapter details are given of the design of all the mechanical and civil components of a MHPS. Firstly the intake structure and general considerations for constructing the powerhouse are discussed, after which a detailed discussion on the design of the pipeline follows. A section in which the focus is on the design and selection of the appropriate turbine for a given site then follows, after which the hydraulic control of the system is addressed. The chapter is then concluded with a short section on the drive system between the turbine and the generator. Pictures of the designed and installed components of the MHPS are attached in Appendix G.

### **4.1 Water Diversion Structures**

The inlet structure comprises of the structure necessary to divert a required amount of water from the river. Usually a permanent diversion weir with an intake mouth, constructed of concrete is used to raise the water level of the river, in order to ensure a constant water supply to the intake. The location of the inlet, whether it is on the side of the riverbed or directly in the course of the river, usually depends on the site characteristics and the space that is available [13].

The most important fact that must be considered when selecting the location of the diversion weir is to ensure that adequate foundations are present. This is of great importance to ensure that the flow of the river does not result in the undercutting of the structures. The presence of good foundations will also ensure a good seal between the diversion weir and the riverbed and sufficient strength of the structures to withstand extreme flood conditions.

Most rivers carry a silt load which is usually seasonally dependent. Challenges in the design of the diversion weir are:

- To avoid the depositing of silt around the diversion weir and the intake, since it can bury the intake and cause unequal flow diversion.

- To avoid silt from entering the pipeline, since this can cause blockages and erosion in the pipeline, valves and turbines.

Water that is diverted from rivers for power generation is usually diverted into a channel where it first passes through a settling basin, before it enters the pipeline (conveyance intake) [16]. In the settling basin, the velocity of the diverted flow is reduced in order to remove the silt load in the water, but the possibility however does exist that these settling basins can be overburdened, which will result in silt entering the pipeline. These channels and settling basins usually take up a lot of space and can become very costly. If the space and characteristics of the inlet site are such that they do not allow for a settling basin, the diverted water will have to enter the pipeline directly through the intake mouth (direct intake) [16]. The diversion weir must then be designed and built in such a way that a small reservoir is created, upstream of the diversion weir. Silt in the water will then deposit as it enters the area of still water and the danger of silt deposition at the diversion weir and intake is reduced. It will however be necessary to clean this reservoir from time to time and thus a flush pipe should be incorporated into the bottom of the diversion weir.

Another problem that has to be dealt with is the floating debris that is carried by the water in the river. To avoid this debris from entering the intake, a trash rack must be designed and placed at the intake. This is basically a metal grill that is made up of a series of evenly spaced parallel bars. A simple covering grill is sufficient for structures with a side intake, since most of the debris is carried past the intake by the river flow. For direct intakes, an angled grill with the bars located vertically upward, is necessary to intercept the floating debris and divert it upwards, over the diversion weir [13]. By varying the net area of the trash rack (the total area minus the frontal area of the bars), the velocity of the water through the trash rack, must be limited to a speed of 1 m/s to avoid the floating debris being attracted to the trash rack. For trash racks that are easily accessible for cleaning, this speed should not exceed 0.75 m/s [17]. Since this trash rack is a hindrance to the diverted flow, a slight head loss is induced. This trash rack head loss is calculated by

$$h_{tr} = K_{tr} \frac{v_{af}^2}{2g} \quad (4.1)$$

where

$$K_{tr} = B_{sc} \left( \frac{s}{b} \right)^3 \sin(\varphi) \tag{4.2}$$

In Equation 4.1 and 4.2,  $h_{tr}$  is the experienced head loss,  $K_{tr}$  is the trash rack coefficient,  $v_{af}$  is the approaching velocity of the flow,  $B_{sc}$  is the shape coefficient of the bars in the trash rack as defined in Figure 11,  $s$  is the thickness of the bars in the trash rack,  $b$  is the opening between the bars in the trash rack and  $\varphi$  is the angle of the bars in the trash rack with the horizontal.

If the trash rack forms an angle,  $\Phi$ , with the approaching flow as shown in Figure 11, then the head loss through the trash rack is increased and the result obtained from Equation 4.2 needs to be multiplied with the correction factors listed in Table 2.

An intake should be designed such that the formation of vortices is avoided, since they can introduce the following problems:

- Non-uniform diversion flows.
- Air entrainment into the pipeline.
- Debris can also enter the pipeline.

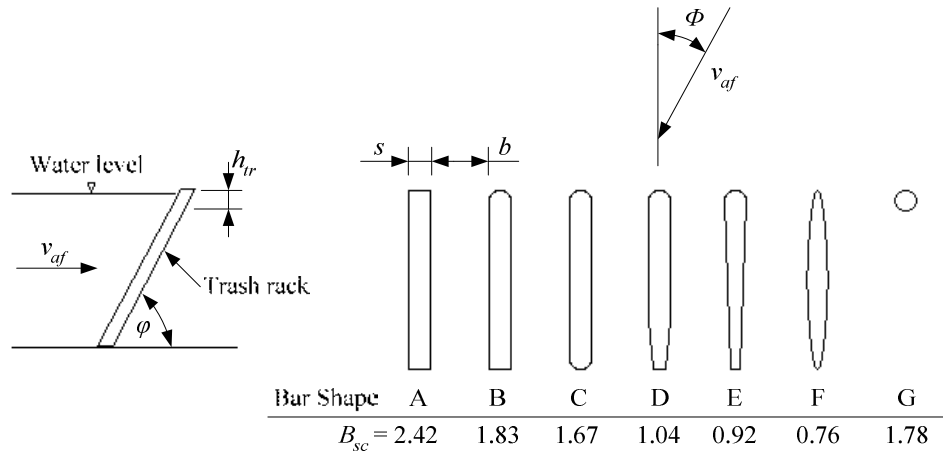


Figure 11: Shape coefficient of different bars to be used in a trash rack [17].

Table 2: Correction factors when  $\Phi > 0^\circ$ ,  $S/b = 0.599$  and  $\varphi = 90^\circ$  [17].

$\Phi$	Bar shape					
	A	B	C	D	E	F
30°	1.46	0.76	0.71	0.43	0.68	0.22
45°	2.05	1.29	1.29	0.94	1.29	0.67
60°	4.26	2.45	2.81	2.19	3.05	1.84

These problems result in higher head losses, lower efficiencies, vibration, cavitation and unbalanced loading of the hydraulic components and machinery of the MHPS. Vortices are usually initiated by the following factors [18]:

- Asymmetrical approach conditions of the flow ( $\Phi > 0^\circ$ ).
- Insufficient submergence of the intake.
- Flow separation and eddy formation.
- Rapid changes in the flow direction.

The first two disturbances are mostly associated with vortex formation. The American Society for Civil Engineers states that the criteria to avoid vortices are not well defined and thus no formula exists that considers all the possible factors that may initiate vortices. It is generally believed that if an intake is well submerged and the approach conditions of the flow are symmetric, it is unlikely that vortices will form. The minimum submergence depth of intakes, to avoid vortices, for symmetrical and asymmetrical approaching flow conditions, is calculated from

$$h_{depth} = C_{af} v_{df} \sqrt{D_{intake}} \quad (4.3)$$

where  $h_{depth}$  is the minimum submergence depth of the intake mouth,  $v_{df}$  is the velocity of the diverted flow,  $D_{intake}$  is the height of the intake and  $C_{af}$  is the approach coefficient of the flow, being 0.7245 for asymmetric approaching flows and 0.5434 for symmetric approaching flows [16]. When deciding on the submergence depth of the intake, it must be noted that a good precaution to avoid deposited silt from entering the intake is to ensure that the intake is located about 0.3 m above the riverbed [19], as shown in Figure 12.

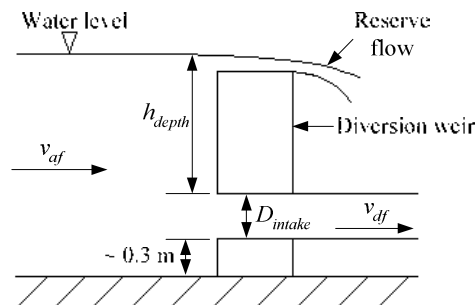


Figure 12: Submergence depth of the intake.

The inlet works of the MHPS at Waterval is located about three metres downstream of a natural weir that exists in the Assegaaibos River. The sediment load of this river is very seasonally dependent, but the advantage of this location is that most of the sediment in the river is deposited at the natural weir, leaving very little sediment that can enter the intake. The riverbed at this location consists of pure Table Mountain sandstone rock and thus ensures good foundations for the concrete diversion weir that was built. Considering costs and the available space at this location, a direct intake to the pipeline was selected. This intake incorporates a flush pipe constructed into the bottom of the weir, to allow for cleaning the sediment that may deposit in the reservoir. The flow area of the designed trash rack for this inlet is  $0.7 \text{ m}^2$  and by using Equation 2.2, the velocity of the flow approaching the trash rack is calculated to be  $0.0286 \text{ m/s}$  for a flow rate of  $20 \text{ l/s}$ . Round bars with a diameter of  $10 \text{ mm}$  and a spacing of  $15 \text{ mm}$  between them was used for the trash rack at Waterval. The trash rack stands at an angle of  $75^\circ$  to the horizontal and the calculated head loss using Equations 4.1 and 4.2 is  $0.042 \text{ mm}$ . Pipeline calculations, which are discussed in Chapter 4.3, showed that the pipeline for this MHPS should have a nominal diameter of  $160 \text{ mm}$  with an inner diameter of  $148.1 \text{ mm}$ . By using Equation 2.2 it is calculated that the diverted flow in the pipeline will have a velocity of  $1.163 \text{ m/s}$ . Due to the characteristics of the diversion weir location, the flow in the river approaching the intake is asymmetric and by using Equation 4.3, it is calculated that the intake should be submerged at least  $0.327 \text{ m}$  below the water level to avoid the formation of vortices.

## 4.2 Powerhouse

The purpose of the powerhouse of a MHPS is to protect the electrical and mechanical equipment required to convert the potential energy of the water into electrical energy, against extreme weather conditions.

General considerations when selecting the location of the powerhouse are discussed in section 2.3.1. The powerhouse is only designed once the design of the generating equipment of the MHPS is completed, since the size, type and configuration of the generating equipment determines the size of the powerhouse. The location of the powerhouse of the MHPS at Waterval had been previously disturbed and is situated  $7 \text{ m}$  away from the river, where the water table is deeper than  $0.5 \text{ m}$ . Hence the environmental impact of constructing the powerhouse is very little and since the foundations of the powerhouse are only  $0.4 \text{ m}$  deep, it is unlikely that they will be

damaged by the water table. To ensure proper ventilation in the powerhouse, to prevent overheating of the generating equipment, provision is made for ventilation holes with filters in the bottom and top of the powerhouse walls.

### 4.3 Pipeline

The pipeline is a closed conduit which carries the diverted water from the inlet, under pressure, to the powerhouse. Depending on the site topography, the pipes and the installation thereof, are usually the most expensive part of a MHPS (Refer to Table 7). It is therefore worthwhile to optimise the pipeline design to obtain optimum performance at a lowest cost.

#### 4.3.1 Design

The dynamics of a fluid in a pipeline between the point where it is diverted into the pipeline and the point where it is released back into the river, induces pipeline losses; hence the net head at the lower point of the pipeline when the fluid is in motion, is less than the gross (static) head. For a given discharge and pipeline length, these losses decrease with increasing pipe diameter, but when increasing the diameter of the pipe, its costs also increases significantly and a compromise needs to be found between the performance of the pipeline and its cost.

Figure 13 shows the energy line along the pipeline of a simplified MHPS. To optimise the performance of the pipeline, the energy equation applies [20]:

$$\frac{p_1}{\gamma} + \alpha_1 \frac{v_{af}^2}{2g} + z_1 = \frac{p_2}{\gamma} + \alpha_2 \frac{v_{dt}^2}{2g} + z_2 + h_l + h_t \quad (4.4)$$

where  $p_1$  and  $p_2$  is the pressure at the top and bottom reservoirs,  $\gamma$  is the specific weight of water,  $\alpha$  is a kinetic energy correction factor which is usually assumed to be unity for flows in a pipeline [20],  $v_{dt}$  is the velocity of the water in the bottom reservoir,  $z_1$  and  $z_2$  is the elevation of the top and bottom water levels of the reservoirs above a certain reference point,  $h_l$  is the accumulative head losses in the pipeline between the two reservoirs and  $h_t$  is the net head that is available for power generation. If the water level of the bottom reservoir is chosen as the reference point, as shown in Figure 13, then the gross head ( $h_g$ ) is equal to  $z_1$ . The approaching velocity of the water in the top reservoir, compared to the velocity in the pipeline, is usually very small as the cross-sectional area of the approaching flow is much bigger than the cross-sectional area of the pipeline; hence the kinetic energy term ( $v_{af}^2/2g$ ) in Equation 4.4 can be neglected.

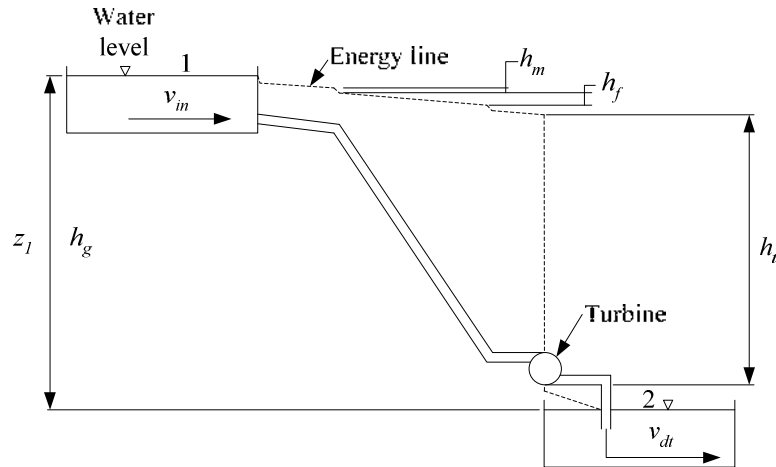


**Figure 13: Energy line of the pipeline of a MHPS.**

Considering this and the fact that for a MHPS the points 1 and 2 at the top and bottom reservoirs in Figure 13 are both located in atmosphere, Equation 4.4 is reduced to

$$h_t = h_g - h_l - \frac{v_{dt}^2}{2g} \quad (4.5)$$

The head losses in the pipeline are expressed as

$$h_l = h_r + h_f + h_m \quad (4.6)$$

where  $h_f$  is the frictional losses caused by wall shear that is distributed along the length of the pipeline and  $h_m$  is the losses induced by a change in magnitude and/or direction of the velocity of the water in the pipeline. These losses that are caused by valves, elbows and other fittings are commonly referred to as minor losses. Several methods do exist to determine the frictional losses that are induced by wall shear in the pipeline and these methods are discussed in great detail in [10, 20 - 22]. The Hazen-Williams equation is widely used in the design of waterworks and if the results obtained from it are compared to those from other methods, it yields fairly accurate results over the range of Reynolds numbers that is commonly found in water distribution systems. The Hazen-Williams equation is however easier to use since the friction coefficient of a pipe material is not a function of the Reynolds number of the flow in the pipeline, as is the case with the Darcy-Weisbach equation. For this study the Hazen-Williams equation was used to calculate the frictional head losses in the pipeline. These losses are expressed by

$$h_f = RQ_{pipe}^{1.85} \quad (4.7)$$

where  $R$  is the resistance coefficient and is expressed as

$$R = \frac{10.59(l)}{C_{HW}^{1.85} D_{pipe}^{4.87}} \quad (4.8)$$

where  $l$  is the length of the pipeline,  $C$  is the Hazen-Williams coefficient of the roughness of the pipe material and  $D_{pipe}$  is the inner diameter of the pipeline. The minor losses in the pipeline are calculated once the number of the different fittings that will be incorporated into the pipeline is known, since the loss coefficients that represent these components need to be known. The minor losses are calculated from:

$$h_m = \frac{8 \sum K}{g} \left( \frac{Q_{pipe}}{\pi D_{pipe}^2} \right)^2 \quad (4.9)$$

where  $K$  is the loss coefficient of each component in the pipeline. The loss coefficients of fittings and the Hazen-Williams coefficients of different pipe materials are attached in Appendix B.2.

According to the Alternate Hydro Energy Centre at the Indian Institute of Technology, the diameter of the pipeline of a MHPS should be selected such that the total head loss in the whole pipeline should not exceed 10 % of the gross head at the design flow, in order to keep the efficiency of the pipeline as high as possible. The ideal is to select the pipe diameter such that the losses in the pipeline are zero, but this is not economically justified. As the costs of a pipeline increase with its diameter, the cost of energy that is lost over the lifetime of the pipeline decreases and thus a least cost solution for finding an optimum pipe diameter is possible. The method to find this solution is:

- i. Calculate the cost of the pipeline for each diameter and plot it.
- ii. By using the design flow rate, calculate the head loss for each pipe diameter by using Equations 4.5 - 4.9 and then calculate the amount of the energy that is lost over the lifetime of the MHPS by using Equations 2.4 and 2.5 for each pipe diameter. By using current electricity tariffs the cost of the lost energy can be calculated and plotted.
- iii. Add the two curves and the optimum pipe diameter will be the one with the lowest total cost.

### ***The Main pipeline***

The main pipeline comprises of all the piping from where the water enters the pipeline until it reaches the powerhouse. Depending on the topography, soil conditions and accessibility of the site, the main pipeline can be installed underneath or above the ground. This fact usually

has a large impact on the decision of the pipe material that is used for the pipeline, since some materials are more suited to exposure to sunlight than others. The most common considerations when selecting a pipe material are summarised in Table 3 and three common pipe materials are compared.

The pipe material selected for the main pipeline at Waterval is uPVC. These pipes come in lengths of 6 m; hence 80 lengths of pipe were used for Waterval. The reason for selecting uPVC piping is that the characteristics of the site are such that the installation of heavy steel pipes would have been very difficult and expensive. The same applies to HDPE pipes of which the joints must be welded together. The gross head at Waterval is 79 m, hence a Class 9 pipe, capable of withstanding a working pressure of 9 bar, was used. All the information regarding the pipe diameter sizes that were considered for Waterval is attached in Appendix B.2. A summary of all the fittings used on this pipeline is also attached in Appendix B.2.

**Table 3: Characteristics of common pipe materials.**

	<b>Steel</b>	<b>Unplasticised Poly Vinyl Chloride (uPVC)</b>	<b>High-Density Polyethylene (HDPE)</b>
<b>Cost</b>	Expensive	Cheapest	Cheap
<b>Friction</b>	It has moderate resistance to flow and its resistance increases as it corrodes	Low resistance to flow	Low resistance to flow
<b>Sunlight</b>	Susceptible to sunlight	Deteriorates when subjected to sunlight but measures do exist to protect it	Susceptible to sunlight
<b>Corrosion</b>	Does corrode	Good corrosion resistance	Good corrosion resistance
<b>Weight</b>	Heavy	Light	Light
<b>Max Pressure</b>	189.9 bar	25 bar	25 bar
<b>Max Diameter</b>	600 mm	500 mm	1000 mm
<b>Jointing</b>	Moderate, pipes are either welded or bolted together	Easy, features a spigot and socket joint; thus the pipes just slide into one another	Difficult, different pipes need to be welded together on site
<b>Fragile</b>	Very resistant to damage	Very fragile, especially at low temperatures	Less fragile than uPVC
<b>Expansion and Contraction</b>	Little	About 10 times more than steel	About 10 times more than steel

The net head that can be used for power generation at Waterval, when using a range of pipe diameters for a constant discharge of 20 l/s, is calculated by programming Equations 4.5 – 4.9 into a Matlab program, while taking the following into consideration:

- The length of the main pipeline is 475 m.
- The actual inner diameter of each nominal pipe diameter is used.
- The Hazen-Williams coefficient for uPVC pipes is 140.
- The sum of the minor loss coefficients is 3.705 (Table B.3).

These results are plotted in Figure 14. From this graph it can be seen that the net available head at the bottom of the main pipeline becomes fairly high for pipe diameters of 160 mm and bigger. It must be remembered that the head losses that exists in the manifold pipeline and draft tube are not taken into consideration here. Hence only the pipe diameters that have a head loss of less than 7.9 m (10 % of the gross head) are considered, in order to account for the head losses in the manifold pipeline and draft tube. Hence from Figure 14 it can be seen that only pipe diameters of 160 mm and bigger are considered.

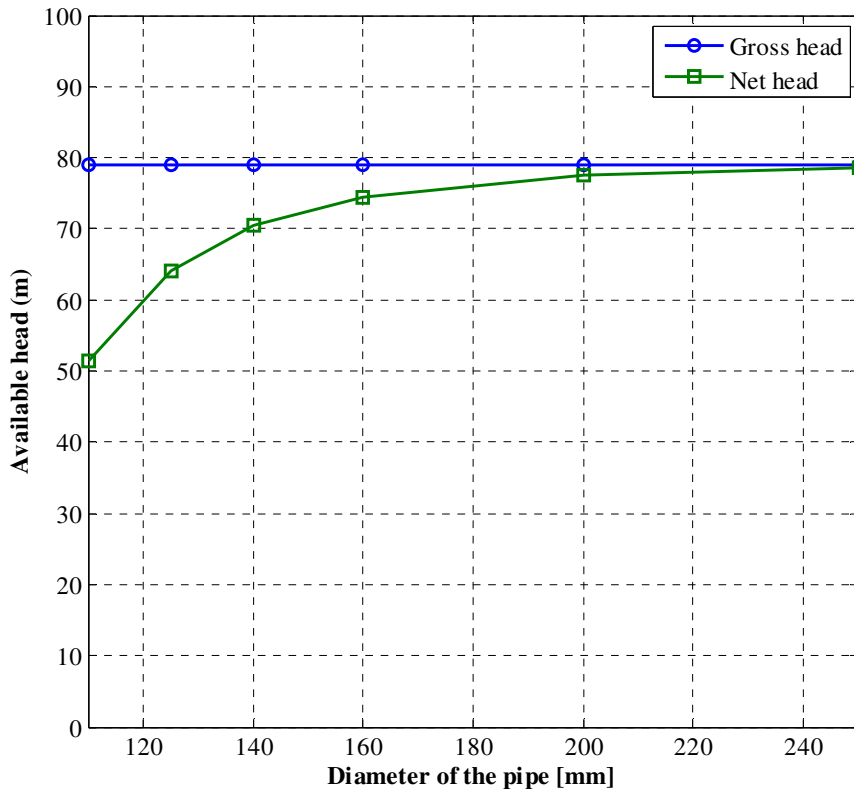


Figure 14: Head available from the main pipeline for various pipe diameters.

The lowest cost solution for this pipeline is obtained by programming Equations 2.4 and 2.5 into a Matlab program with the following taken into consideration:

- A system efficiency of 59.5 % (70% for the turbine and 85 % for the generator).
- A lifetime of 20 years.
- Pipe costs that are given in Appendix B.2.
- An electricity tariff of 46.27 c/kWh [35].

These results are plotted in Figure 15. From this figure it can be seen that the sum of the pipeline cost and the present value of the energy that is lost over the lifetime of the MHPS is the lowest for a nominal pipe diameter of 160 mm, hence this is the optimal size for the MHPS at Waterval.

The characteristics of the site are such that it allows for one half of the main pipeline to be buried under the ground while the other half is installed above the ground. The part that is installed above the ground is covered with paint to reduce the deterioration as a result of being exposed to ultraviolet light.

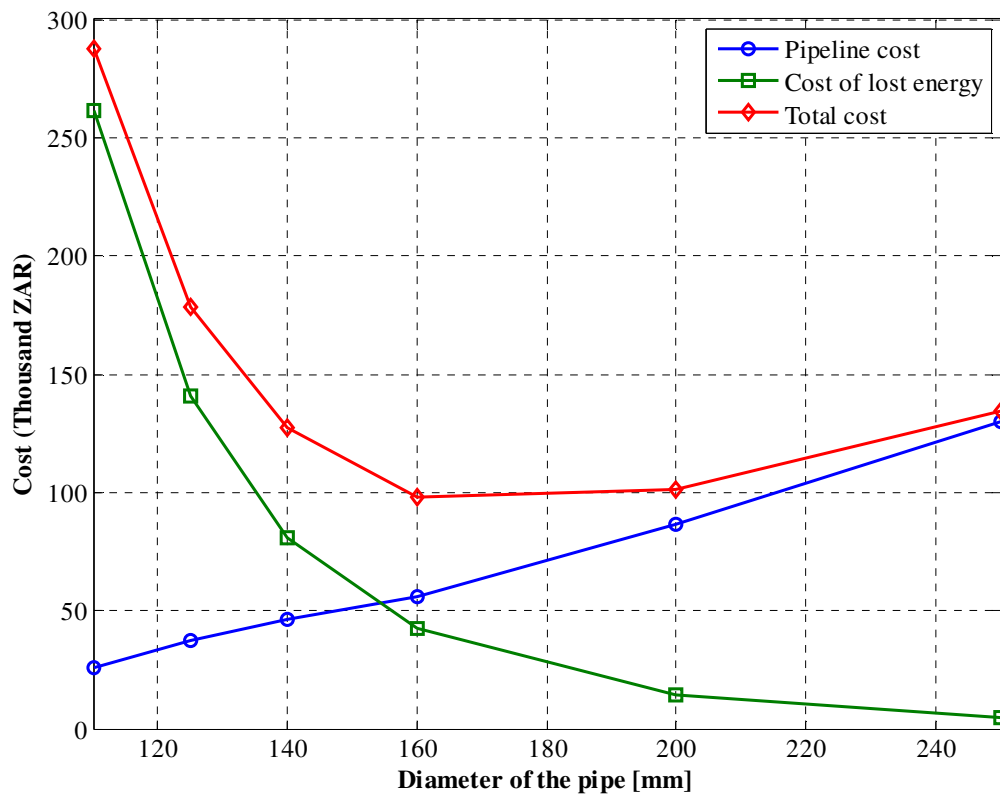
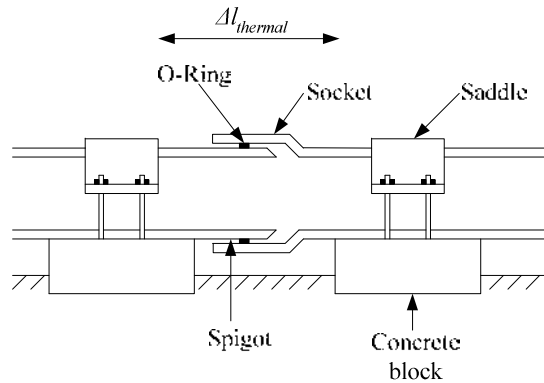


Figure 15: Lowest cost solution of the main pipeline.

The above-ground part of the main pipeline is exposed to large day and night temperature variations when there is no flow in the pipeline. Due to the large thermal expansion coefficient of uPVC, this length of the pipeline experiences significant thermal expansion and contraction. The change in length of a pipeline due to thermal expansion and contraction is calculated from

$$\Delta l_{thermal} = \alpha_t l_{initial} \Delta T \quad (4.10)$$

where  $\Delta l_{thermal}$  is the change in length,  $\alpha_t$  is the coefficient of thermal expansion,  $l_{initial}$  is the initial length of the pipe and  $\Delta T$  is the difference between day and night temperatures. The thermal expansion coefficient of uPVC is  $90 \times 10^{-6} \text{ } ^\circ\text{C}^{-1}$ . With a realistic maximum change in temperature at Waterval of 30  $^\circ\text{C}$ , the change in length of a 6 m uPVC pipe is calculated to be 16.2 mm. To account for this change in length of each pipe, the above ground pipes are fixed to the ground by means of PVC saddles that are bolted to boulders and concrete blocks. The saddles allow for radial and linear thermal expansion and contraction of the pipeline. uPVC pipes feature spigot and socket joints, with O-rings as gaskets, and this accommodates the linear thermal expansion and contraction of the main pipeline, as shown in Figure 16.



**Figure 16: A spigot and socket joint with saddles on each side of the joint**

### ***The Manifold pipeline***

The manifold pipeline is the part of the pipeline that conveys the water from the main pipeline to the turbine. It usually branches in the powerhouse into additional lines to accommodate a bypass line or if applicable, more turbines. Valves usually exist in this pipeline which are used to control the flow inside the powerhouse. Other fittings like bends and reducers are also used to fit the diameter of the main pipeline to the diameter of the inlet of the turbine.

The layout of the hydraulic system in the powerhouse at Waterval is represented in Figure 17. The manifold line of this MHPS has two branches; one that conveys the pressurised water to the turbine with the other one only functioning as a bypass line which is discussed later.

The following components, all with a nominal diameter of 110 mm and an inner diameter of 101.7 mm, add to the head loss experienced in the manifold line:

- uPVC Pipe with a length of 2 m.
- An isolation gate valve that is used to isolate the control valves and turbine from the main pipeline during shut down of the MHPS.
- A Bellow rubber joint that dissipates vibrations in the manifold line.
- A T-junction joint to provide for the bypass pipeline that is discussed in Chapter 4.5.
- A hydraulic control globe valve.
- A reducer to fit the 110 mm pipe to the 50 mm inlet diameter of the turbine.

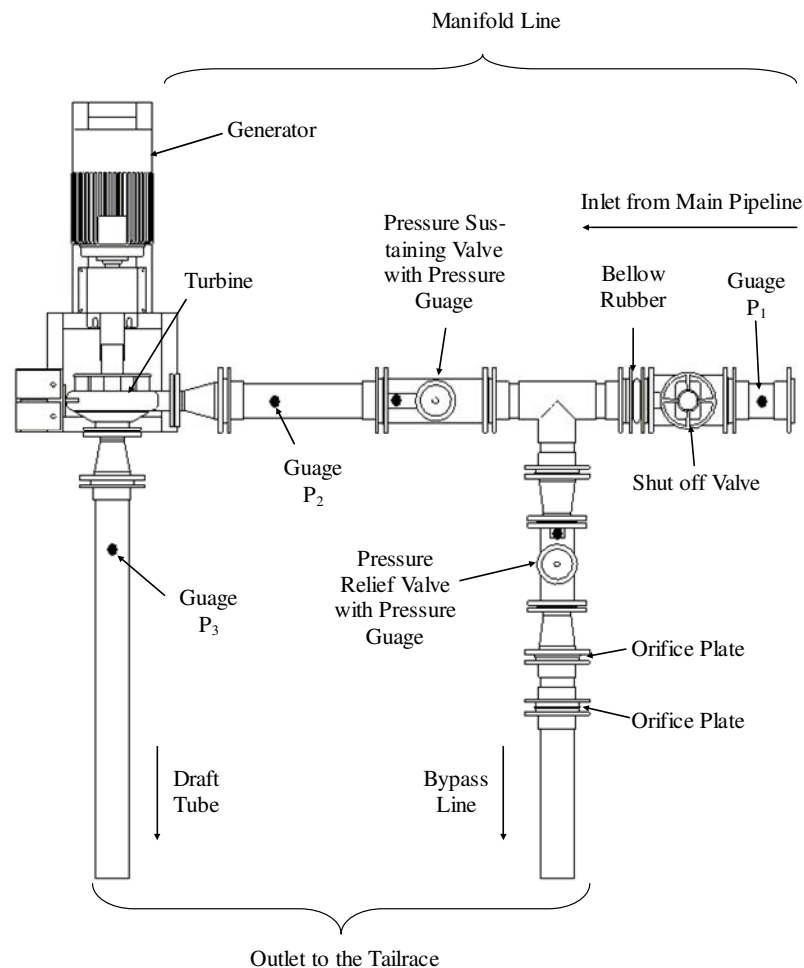


**Figure 17: Layout of the hydraulic system in the powerhouse.**

With all the valves in the manifold line considered as fully open, the collective minor loss coefficient is 6.005 (Table B.3). By using Equations 4.7 – 4.9, the total head loss in the manifold line for a flow of 20 l/s is calculated as 1.97 m.

### ***The Draft tube***

A draft tube is only used in MHP systems where reaction turbines are used. The velocity of the flow at the outlet of the turbine is usually very high, and so is the kinetic energy loss if the water is discharged directly into the tailrace. To reduce this kinetic energy loss, the draft tube that is submerged in the tailrace, is connected to the outlet of the turbine to form a continuous stream of water between the turbine and the tailrace. Generally the cross sectional area of this tube is gradually increased over its length to reduce the velocity of the water that flows through the draft tube. The reduced velocity at the outlet of the draft tube results in a reduced kinetic energy loss. The reason for submerging the draft tube outlet is to make use of the full head between the water levels of the intake and the tailrace.

Various designs for draft tubes exist and the layout of a typical draft tube is shown in Figure 18. When designing a draft tube for a specific turbine, the exit diameter of the turbine needs to be known, since [23] recommends that the dimensions of the draft tube should be such that the following are satisfied:

- $\frac{l_{dt}}{D_{te}} \leq 9$ , where  $L_{dt}$  is the length of the draft tube and  $D_{te}$  is the diameter of the outlet of the turbine.
- $\frac{A_{dt}}{A_{te}} \leq 4$ , where  $A_{dt}$  is the cross-sectional area of the draft tube outlet and  $A_{te}$  is the cross-sectional area of the turbine outlet.
- $\theta \leq 8-12^\circ$ , where  $\theta$  is the angle at which the walls of the draft tube diverge.

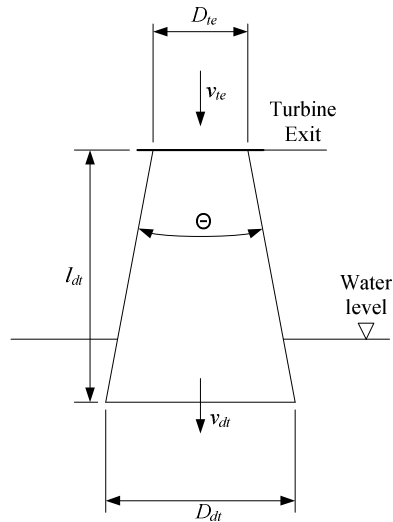


**Figure 18: A typical draft tube [23].**

The design of the draft tube of the MHPS at Porterville was based on commercially available components. The draft tube consists of the following:

- A gradual expansion joint that is bolted to the turbine outlet, where the nominal diameter expands from 65 mm (turbine outlet diameter) to 110 mm; the length of the expansion joint is 101.6 mm.
- uPVC Pipe with a nominal diameter of 110 mm and a length of 3 m.
- A 45° bend with a nominal diameter of 110 mm.

The actual diameter of the draft tube outlet is 101.7 mm. For a design flow rate of 20 l/s, the kinetic energy loss ( $v_{dt}^2/2g$ ) at the outlet of the draft tube is calculated to be 0.309 m, which is much less than 1.85 m if the water is to be discharged directly into the tailrace from the turbine outlet. With the minor loss coefficients of the draft tube that add up to 0.13 (Table B.3) and using Equations 4.5 – 4.9, the total head loss of the draft tube is calculated as 0.2073 m, for a design flow rate of 20 l/s.

With all the information of the whole pipeline known, the final system curve of the pipeline at Waterval, from the intake to the tailrace is determined using Equation 4.4 and the results are shown in Figure 19. This is done by programming the information of each section of the pipeline and Equations 4.5 – 4.9 into a Matlab program.

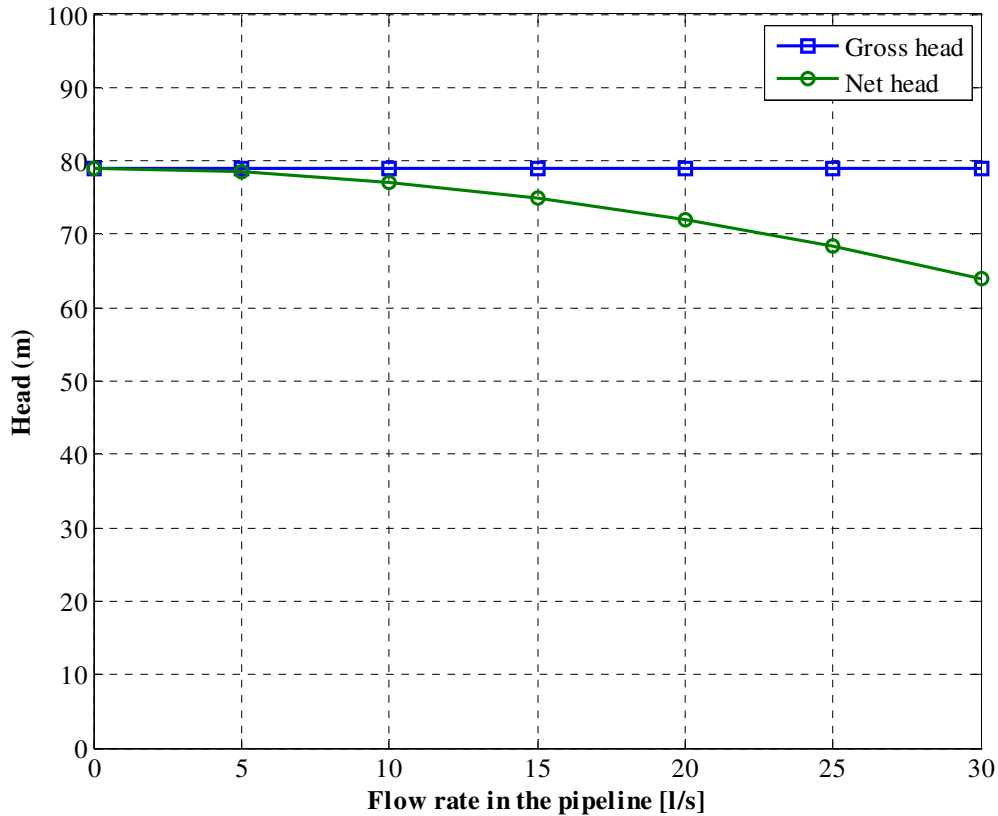


**Figure 19: Final system curve of the whole pipeline.**

From this final system curve it can be seen that the total head loss of the whole pipeline as a result of the high loss coefficient of the pressure sustaining valve in the manifold line increases rapidly for flows larger than 10 l/s. The total head loss at the design flow rate of 20 l/s is 6.98 m, which is within the 10 % limit of the gross head of 79 m. The efficiency of the pipeline at the design flow is calculated to be 91.2 %.

### 4.3.2 Water Hammer

Sudden changes in the velocity of water in a pipeline results in pressure transients that develop along the length of the pipeline, a phenomenon known as water hammer. In hydro power systems, water hammer is usually caused by (i) sudden opening or closure of valves at the bottom of the pipeline, (ii) by changes in turbine operation or (iii) by pipe bursting.

If the velocity of the water at the bottom of the pipeline is changed by  $\Delta v$ , the pressure at that point will also change with  $\Delta p$  and a pressure wave will be developed that will move back and forth in the pipeline until dissipated by friction in the pipeline [22].

The change in pressure due to the change in the velocity of the water is calculated from

$$\Delta p = -\rho_w a \Delta v \quad (4.11)$$

where  $\Delta p$  is the pressure change and  $a$  is the velocity of the pressure wave in the pipeline. From Equation 4.11, it can be seen that a reduction in the velocity of the water will result in a pressure rise ( $+\Delta p$ ) and an increase in the velocity will result in a pressure drop ( $-\Delta p$ ). With the assumption that the developed pressure waves cause the water in the pipeline to compress slightly and the walls of the conduit to deform somewhat, the speed of the pressure waves is calculated from

$$a = \sqrt{\frac{\frac{E_{water}}{\rho_w}}{1 + \frac{D_{pipe} E_{water}}{t E_{pipe}}}} \quad (4.12)$$

where  $E_{water}$  is the modulus of elasticity of water,  $t$  is the thickness of the conduit walls and  $E_{pipe}$  is the modulus of elasticity of the pipe material. Care must be taken to ensure that the change in pressure plus the initial pressure of the water in the pipeline, before its velocity was changed, does not exceed the maximum pressure rating of the pipeline. To achieve this, the velocity of the water needs to be changed gradually. The time it takes for a pressure wave to travel from the bottom of the pipeline to the intake and back, also known as the reflection time, is calculated from

$$t_r = \frac{2L}{a} \quad (4.13)$$

where  $t_r$  is the reflection time. It is preferred that the velocity of the water in the pipeline is changed gradually over time steps greater than the reflection time, since earlier pressure waves return to the bottom of the pipeline as waves with low pressure and hence the risk of high pressures during further stages of velocity changes are reduced [20 - 23].

The modulus of elasticity of water and uPVC is 2.2 GPa and 2.7 GPa respectively. By using this in Equation 4.12 it is calculated that a pressure wave in the pipeline at Waterval will travel at a speed of 321.8 m/s. Considering the water in the pipeline at standstill, then the maximum pressure rise can that can be accommodated is 1.1 bar. By using this in Equation 4.11 it can be seen that the maximum instantaneous change in the velocity of the water should not exceed 0.34 m/s. From Equation 4.13 it is calculated that the reflection time of the pipeline is

2.95 s, and thus to avoid any damage to the pipeline, the velocity of the water in the pipeline should never change instantaneously with more than 0.34 m/s every 2.95 s.

Several measures exist that can be incorporated to reduce the risk of water hammer in a pipeline. These include:

- Increasing the diameter of the pipeline in order to have low initial velocities at the design flow rate, but with the cost of the pipeline remaining at values that are justified economically.
- Usage of another pipe material to reduce the velocity of the pressure wave in the pipeline.
- Ensuring longer opening and closing time of valves at the bottom of the pipeline.
- Installation of a bypass line around the turbine, which usually features a pressure relief valve that opens according to certain preset pressures. To deal with water hammer problems at Waterval, a bypass line is installed, but this is discussed in Chapter 4.5.

### 4.4 Hydraulic Turbine

The turbine is the mechanical machine that converts the kinetic energy of the pressurised water in the pipeline into rotational energy. As discussed in section 1.2, various turbines exist that can be used in a MHPS. Figure 20 presents the range of heads and flow rates for which different pumps can be used to operate as turbines. The available head and flow at Waterval falls well within the range of a radial / centrifugal PAT.

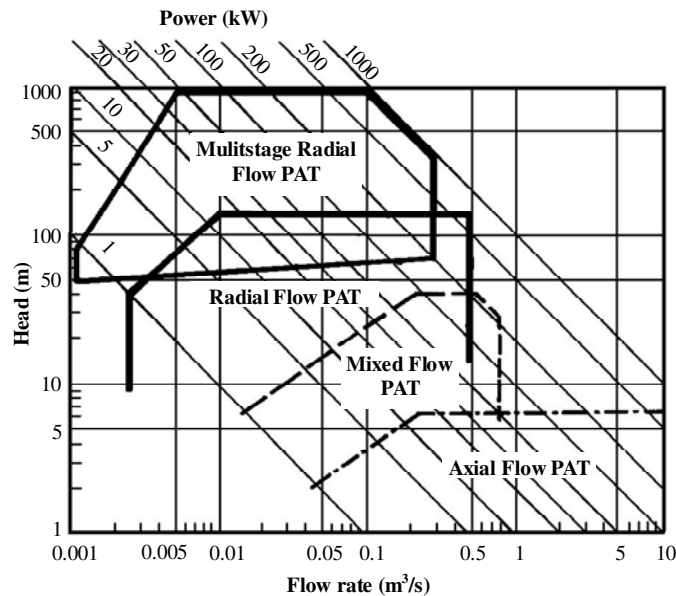


Figure 20: Range of application of different PAT types [23].

The primary reason for selecting a PAT for the MHPS at Waterval is its major cost advantage. When comparing a PAT to conventional turbines, it is found that it also has the following advantages:

- Pumps are commercially available in a number of different sizes which make them suitable to be used over a wide range of heads and flow rates as shown in Figure 20.
- Pumps and their spare parts are easily available since they are mass produced.
- Mostly the installation of pumps is relatively easy and no high level qualifications or special equipment is necessary for doing basic maintenance on pumps,
- No big modifications need to be made for a pump to operate in reverse as a turbine. In turbine mode the impeller rotates in the reverse direction and the only major modification is that the nut that holds the impeller in place must be fastened to the shaft, either by using a locking adhesive or by using a nut with a split pin through it.

A PAT has the disadvantage that its peak efficiency is lower than that of a conventional turbine. Since a PAT does not incorporate any form of hydraulic control like a conventional turbine, the efficiency drops significantly when operating at flow rates other than the design flow rate. Hence unless using multiple PATs, it cannot be used in applications where a wide range of flows needs to be accommodated.

#### **4.4.1 Centrifugal Pump as Turbine Principle**

As mentioned in section 1.2, a centrifugal pump that operates in reverse as a turbine, works on the same principle as a Francis turbine. Water enters the casing of the PAT through the inlet and then flows inward through the impeller as shown in Figure 21. The water then exits through the eye of the impeller and discharges into the tailrace through a draft tube.

The performance of a pump and a PAT are usually presented in diagrams where the head developed or absorbed by the machine is plotted versus the flow through the machine, with typical curves shown in Figure 22. From this it can be seen that the flow through a PAT increases continuously with increasing head, but for a pump, it decreases with increasing head. Also, a PAT only starts to deliver power once the flow through the PAT exceeds a certain minimum. The power output then increases with increasing flow and head. For a pump, the power needed is a minimum at maximum head, and increases with decreasing head.

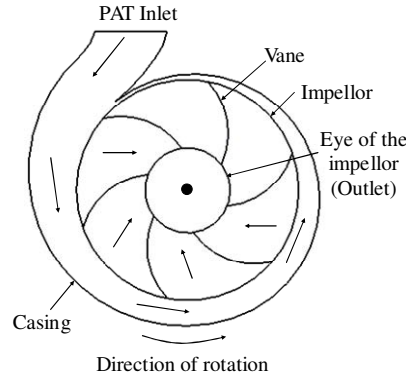


**Figure 21: Basic flow path of water in a PAT.**

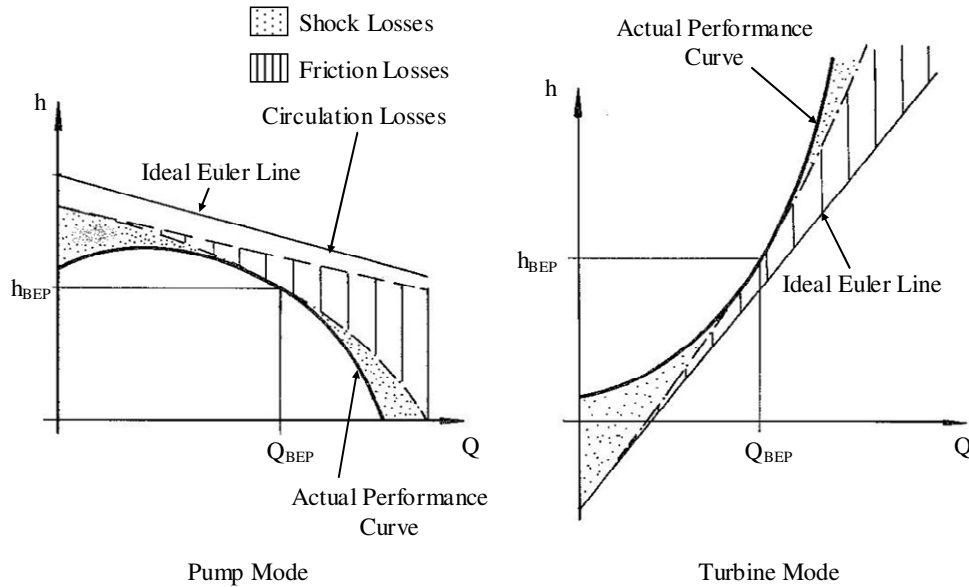


**Figure 22: Characteristic curves of a pump and a PAT for both ideal and non-ideal conditions [23, 24].**

The most important difference between the performance curves of the two modes of the same pump is that the Best Efficient Point (BEP) lies at different head and flow conditions for pump mode than for turbine mode. The performance of a pump was originally described by Euler according to ideal conditions (no losses) and these conditions are also shown in Figure 22. However, these ideal conditions are not achievable in practice as actual losses do exist. These losses differ for the two operating modes, and are the reason for the difference of the BEP between the two modes [23, 24]. These losses are discussed hereafter with reference to the performance curves shown in Figure 22.

### ***Mechanical friction losses***

These losses are due to friction between the rotating shaft of the pump and its stationary casing and occur in the bearings and the stuffing box packing. They are however the same for both pump and turbine mode of a pump, and increase proportionally with the square of the flow rate through the machine [23].

### ***Shock losses***

The angles of the vanes in the impeller and of the casing are designed to match those of the fluid at a certain design point, in order to obtain optimal performance at this flow rate. Misalignment between all these angles occurs when flow rates other than the design flow rate are experienced, which results in losses commonly known as shock losses. No shock losses are present at the design point, but they increase with the square of the difference between the operated and design flow rates [23, 25].

If a pump is operated in such a way that shock losses are experienced, ideal energy transfer from the impeller to the water is not achieved and the head generated by the pump is lower than in ideal conditions. The energy transfer in a PAT occurs in the opposite direction, and in order for a PAT to maintain operation at optimum flow, an increased pressure is necessary, hence shock losses are added to the ideal head [23].

### ***Frictional losses***

As the water moves through the impeller vanes and the casing, frictional losses occur. In pump and turbine mode, these losses increase with the square of the flow rate through the machine. In pump mode these losses decrease the head generated by the pump, but for turbine mode, to remain operating at optimum flow rate conditions, these frictional losses are added to the required head [23].

### ***Leakage losses***

This loss occurs as a result of water leakage from the high pressure side at the impeller tips to the low pressure side at the eye of the impeller, through the small clearance between the impeller and the casing. Hence in a pump the total pumped flow is less than the ideal flow. In a PAT, this leaking water does not contribute to the energy transferred from the water to the

impeller. Hence the flow approaching the PAT must be more than the ideal flow to maintain operation at optimum conditions.

**Circulation losses**

The pressure distribution in the channels of a rotating impeller of a pump in pump mode is presented in Figure 23. A high pressure region exists along the pressure side of the vane and a low pressure region exists along the suction side of the vane. This pressure distribution results in the velocity distribution in the channel being non-uniform, with a lower velocity in the high pressure region and a higher velocity in the low pressure region. According to [24], the rotation of the impeller now produces a secondary circulation current within the channels of the impeller. This causes the relative velocity vector of the water to leave the impeller at an angle  $\beta'$  and not at the blade angle  $\beta$ , as predicted by Euler when he assumes the impeller to have an infinite number of vanes. This slight deflection reduces the tangential velocity component of the water, which produces a reduction in the head that is generated by the pump. This loss is known as the circulation loss in a pump.

In a PAT, where the flow through the pump is reversed, this circulation loss now occurs at the inner eye of the impeller. Seeing that the diameter of the eye of the impeller is much smaller than the outer diameter of the impeller, the circulation loss in turbine mode is so small that it can be neglected [23].

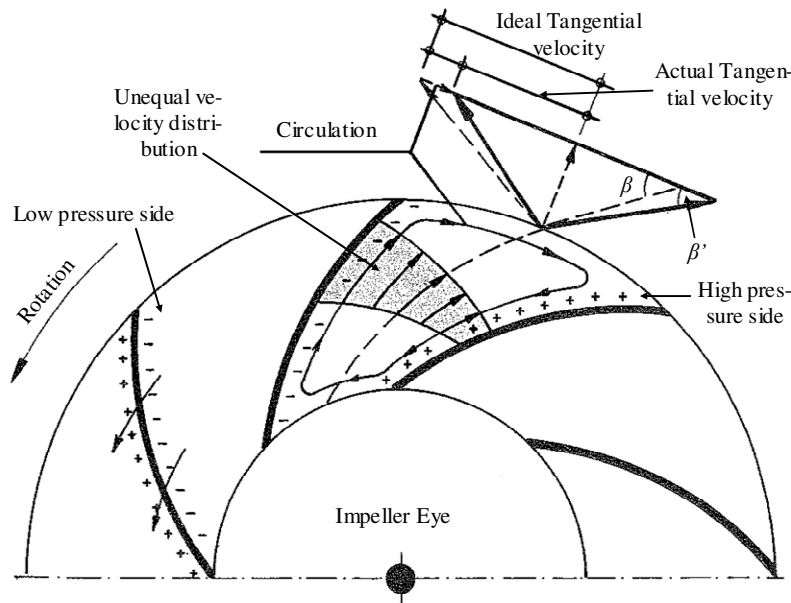


**Figure 23: Velocity and pressure distribution in the impeller of a pump [23, 24].**

The difference in performance between the pump and turbine mode of centrifugal pumps is not necessarily the same for pumps of the same size from different manufactures or for pumps of different models from the same manufacturer.

From the above it is deduced that for a specific site with certain head and flow conditions, a bigger pump must be selected for pump mode than for turbine mode. Since pumps are exclusively designed for pumping applications, the selection of a standard centrifugal pump usually involves the review of easily available pump mode performance diagrams to find a pump that delivers a required flow at a certain head and optimum efficiency. Turbine mode performance data of pumps are not yet easily available, hence turbine mode conditions need to be converted to pump mode conditions in order to select a suitable PAT for a certain application. The turbine mode performance of a pump then needs to be predicted from its pump mode performance diagrams. This process is discussed in the following section.

#### **4.4.2 Selecting a PAT and Predicting its Performance**

Research on using pumps as turbines has been done for almost 80 years. Over the years, a number of methods were developed to predict the turbine mode performance of pumps from readily available pump mode performance data, but none of these methods appeared to be 100 % reliable. Experimental results deviated with  $\pm 20$  % from the theoretical results obtained from these methods [26]. Hence it has become a great challenge to select a proper pump to operate as turbine for a specific application. A basic method to select a PAT is described in [26].

The method used to select a PAT for the MHPS at Waterval is similar to the one used by the PAT group at KSB pumps in Germany. This PAT selection method is based on results obtained from a large number of PATs that have been tested by them over the years [23]. It should be noted that the method discussed in this section only applies to single stage radial flow pumps.

The necessary working diagrams that are used in this method for selecting a PAT are attached in Appendix C.1. The very first step is to calculate the specific speed of the proposed installation. The specific speed is a dimensionless parameter used to classify turbine sizes and types, and it is calculated by

$$n_{qt} = n_t \frac{\sqrt{Q_t}}{h_t^{\frac{4}{3}}} \quad (4.14)$$

where  $n_t$  is the rotational speed of the PAT. This speed depends on the drive system that is used between the PAT and the generator. Should it be coupled directly, then a synchronous speed of 1 500 or 3 000 rpm must be used. These speeds are suited for synchronous generators, but if an induction generator is used, this operating rotational speed must be selected about 3 % higher than the synchronous speed, in order to allow for slip. It must also be ensured that the chosen speed does not exceed the maximum permissible speed as specified by the manufacturer of the pump. The pump-mode specific speed is calculated from

$$n_{qp} = \frac{n_{qt}}{0.89} \quad (4.15)$$

where the value of 0.89 is a result obtained by [23] from test results of various PATs. If the pump mode specific speed is found to be lower than 15, then a PAT should not be used [23]. The efficiencies of these PATs are very low and their turbine mode performance cannot be predicted accurately. The pump mode specific speed can be increased by increasing the turbine mode speed. Alternatively, the turbine mode head and flow can also be varied, but it must be ensured that the power output of the PAT remains acceptable. The conversion factors used to transform the turbine mode design conditions to pump mode design conditions depend on the estimated efficiency of the machine. The diagram presented in Figure C.1 provides maximum pump efficiencies, but as a function of pump mode rated flow versus pump mode specific speed. For a first estimation, this rated pump mode flow rate is calculated from

$$Q_p = \frac{Q_t}{1.3} \quad (4.16)$$

where  $Q_p$  is the rated pump mode flow rate and 1.3 is a sufficient average flow conversion factor [23]. With the maximum pump mode efficiency known, the conversion factors to obtain pump mode head and flow rate can be read from the diagrams in Figures C.2 and C.3. The BEP pump mode design parameters are calculated from

$$h_p = \frac{h_t}{C_h} \left[ \frac{n_p}{n_t} \right]^2 \quad (4.17)$$

$$Q_p = \frac{Q_t}{C_q} \left[ \frac{n_p}{n_t} \right]$$

where  $h_p$  is the pump mode head and  $Q_p$  is the pump mode flow rate.  $C_h$  and  $C_q$  represent the head and flow rate conversion factors respectively. It is very likely that the selected turbine mode

speed of a pump will differ from its pump mode speed at the BEP. To account for this, the affinity laws are incorporated into Equation 4.17, where  $n_p$  represents the rated pump mode speed of the pump at its BEP. The rated pump mode speed is available from the pump performance diagrams.

The calculated pump mode head and flow rate are then used to select a suitable pump from pump performance diagrams. It is unlikely that these operating conditions will match exactly with the BEP of any pump. If no standard available pump matches these required conditions, then the above PAT selection process should be repeated, using a different PAT speed. If there is still no match, the operating point of the PAT, i.e. the design head and flow rate, should be altered.

Usual practice is to select a pump with a rated BEP flow rate slightly less than the design pump mode flow rate, which implies that the pump in turbine mode will be slightly overloaded, i.e. it will operate at a flow rate beyond its BEP. This is advantageous, since the operating point of the PAT will lie in a relatively flat area of the efficiency curve, hence if the flow rate through the PAT drops slightly, the efficiency of the PAT will not decrease significantly.

### ***PAT Performance prediction***

To predict the actual turbine mode performance of the selected pump, the specific speed of the selected pump must be calculated from

$$n_{qps} = n_p \frac{\sqrt{Q_{ps}}}{h_{ps}^{\frac{3}{4}}} \quad (4.18)$$

where the subscript,  $ps$ , denotes the flow rate and head values of the selected pump, at its BEP. Using this specific speed and the efficiency of the selected pump at its BEP, new head and flow rate conversion factors are read from the diagrams in Figure C.2 and C.3. The turbine mode BEP head and flow rate values of the selected pump are calculated from:

$$h_{ts\_BEP} = C_{hs} h_{ps} \left[ \frac{n_t}{n_p} \right]^2$$

$$Q_{ts\_BEP} = C_{qs} Q_{ps} \left[ \frac{n_t}{n_p} \right] \quad (4.19)$$

where  $h_{ts\_BEP}$  is the BEP turbine mode head and  $Q_{ts\_BEP}$  is the BEP turbine mode flow rate of the selected pump.

To account for the uncertainty of the PAT yielding exactly the calculated BEP parameters, [23] suggests that a possible maximum and minimum BEP should be calculated by using the following uncertainty factors:

$$\begin{aligned} h_{ts} &= h_{ts\_BEP} \pm 10\% \\ Q_{ts} &= Q_{ts\_BEP} \pm 7.5\% \end{aligned} \quad (4.20)$$

The maximum efficiency of a pump in turbine mode is expected to be about 3 % less than the pump mode maximum efficiency [23]. By using this and the results obtained from Equation 4.20, the maximum and minimum power output of the selected PAT can be calculated from

$$\begin{aligned} P_{ts\_max} &= (\eta_{ts}) \rho_w g h_{ts\_max} Q_{ts\_max} \\ P_{ts\_min} &= (\eta_{ts}) \rho_w g h_{ts\_min} Q_{ts\_min} \end{aligned} \quad (4.21)$$

where  $P_{ts\_max}$  is the maximum output power and  $P_{ts\_min}$  is the minimum output power,  $\eta_{ts}$  is the turbine mode efficiency of the selected pump,  $h_{ts\_max}$  and  $h_{ts\_min}$  are the maximum and minimum calculated heads respectively and  $Q_{ts\_max}$  and  $Q_{ts\_min}$  are the maximum and minimum calculated flow rates from Equation 4.20 respectively. Provision is also made for performance of the selected PAT away from its BEP, i.e. at part flow conditions. Part flow conditions are taken as 80, 90, 110 and 120 % of the actual BEP turbine mode flow rate of the selected pump. Diagrams, giving PAT head and power output correction values for these altered flow conditions, have also been developed from various test results by the German Mini Hydro Power Group and these are presented in Figure C.4 and C.5. Maximum and minimum part flow values are obtained by multiplying the maximum and minimum flow rates obtained from Equation 4.20 with each of the above mentioned part flow conditions. Maximum and minimum values of the head and power output of the PAT at part flow conditions are obtained by multiplying the correction factors read from Figures C.4 and C.5, with the head and power output results obtained from Equations 4.20 and 4.21. With all of these known, maximum and minimum predicted performance curves of the PAT can be plotted. An example of this is shown in Figure 24. The possible operating range of the PAT then lies between the points where these maximum and minimum predicted performance curves intersect with the system curve.

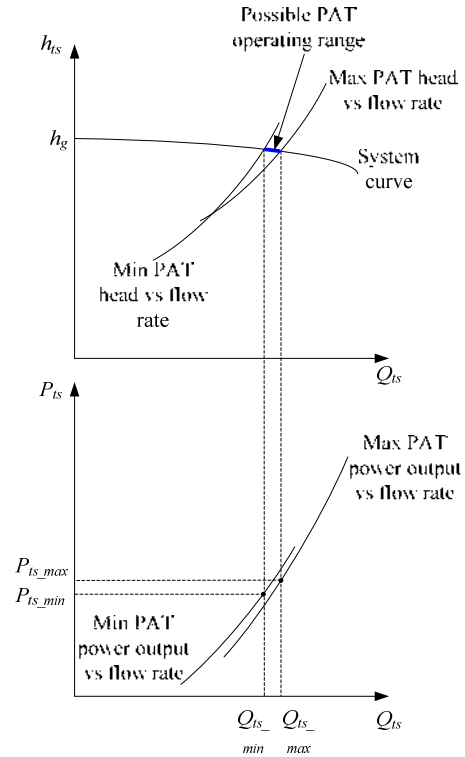


Figure 24: Possible operating range of a PAT [23].

**Runaway conditions**

When a PAT is in operation and the load on the generator is suddenly rejected, the power output of the PAT will become zero. In this case, the speed of the turbine increases, whereby the PAT starts to act as a valve, hence the flow rate through the PAT reduces and the head at the PAT increases. The operating point of the PAT then moves along the system curve to a point where a certain fixed head has been reached. This new operating point is known as the point of runaway. Runaway conditions for each pump differ as they are functions of the pump mode specific speed of the pump. This phenomenon is very dangerous since the sudden change in flow rate will initiate water hammer in the penstock and it is also possible that the runaway speed of the PAT will be beyond safe limits [23]. Hence it is crucial to calculate the runaway conditions and to verify with the manufacturers of the generating machines that these conditions are within acceptable limits. If not, certain measures must be taken to bring the PAT to safe operating conditions once runaway has occurred.

In order to determine the runaway conditions of a PAT, a no-load line needs to be developed. The intersection of this line with the system curve gives the steady state runaway head and flow rate of a specific PAT. To determine this line, four to five head values near the

expected runaway point must be assumed. The runaway flow rate for each of these head values needs to be calculated from

$$Q_{tsr} = \kappa Q_{ps} \left[ \sqrt{\frac{h_{tsr}}{h_{ps}}} \right] \quad (4.22)$$

where  $Q_{tsr}$  is the runaway flow rate of the PAT and  $\kappa$  is a flow correction factor that is read from the diagram attached in Figure C.6. The symbol,  $h_{tsr}$ , represents the assumed runaway heads, which is usually about 100, 120, 160, 200 and 250 % of the BEP pump mode head of the selected pump [23]. Once the runaway head and flow rate are known, the steady state runaway speed of the PAT is calculated from:

$$n_{tsr} = \varepsilon n_{ps} \left[ \sqrt{\frac{h_{tsr}}{h_{ps}}} \right] \quad (4.23)$$

where  $n_{tsr}$  is the steady state runaway flow rate of the PAT and  $\varepsilon$  is a speed correction factor that is read from the diagram attached in Figure C.7.

Standard methods to deal with runaway problems do exist. Mechanical braking of the PAT is a first option to restore the operating speed of the PAT to safe limits, but this method does not solve the water hammer problems that are induced in the pipeline after runaway has occurred. The other method is to have a bypass line with one end connected to the manifold pipeline and the other end open to the atmosphere. A valve that is installed in this line is then preferably opened automatically due to higher pressures sensed and the pressure transients in the pipeline are reduced. With the bypass valve open the pressure upstream of the PAT may be slightly lower. The result is that the rotational speed is also slightly lower, but this may still not be within acceptable limits.

### ***Selected PAT for the MHPS at Waterval***

For the MHPS at Waterval, pumps from KSB pumps are considered for use as a turbine. All the analytical results of calculations to select a PAT are summarised in Table C.1. The available head and flow for power generation is 72.02 m and 20 l/s respectively. The radial flow pumps are rated for pump mode operational speeds of either 1 450 rpm or 2 900 rpm. The difference is the heads that can be accommodated. From performance diagrams, it is deduced that the heads accommodated by the pumps having a rated speed of 1 450 rpm, are too low for

this application, hence a pump with a rated pump mode speed of 2 900 rpm is selected. An induction generator is used for this MHPS and as the PAT and generator are coupled directly, the PAT will have to operate slightly beyond 3 000 rpm. For an induction generator to operate at its rated specifications, it needs to be driven about 3 % beyond its synchronous speed [25]. A shaft speed of 3 080 rpm is chosen. For these turbine mode conditions, a pump mode head and flow rate of 37.15 m and 12.7 l/s respectively are calculated. This operating point lies within the range of the ETA 50-200 model pump. The performance diagram of this pump can be seen in Figure C.8. The problem with this pump is that the required operating point is below the BEP of the pump; hence the pump will not operate near its BEP in turbine mode. The second problem is that the impeller of the pump will have to be trimmed and the effect of this on turbine mode performance is not known. Hence a smaller pump, the ETA 50-160 model, is considered and its performance diagram is presented in Figure C.9. The required operating point together with the BEP values of this pump, is summarised in Table 4.

The BEP flow rate of this pump is still more than the required flow rate; hence this pump will not operate slightly beyond its BEP in turbine mode. The turbine and generator are coupled directly, hence it is not an option to alter the speed as it is preferred that the generator is driven at a maximum speed of 3 090 rpm, as is mentioned above. The only option is to adjust the design turbine mode head and flow rate, so that they are slightly more than the BEP turbine mode operating conditions of this pump. After reconsidering the flow rates in the river, it was decided to adjust the turbine mode flow rate to 24 l/s. By adjusting the pressure sustaining valve that is incorporated into the manifold line, the head losses in the pipeline can be increased to obtain an available head of 55.35 m at a flow rate of 24 l/s as shown in Table 4. When considering the efficiencies at the different operating points in Figure C.9, it was calculated that the power output of this adjusted operating point remains almost the same as for the original operating point. The predicted PAT performance curves of the selected pump are shown in Figures 25 and 26.

**Table 4: Turbine and pump mode operating conditions considered at Waterval.**

	Original operating point		Adjusted operating point		Considered pump	
	Turbine mode	Pump mode	Turbine mode	Pump mode	Turbine mode BEP	Pump mode BEP
<b>Head (m)</b>	72.02	37.15	55.35	33.4	52.32	32.6
<b>Flow rate (l/s)</b>	20	12.4	24	17	23.45	16.67
<b>Speed (rpm)</b>	3 080	2 900	3080	2900	3080	2 900

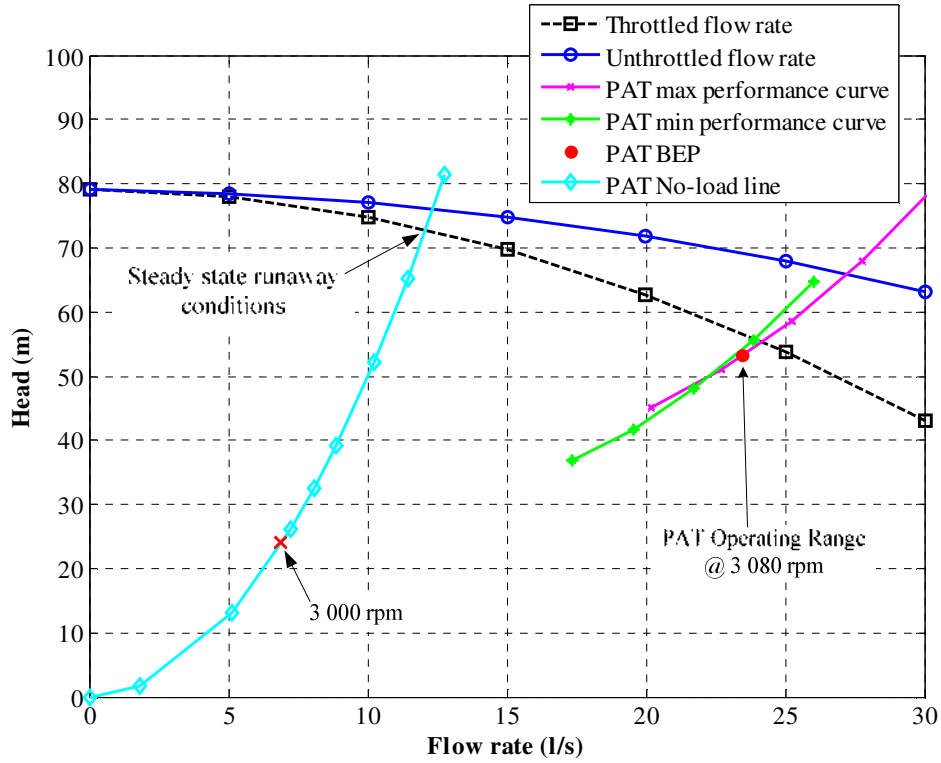


Figure 25: Predicted performance of the selected PAT.

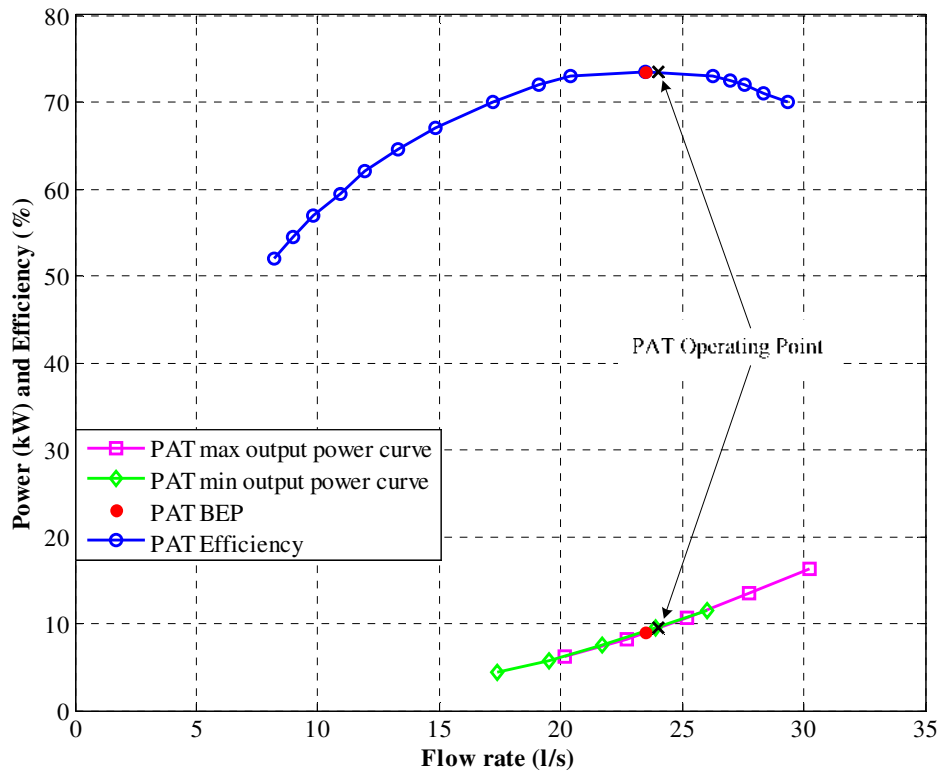


Figure 26: Predicted power output and efficiency of the selected PAT.

These graphs show that if the PAT is operated at a head of 55.35 m and a flow rate of 24 l/s, it will operate beyond its BEP and will yield a power output of about 9.5 kW with an efficiency of about 73 %. The no-load line of the PAT is predicted as described earlier and is also displayed in Figure 25. These predictions show that the lowest flow rate that can be used before the speed of the PAT reaches 3 000 rpm, which is the speed at which the generator stops delivering power, is 6.85 l/s. However, it is not recommended to operate the PAT at this point as the pressure drop over the valves upstream of the PAT will be very high. Hence the possibility exists that cavitation at these valves will occur.

The steady state runaway conditions of the PAT are also shown in Figure 25. The runaway head and flow rate of the PAT are 72.5 m and 12 l/s, respectively. The speed correction factor,  $\varepsilon$ , for the PAT is read from Figure C.7 as 1.205. By using Equation 4.23 it is calculated that the runaway speed of the PAT is 5 211 rpm. The pumps manufactured by KSB pumps are not designed to operate at this speed for long periods. To reduce this speed, a bypass line is incorporated into the manifold line, which is discussed in more detail in Chapter 4.5.

#### 4.4.3 Cavitation

As the water flows through the impeller of a PAT, the velocity of the water increases and as it leaves the eye of the impeller to exit the PAT it enters into a low pressure region. If the pressure of the water in this region falls below the vapour pressure of water, some of the water vaporises, thereby causing bubbles to form within the flowing water. As these bubbles move with the water to regions where the pressure is again higher than the vapour pressure, they collapse. This phenomenon is known as cavitation and it induces noise, flow instability, vibration and also results in serious surface damage [20 - 24]. To prevent cavitation in a PAT, a certain backpressure known as the Net Positive Suction Head (NPSH) is required at the PAT outlet. Two criteria exist, that must be compared to each other when analysing the cavitation performance in a PAT, and these are:

- The requirement criterion ( $NPSH_R$ ) is a function of the impeller geometry and depends on the specific speed of the PAT.
- The availability criterion ( $NPSH_A$ ) depends on the MHPS conditions, i.e. draft tube design, height of the PAT above the tailrace level etc.

To avoid the danger of cavitation in a PAT, the  $NPSH_R$  must always be smaller than the  $NPSH_A$ . The  $NPSH_R$  for a certain PAT is calculated from

$$NPSH_R = \sigma_T (h_t) \tag{4.22}$$

where  $\sigma_T$  is the dimensionless Thoma number that is read from Figure C.10. The hydraulics downstream of the PAT are presented in Figure 27, and with reference to this figure, the  $NPSH_A$  is calculated from

$$NPSH_A = \frac{p_{atm}}{\rho_w g} + h_{dt} - \left[ \frac{v_{te}^2}{2g} + \frac{p_v}{\rho_w g} + h_s \right] \tag{4.23}$$

where  $p_{atm}$  is the atmospheric air pressure,  $h_{dt}$  is the friction and minor losses in the draft tube,  $v_{te}$  is the velocity of the water at the PAT outlet,  $p_v$  is the vapour pressure of water and  $h_s$  is the height of the highest point of the blades of the impeller above the tailrace water level. Note that the atmospheric pressure changes with the height of the MHPS above sea level and that the vapour pressure of water changes with temperature. These relations is shown in Figure C.11 and given in Table C.2.

A tailrace dam is built next to the powerhouse at Waterval, to provide a fixed tailrace water level at almost the same height of the PAT, hence increasing the  $NHPS_A$ . The water flows from the draft tube into this dam, before it flows back freely to the river.

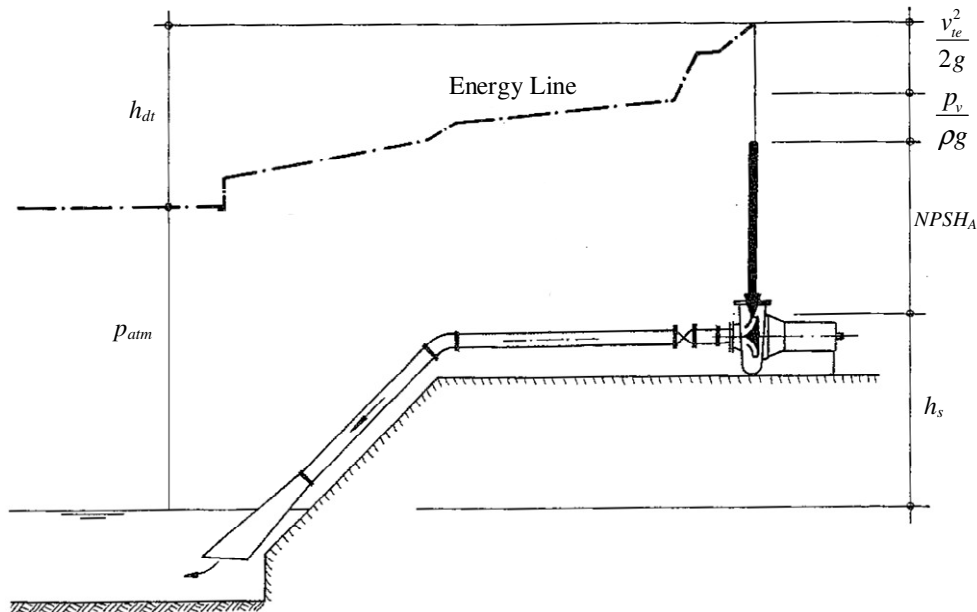


Figure 27: Hydraulics at the outlet side of a PAT [23].

The Thoma number for the PAT at Waterval is found to be 0.12. Using Equation 4.22, the  $NPSH_R$  to avoid cavitation of the PAT is calculated to be 6.642 m, for a flow rate of 24 l/s. The  $NPSH_A$  for the MHPS at Waterval is calculated by considering the following:

- Atmospheric pressure is 0.98 bar for a site that is 250 m above sea level.
- Vapour pressure of water is 2.34 kPa at a temperature of 20 °C.
- By using Equations 4.5 – 4.9, the draft tube losses are calculated as 0.292 m for a flow of 24 l/s.
- The impeller of the PAT has a diameter of 0.169 m, and the centre of the impeller is located 0.135 m above the tailrace water level.

From Equation 4.23, the  $NPSH_A$  is calculated as 7.17 m, which is more than the  $NPSH_R$ . Hence if the PAT maintains operating at a head of 55.35 m and a flow rate of 24 l/s, cavitation at the PAT will not occur.

Cavitation can also occur at the valves installed in the manifold line, when the pressure drop across them becomes too big. The control valves used are usually sized by their suppliers, such that cavitation does not occur near its operating point. The pressure sustaining valve for Waterval is sized such that cavitation only initiates when the pressure drop across the valve increases beyond about 3.5 to 4 bar. Hence this limits the extent over which the valve can be throttled for PAT operating points.

## 4.5 Hydraulic Control System

The hydraulic control of a MHPS entails flow control in the powerhouse and the protection of the pipeline against water hammer (section 4.3.2). The usage of a PAT in a MHPS requires hydraulic valves in the manifold line for flow regulation, since PATs do not have built-in hydraulic control devices such as guide vanes or needle valves. It is common practice to install a manually operated isolation valve at the bottom of the pipeline, upstream of the PAT, in order to allow or disallow flow through the MHPS. This valve can also be used to control the flow through the PAT manually. As explained in section 4.4.2, sudden load rejection on the generator will increase the rotational speed of the PAT and water hammer will be induced in the pipeline. In order to protect the PAT against these conditions and the pipeline against water hammer, it is

preferable to use automated valves rather than the isolation valve for controlling the flow through the MHPS.

Referring to Figure 17, the manifold line of the MHPS at Waterval divides into a bypass line and a line that supplies the PAT with water. An isolation valve that is used solely for the on or off mode of the MHPS is installed at the front of the manifold line. When this valve is closed, it isolates the rest of the manifold line, the bypass line, the PAT and the draft tube from the main pipeline. To control the flow through the PAT, a pressure sustaining valve is used. This valve maintains a certain preset downstream pressure on the PAT and as the flow rate is related to the pressure, constant flow rate is ensured. Since the head loss over this valve increases as it closes and decreases as it opens, the valve is also used to throttle the flow rate through the PAT to the required operating point, thereby ensuring PAT operation near its BEP. When runaway has occurred, this valve senses the increase in downstream pressure at the PAT and adjusts itself to maintain the preset pressure on the PAT. As this valve throttles, the system curve changes as shown in Figure 28, and the runaway point shifts down the no-load line until the preset downstream pressure has been reached.

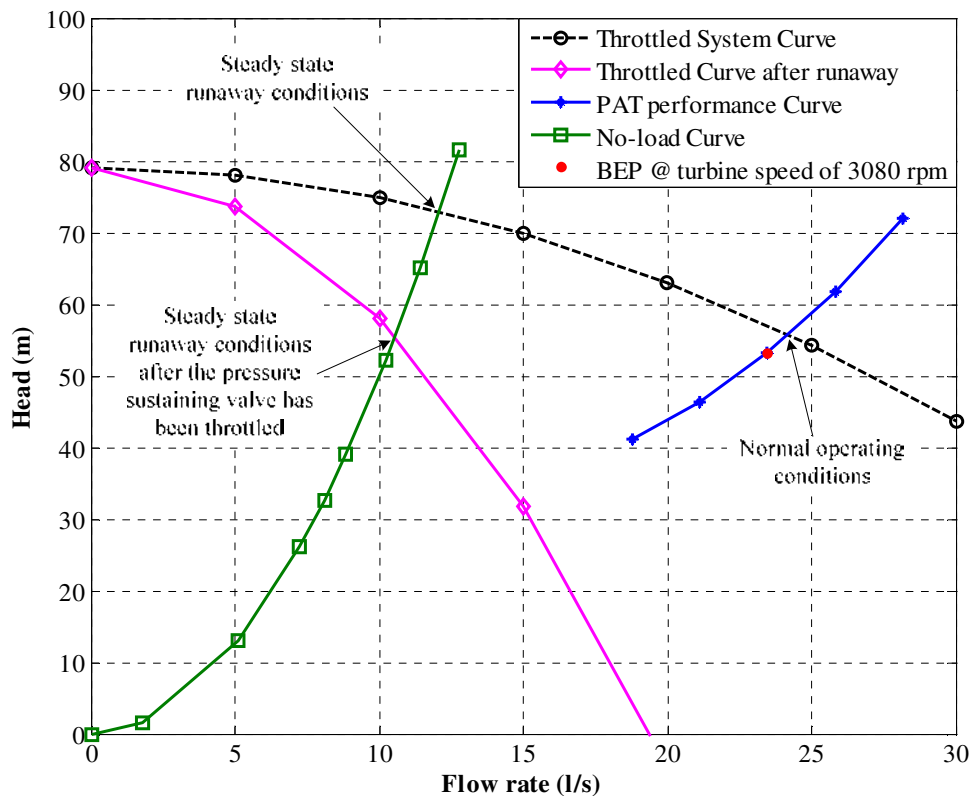


Figure 28: Final runaway conditions after the pressure sustaining valve has throttled to the preset pressure.

The runaway head and flow rate at this throttled point is 55.35 m and 10.5 l/s, respectively. From Equation 4.23 the runaway speed of the PAT and the generator at this point is calculated as 4 553 rpm, which is acceptable. A solution to reduce the speed even more is to have a second solenoid activated downstream pressure setting on the pressure sustaining valve so that when the load on the generator is rejected, the solenoid activates the pressure sustaining valve to throttle to a much lower pressure. This is not currently implemented at Waterval.

The bypass line that branches from the manifold line, features a pressure relief valve, which is usually closed and only opens when certain preset pressures are exceeded, hence serving as a protection for the pipeline against water hammer. Two orifice plates are installed downstream of the pressure relief valve to overcome the problem of cavitation on the pressure relief valve. These orifice plates are sized so that the pressure drop across each of them does not exceed 2.5 bar. This is done to limit cavitation at each of the orifice plates.

When starting the MHPS, the isolation valve is simply opened until the PAT has reached synchronous speed. The induction machine is then started and now operates as a motor at no load. As the isolation valve is opened further, the speed of the PAT and the induction machine increases beyond 3 000 rpm and the induction machine starts delivering active power. The isolation valve is then opened fully, with the pressure sustaining valve ensuring that the required head and flow rate is delivered to the turbine. When stopping the PAT, the isolation valve is closed, but it is operated according to the specified limits described in section 4.3.2.

#### **4.6 Drive System between the PAT and the Generator**

This system connects the shafts of the turbine and the generator and it transmits the shaft power developed by the turbine to the shaft of the generator. Several drive systems exist, each of them having its own advantages and disadvantages. The type of drive system that is to be used usually depends on the speed ratio of the turbine and generator shafts. The output speed of the drive system should match a synchronous speed of 900, 1 500 or 3 000 rpm if a synchronous generator is used. If an induction generator is used, then the output speed of the drive system must be about 3 % greater than these synchronous speeds in order for the machine to operate according to its rated specifications [27]. Each of these drive system options is discussed in this section.

### ***Direct coupling***

The two shafts are coupled directly. This option is only applicable to systems where the speeds of the turbine and generator shafts are the same. This type of shaft connection has a very high efficiency and it involves little maintenance and little or no additional radial load on the shaft and the bearings of both the turbine and the generator. Although modern direct couplings allow for some angular and positional displacement of the two shafts, it must be attempted to align the two shafts as closely as possible, in order to eliminate unnecessary strain on the couplings and to reduce noise that can be induced by these couplings.

### ***Belt and pulley coupling***

Three types of belts are available that can be used. These are flat belts, V-belts and timing belts. All three of these belt types have the disadvantage that they need maintenance. They can be used in systems where the shafts of the turbine and the generator rotate at the same speeds or at different speeds.

Firstly V-belts are the most common of the three. They can take up some angular misalignment and can be used on systems with high speed ratios. V belts put some extra loading on the shaft and bearings of the machines and their efficiency is in the order of 85 – 95 %. Depending on the size of the installation, multiple belts may be necessary.

Flat belts have higher efficiencies than V-belts and can also be used on systems where high speed ratios are required. Since the tension in these belts needs to be very high, it induces big radial loads on the shafts as well as on the bearings of the machines. These belts can take up very little angular misalignment.

Lastly the timing belt is a flat belt with teeth on its surface and it runs on a toothed pulley. It does not slip and of the three types of belts, it has the highest efficiency. The tension in the belt is also the lowest of the three types hence the extra radial forces on the bearings and shafts of the machines are reduced. This belt can accommodate very large speed ratios [13].

### ***Gearbox***

Gearboxes allow for very big speed ratios, but are preferably only used in large systems where the power and torque exceed the maximum of belt drives. A gearbox must always be

considered as the last alternative due to its cost and the maintenance it requires. A gearbox also requires that all the shafts are aligned properly.

### ***Chain and Sprocket***

Chains running on sprockets have very high efficiencies and very large speed ratios can be accommodated. They also allow for little angular misalignment between the shafts of the turbine and generator, but require maintenance. If they are not lubricated correctly, their lifetime decrease significantly.

To keep the cost and the maintenance of the MHPS at Waterval to a minimum, a direct drive system between the PAT and the generator is used. Toothed couplings are located on both ends of the shafts. They push and lock into one another with a rubber block that is located between the respective contact surfaces. This rubber block allows for a small level of angular misalignment between the two shafts.

## 5. Electrical Design

In this chapter all the electrical aspects of a grid-connected MHPS are dealt with. Firstly the generator that is connected to the PAT at Waterval is discussed thoroughly. A section on the transmission of the generated electrical energy is then presented where after the interconnection of a MHPS with the load and the grid is discussed.

### 5.1 Generator

The generator is the machine that converts the rotational energy produced by the turbine, into electrical energy. As mentioned in section 1.2, two main types of AC generators exist: (i) synchronous generators and (ii) asynchronous generators. As the cost of a synchronous motor with the accompanying switchgear for synchronizing to the grid is often not economically justified for use in small power generation systems, these were not considered as an option for the MHPS at Waterval and are not discussed in this study.

Two types of induction generators exist that can be used for power generation. The stators of these machines are the same, each having a conventional three phase winding that is connected to the load or grid. The difference between the machines is the type of rotor winding that is used. Firstly the doubly-fed induction generator (DFIG) has a rotor that consists of a three phase winding that is connected to slip rings on the rotor [27]. The terminals of the slip rings are connected through a modern inverter system to a three phase supply. The purpose of the inverter is to control the frequency of the rotor current. Hence the speed of the generator can be controlled. This generator is often used in special embedded generating systems where speed control is necessary, for example in wind generation systems. An accompanying inverter for this generator increases the cost substantially; hence if speed control of the generator is not required then this is not an option for a low cost MHPS.

The other type of rotor winding used is known as the squirrel-cage rotor. These rotors consist of solid bars of a conducting material that are embedded in slots. All these conducting bars are short-circuited at their opposite ends [27]. These machines are more often found in a variety of small power generation plants, mainly due to the fact that they are the cheapest and most robust of all the generator types. Another advantage of the squirrel-cage induction generator is that it has no rotor windings and slip rings, hence maintenance and total life cycle

cost is reduced. Unlike synchronous generators, they do operate at lower efficiencies and power factors. However, they have the advantage that no expensive synchronising equipment is required, since the output voltage and frequency of the induction generator is determined by the power system to which it is connected [7].

The induction generator has a need for reactive power to develop the necessary magnetic field in the machine. Hence it is well suited for grid-connected applications where the grid supplies the necessary reactive power. The disadvantage is that induction generators operate at lower power factors, and that the reactive power supplied by the grid causes more losses in the grid. If required by the distributor that power factor correction of the generator must be done, the usual practise is to connect power factor correction capacitors to the terminals of the machine. If a sufficient amount of capacitors, that supply all the required reactive power are installed, the danger exists that the generator will continue generating power upon de-energising of the grid [28]. This is known as self-excitation and should be avoided at all times. This is further discussed in Chapter 5.3.2.

Self-excitation of an induction generator can also occur if the load to which the generator is connected consists of enough capacitance to provide the necessary reactive power. Prior to connecting the induction generator to the grid, the load capacitance should be known. It should be ensured that this is less than that required by the generator to become self-excited. If not, then suitable switchgear should be installed to prevent self-excitation of the generator.

The capacitance required for an induction generator to become self-excited is calculated according to the method described in [27]:

$$S = \sqrt{3}V_L I \quad (5.1)$$

where  $S$  is the apparent power,  $V_L$  is the rated line voltage of the induction generator and  $I$  is the rated current of the induction generator. The rated current and voltage of the machine is obtained from the manufacturer's catalogue. The minimum total reactive power required is calculated from

$$Q = \sqrt{S^2 - P_{IM}^2} \quad (5.2)$$

where  $Q$  is the reactive power.  $P_{IM}$  is the rated active power of the induction machine and is calculated from

$$P_{IM} = S \cos \theta \quad (5.3)$$

where  $\cos\theta$  is the power factor of the machine that is obtained from the manufacturer's catalogue. The capacitive reactance required per phase is calculated from

$$X_c = \frac{V_L^2}{3Q} \quad (5.4)$$

The minimum required capacitance is calculated from

$$C = \frac{1}{2\pi f X_c} \quad (5.5)$$

where  $C$  is the required capacitance and  $f$  is the frequency at which the induction machine operates.

The size of the induction generator necessary for a specific MHPS installation is determined by the output power of the turbine. The required number of poles of the generator is determined by the output speed of the drive system that connects the shafts of the generator and the PAT. The number of poles is determined from

$$p_{IG} = \frac{120f}{n_s} \quad (5.6)$$

where  $p_{IG}$  is the number of poles and  $n_s$  is the synchronous speed of the rotating magnetic field in the induction machine.

The efficiency of a commercially available induction motor is only supplied for the machine operating as a motor. When calculating exact MHPS efficiency and power output, it is assumed that the efficiency of a commercially available induction motor remains the same for generator mode.

The reason for selecting a squirrel-cage induction generator for the MHPS at Waterval is the numerous advantages that it has with respect to other generator types, as discussed above. The output shaft power of the PAT selected for the MHPS at Waterval, is about 9.5 kW. The shafts of the turbine and generator at Waterval are directly connected. Hence the shaft speed of the generator is 3 080 rpm, with the synchronous speed of the rotating magnetic field in the induction motor being 3 000 rpm. By connecting the generator to a grid with a frequency of 50 Hz, it is calculated from Equation 5.6 that the induction generator must have two poles.

Commercially available induction motors with a rated mechanical power output of 7.5 and 9.2 kW exist. The rated full load efficiencies of these two motors are 87 and 86.3 %

respectively. Hence the rated full load power input of these two motors is 8.62 and 10.7 kW respectively. From this it is concluded that the induction motor with a rated power output of 7.5 kW is too small for the MHPS at Waterval. Hence the induction motor with a rated power output of 9.2 kW is selected. The selected induction motor has a rated full load speed of 2 870 rpm. At full load, it draws a rated current of 16.88 A from a 400 V AC source. The motor also has a full load power factor of 0.89. From these induction motor ratings, it is calculated that if the PAT operates slightly beyond its BEP at a flow rate of 24 l/s, the electrical power output at the terminals of the induction generator is about 8.1 kW. Measured generator mode results of this induction machine are presented in Chapter 6.3.

To investigate the probability of whether or not this generator will become self-excited without connecting capacitors to its terminals, it is calculated from Equations 5.1 to 5.5 that this generator requires a capacitance of at least 318.3  $\mu\text{F}$  per phase, to become self-excited. This aspect is further discussed in Chapter 5.3.3.

## 5.2 Transmission Cable

The transmission cable is an insulated group of conductors that transfers the generated power from the powerhouse of the MHPS to the point of interconnection with the load and accordingly with the grid. For Waterval, an underground power cable is used as it is safer for the environment than overhead lines.

Underground power cable design for MHP systems mainly entails the selection of the right conductor size. This is dependent on the voltage drop between the two ends of a cable. This voltage drop needs to remain within certain limits. According to the South African National Standard's Wiring Code (SANS 10142-1:2003) [34] the voltage drop over the length of the cable should not exceed five percent of the standard voltage, for example 20 V for a 400 V three phase circuit. Values of the voltage drop for different copper conductor sizes are given in Table D.1. The voltage drop over a certain length of power cable is calculated from

$$V_d = C_v l_{cable} I \quad (5.7)$$

where  $C_v$  is the voltage drop of the specific conductor size found from Table D.1,  $l_{cable}$  is the length of the cable and  $I$  is the rated current that will flow through the cable.

The powerhouse of the MHPS at Waterval is located 210 m away from the distribution board where it is connected to the PCC. By using Equation 5.7, for a rated current of 16.9 A

generated by the induction generator, the voltage drop when using a 10 mm<sup>2</sup>, four core, armoured and insulated PVC cable, is calculated to be 15.6 V. This is below the maximum limit of 20 V.

### **5.3 Interconnection with the Grid and Switchgear**

When connecting any generator to a load and/or a grid, the primary concerns are human safety, power system safety and quality of the power that is generated. To ensure this, a standard or code that stipulates all the necessary requirements for interconnecting a generator to the distribution network of the local supplier exists. Eskom does have such a standard for the interconnection of generators to the grid, but this is not applicable to systems having a generating capacity of 100 kW and less (micro power generation systems) [29]. The reason for this might be that the size of a micro power generation system is so low that it is unlikely that it will cause any substantial instability to the grid. However, once the number of these micro power generation systems exceeds a certain limit, a special standard for these systems will have to be developed to address any possible instability that may occur, for example, extensive reactive power consumption of induction generators that causes extra losses in the distribution grid.

To get an idea of the necessary requirements and safety measures that need to be in place when interconnecting a micro power generation system to the grid, grid codes and interconnection guidelines that are used elsewhere, were consulted [30 – 33]. From these guidelines, general and specific technical and operating requirements for small induction generators that are connected to the distribution network were obtained. These requirements are discussed hereafter.

#### **5.3.1 General Interconnection Requirements**

Any party that wishes to connect and synchronise a generator to the distribution network, must prior to the interconnection, have approval from the distributor or the legal entity that is responsible for approving generator interconnections to the grid. This is required by the Electricity Regulation Act 6 of 2006. The full technical application of the proposed interconnection power generation system is reviewed by the distributor prior to reaching an interconnection agreement with the owner of the private power generating system. The technical data need to be reviewed by the distributor to ensure that certain power quality measures are met

in order to ensure that the generator does not cause any instability to the grid. This agreement also ensures safe operation of the system over its designed lifetime, if it is properly maintained, since all the switchgear and protection equipment need to comply with certain standards and regulations.

It is the responsibility of the owner of the power generating system to ensure that all his equipment is maintained properly. Good maintenance ensures good protection of the system and also protects the operators of the systems against any fault conditions.

If the generating system is not intended for own use only, but also for commercial use such as to sell electricity to or through the distribution network, extra metering instruments need to be installed at the PCC. This metering equipment is supplied by the distributor and is also operated and maintained by the distributor. The intention of selling electricity results in an additional power purchase agreement (PPA) that must be settled between the owner of the generating system and the distributor. Eskom is not currently purchasing power from hydro power systems smaller than one megawatt, but they are busy researching methods to compensate owners that deliver energy to the grid.

### **5.3.2 Operating Requirements**

Once the generator is connected to the grid, the owner must at all times comply with the terms and conditions of the interconnection agreement and the net metering agreement or PPA, if applicable. All the equipment must be maintained according to best practice at all times and whenever required by the distributor, the system must cease operation.

#### ***Synchronization***

Grid-connected induction generators, without capacitor banks, cannot generate power prior to their connection with the grid. As the grid supplies the necessary excitation current, the voltage and frequency of the induction generator are determined by the grid and therefore no synchronizing equipment is required for these generators. Accordingly, no voltage, power factor or frequency control is required for these generators.

### ***Islanding***

Islanding happens when a grid-connected self-excited induction generator continues to keep the grid energised whenever the grid is intentionally or unintentionally de-energised by the distributor. This is not allowed to happen in any circumstance. The general requirement is that any grid-connected generator should cease operation within two seconds after the grid has intentionally or unintentionally been islanded. The advantage of induction generators that is excited by the grid is that they will automatically cease operation upon de-energising of the grid, providing that the load does not have enough capacitance to supply reactive power to the generator.

The interconnection agreement determines whether reactive power for induction generators is supplied by the grid or whether the owner is responsible for installing capacitor banks to provide the required reactive power. Some distributors allow that all the necessary reactive power is drawn from the grid in order to reduce the possibility of islanded operation. Other distributors only supply reactive power for systems up to a certain capacity, while others require that the owner should supply all the necessary reactive power in order to correct the power factor of the generator to be as close to unity as possible. Whenever capacitors are installed at or near an induction generator for power factor correction, extra costs are necessary for hardware and software to avoid islanded operation of self-excited induction generators. Depending on the size of the system, this may not be economically justified.

### **5.3.3 Switchgear Requirements**

The switchgear required for a generator that is connected to the grid, differ for grid excited induction generators, self-excited induction generators and synchronous generators. The switchgear required for a grid excited induction generator is much simpler than and not as costly as the other types of generators, since no synchronizing equipment is necessary. No short circuit electrical protection for the generator is required since it provides its own protection against short circuits as the output power drops to zero when excitation is lost. Usually no anti-islanding equipment is necessary. To confirm this, it must be verified that the load to which the generator is connected does not consist of enough capacitance to supply the necessary reactive power to the generator in the event of grid de-energising.

As the flow through the PAT of the MHPS at Waterval is not shut-off when the grid is de-energised, the generator keeps on turning and if sufficient reactive power is available, it can become self-excited. Hence it is possible that an island can form. To determine whether the load of Waterval consists of enough capacitance to let the induction generator become self-excited, the reactive power profile of the load in the event of grid de-energising was investigated. The reactive power consumption of Waterval for the month of April 2008 is presented in Figure 29. The seven spikes in reactive power consumption of the load represent the times when the irrigation pumps are powered. Also shown in the graph is the voltage profile of the power consumed, since the voltage is used to see if the grid is energised or not. If any form of charged capacitance exists in the load at the time of grid de-energising, then reactive power would have been exported to the grid, if not consumed in some of the equipment in the load itself.

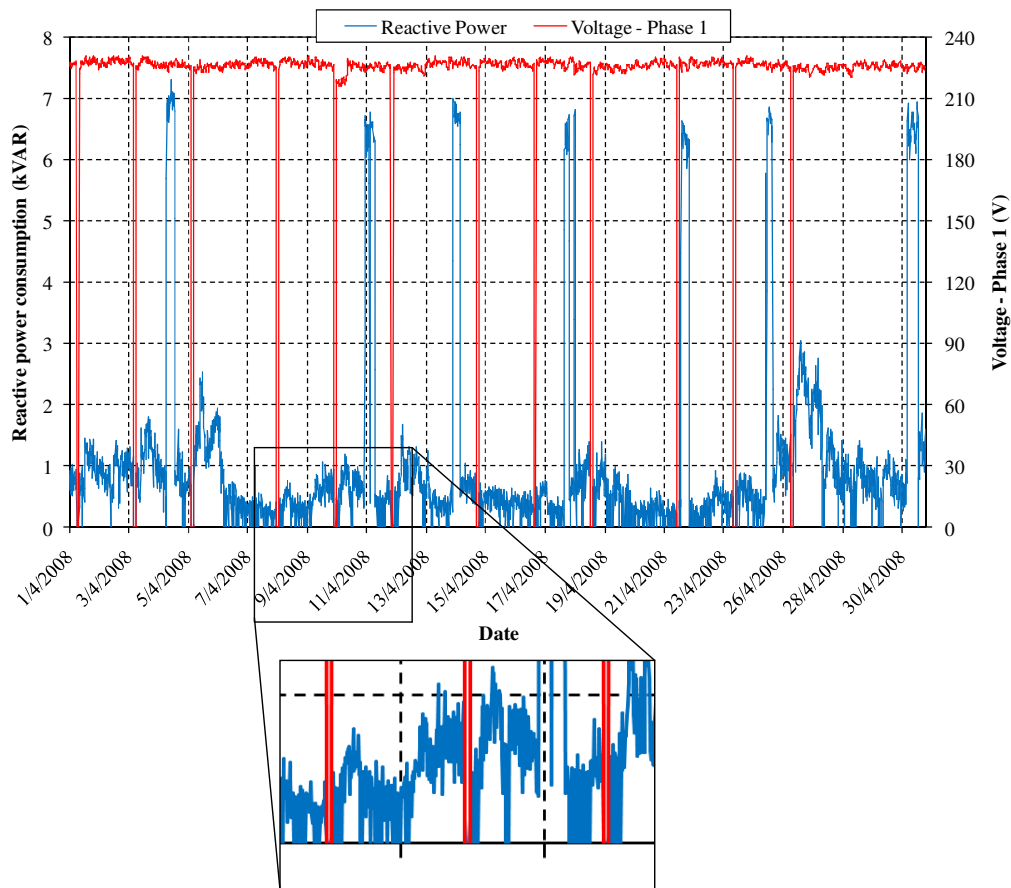


Figure 29: Reactive power consumption and voltage of the load.

The capacitance of this exported reactive power is then calculated and matched to the required capacitance of the induction generator to see whether it would be sufficient for the generator to become self-excited. From the reactive power profile of Waterval, it is clear that no reactive power is exported to the grid when the grid is de-energised. Hence no capacitance exists in the load that would be sufficient to supply the generator with the necessary reactive power to become self-excited. It is thus concluded that no anti-islanding electrical protection is necessary for the MHPS at Waterval.

A single line diagram of the electrical connection of the grid with the load and the MHPS at Waterval is presented in Figure 30. The complete electrical wiring diagrams of the MHPS and the PCC are attached in Appendix D.2. A discussion on the switchgear used for connecting this MHPS to the load and grid is presented hereafter. Switchgear requirements for other sizes and types of generators can be found in [30 - 33].

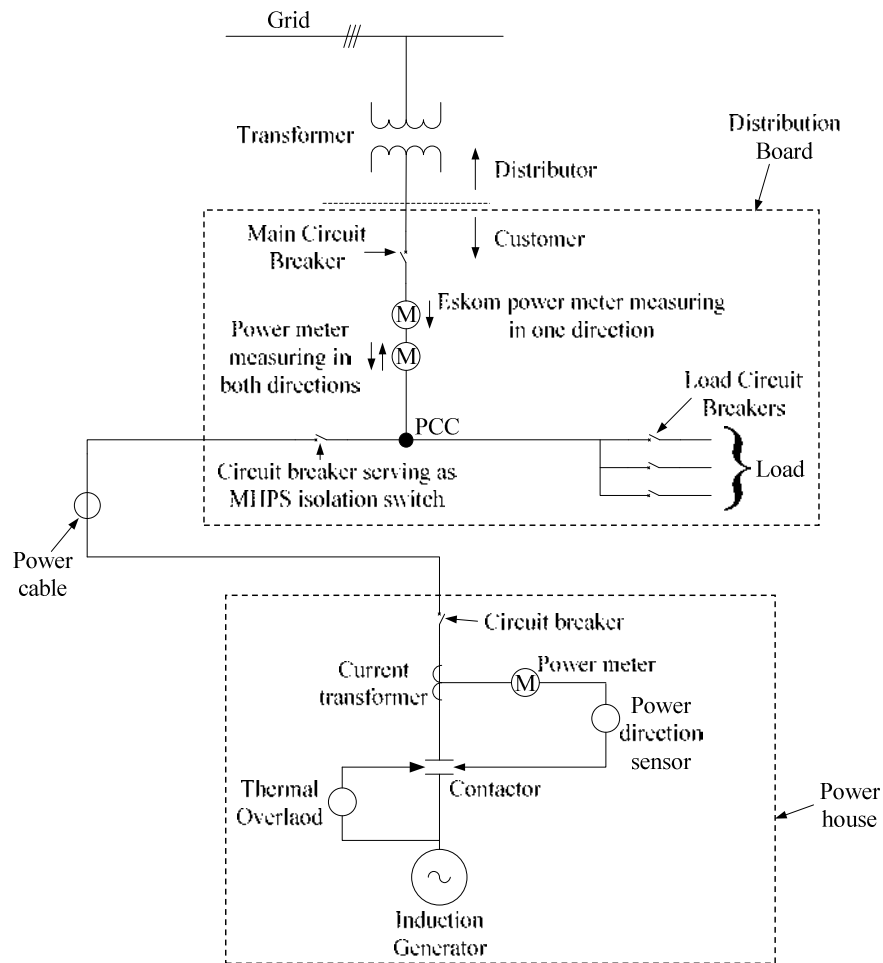


Figure 30: Single line diagram of the induction generator that is connected to the grid at Waterval.

### ***Main Disconnection Point***

The powerhouse where the generator is located and the PCC are not necessarily located next to or close to each other. An isolation switch must be incorporated between the generator output terminals and the PCC in order to isolate the grid and load from the MHPS. This switch should be located at the PCC in order to be accessed easily by any party having the right to access the switch. For a three phase generator, it must be provided that this switch simultaneously isolates all three phases.

Due to very limited space in the existing distribution board at Waterval, a circuit breaker is used as an isolation switch. This circuit breaker has a maximum current rating of 25 A, and also protects the power cable between the powerhouse and the PCC against overcurrent conditions.

### ***Overcurrent Protection***

Circuit breakers are commonly used as protection devices against fault overcurrent conditions. It is advisable to have the generator connected to the grid via two circuit breakers, since if there is only one, the failure of the breaker could result in unsafe operation of the MHPS. The circuit breaker in the powerhouse is also used as a disconnection switch, for isolating the generator and the rest of the MHPS electrical equipment from the grid and the load. This circuit breaker has a current rating of 20 A and serves as the primary overcurrent protection breaker, while the one at the PCC also serves as backup protection for the generator. Both these breakers are rated for a line to neutral phase voltage of 230 V and also serve as protection against over voltage conditions.

### ***Under Voltage Protection***

A three phase contactor is incorporated into the electrical circuit of the MHPS at the powerhouse at Waterval with its coils energised by the grid. Upon de-energising of the grid, the contactor automatically isolates the generator from the grid and load, since the grid voltage becomes zero. The contactor is wired in such a way that when the grid is re-energised it does not engage automatically. Hence the generator has to be started again manually. The contactor will also isolate the generator from the grid upon sensing a voltage dip that is lower than the minimum voltage on which the contactor opens. The contactor also features a thermal overload

on all three the phase currents, which trips the contactor once a preset thermal limit on the conductors is sensed.

### ***Reverse Power Protection***

When the hydraulic system of the MHPS for some or other reason malfunctions resulting in that the rotational speed drops to below the synchronous speed, the generator will start to operate as a motor. Hence active power is consumed from the grid instead of being delivered to the grid and load. At Waterval this condition is prevented by means of an electricity meter located at the generator. This meter has a directional current relay that is connected to the contactor. As soon as the meter senses active power flowing in the reverse direction, it de-energises the coils of the contactor, hence causing the MHPS to cease operation. Upon the contactor opening, a normally open switch is activated which turns on a light that indicates that a fault condition has been sensed.

### ***Net Metering***

Net metering is a system whereby energy is measured in both directions to know at the end of a billing period whether the net amount of energy has been exported or imported. This needs to be known in order to determine whether the owner of a power generating system should be billed or compensated for energy. In South-Africa, this system has not yet been implemented for systems having a generating capacity of below 100 kW, although it is currently in the research phase. As shown in Figure 30, Eskom currently only has meters installed at the PCC at Waterval that measure the active energy consumption of the load. However, two additional non-Eskom electricity meters, one in the powerhouse and one at the PCC, are installed in order to monitor the exporting and importing of energy at the PCC. The meter in the powerhouse measures and logs the generated hydro power, while the meter at the PCC measures and logs all imported and exported active and reactive energy. The meter at the PCC does not compensate for transformer losses of energy that is exported to the grid. When a dedicated Eskom meter is installed to measure the exported energy, it should be internally compensated for transformer losses.

## **6. Field Implementation and Testing**

In this chapter the results obtained from the installed MHPS are dealt with. Upon completion of the MHPS design, the implementation of the system began and this was divided into three phases. Results of each of these phases are presented in this chapter, with the main focus being on the performance of the installed MHPS.

### **6.1 Pre-Construction Phase**

The pre-construction phase basically consists of getting the necessary approvals from the applicable authorities for the implementation of the MHPS at Waterval, as discussed in Chapter 3. This process started on the 3<sup>rd</sup> of September 2007, with a site meeting with representatives from DWAF and Cape Nature. They gave environmental clearance for the project, subject to the following conditions:

- A minimum reserve needs to remain in the river at all times.
- An EIA needs to be undertaken with the BAR being authorised by DEA&DP.
- All activities associated with the implementation of this MHPS, must at all times comply with the conditions on which the BAR is approved.

After this site meeting, the impact assessment for the proposed MHPS commenced. A draft BAR was made available for the I&APs during the public participation process, which started on the 1<sup>st</sup> of November 2007 and lasted for a period of 30 days. The final BAR together with an EMP was compiled and submitted to DEA&DP on the 14<sup>th</sup> of January 2008. The BAR was approved with the record of decision received on the 6<sup>th</sup> of March 2008 and construction of the MHPS was to start after the necessary appeal periods ended.

### **6.2 Construction Phase**

Construction of the MHPS at Waterval started on the 1<sup>st</sup> of April 2008. As already mentioned, the difficulty and complexity of the construction activities of MHP systems are strongly site dependent, but usually there is no need for large and elaborate civil works. To verify this statement, all the construction was done by the author with the help of employees of Waterval.

Natural forces played a major role in the time it took to construct the MHPS at Waterval. Specifically rain and fire played a significant role as they extended the construction period and limited the number of employees that could help. The construction period extended over a total of 212 working days, of which only 89 could be used effectively for construction. Figure 31 shows a breakdown of the number of days it took to complete the different activities. As mentioned in section 4.3.1, the length of the underground pipeline is 240 m, with the above-ground pipeline length being 235 m. Although the pipeline section above the ground is slightly shorter than the underground section, it took 27 days longer to install the above-ground section. This is due to the fact that various concrete foundations had to be built and a number of constructions into boulders had to be made to keep this part of the pipeline in its position. Construction was completed on the 27<sup>th</sup> of February 2009. A layout of the completed MHPS at Waterval is presented in Figure E.1.

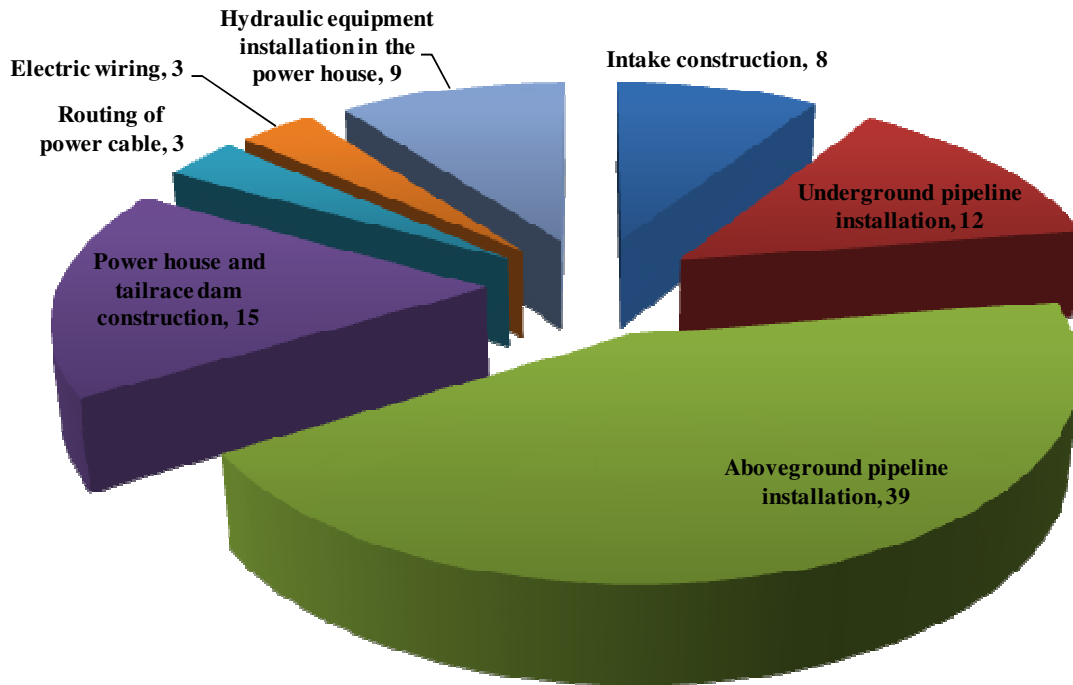


Figure 31: Construction activities with the number of days it took to complete each.

### 6.3 Operational Phase

Upon completion of the pipeline installation, before the hydraulic equipment in the power house is installed and to comply with the EMP of the BAR, a small amount of water was allowed

to flow through the pipe to clean it. It was then filled with water and in order to avoid excessive water hammer and initial shock in the pipeline, it was filled at a rate of about 0.6 l/s over a time of three hours and 30 minutes. The pipeline then remained full of water for a day, in order to inspect the stability of the above-ground part of the pipeline. It has also been verified that the pipeline expands and contracts during night and day temperatures within acceptable limits. The maximum displacement at a single joint is measured as 11 mm for a change of about 12 °C between day and night temperatures. The pipeline has then been drained to test whether the installed air and drain valves work properly.

### ***Pipeline performance testing***

The MHPS has five pressure gauges installed in the hydraulic system inside the powerhouse, as is shown in Figure 17. These gauges are used to measure the respective pipeline losses and for setting the necessary PAT operating points.

The first that has been verified with the pipe filled with water is the measured gross head of the MHPS. Gauge  $P_1$  shows a reading of 8 bar at zero flow. This gauge is located 110 mm above the centre of the pipeline, and to obtain the exact gross head, this 0.11 m must be added to the gauge reading. Hence the actual gross head is found to be 80.11 m, which compares fairly well with the 79 m that has been measured with the GPS as discussed in Chapter 2.3.1. The usage of pipeline pressure for height measurement is the most accurate method; hence the reason for the deviation between the two measurements is due to the accuracy of the “Garmin V” GPS that was used on Waterval.

The performance of the installed MHPS has been measured for flow rates up to 30 l/s. All the measured values are summarised in Tables E.1 and E.2 in Appendix E.2, and the performance curves obtained from these measurements are presented in this chapter. The main pipeline losses are measured with readings obtained from pressure gauge  $P_1$  and by adding the offset distance of 110 mm to each reading. The flow rate through the pipeline is calculated by measuring the time it takes for a certain volume of water to pass through the system. The measured results of the losses in the main pipeline, together with the predicted losses as is discussed in section 4.3.1 are plotted in Figure 32. The predicted losses correspond very well with the actual measured losses in the main pipeline. The difference between these two curves is because of the fact that the predicted losses were calculated for a gross head of 79 m, while the

actual gross head is measured to be 80.11 m. It does however seem that the difference between the predicted and measured results increases with increasing flow, but this can be a result of inaccurate flow measurements.

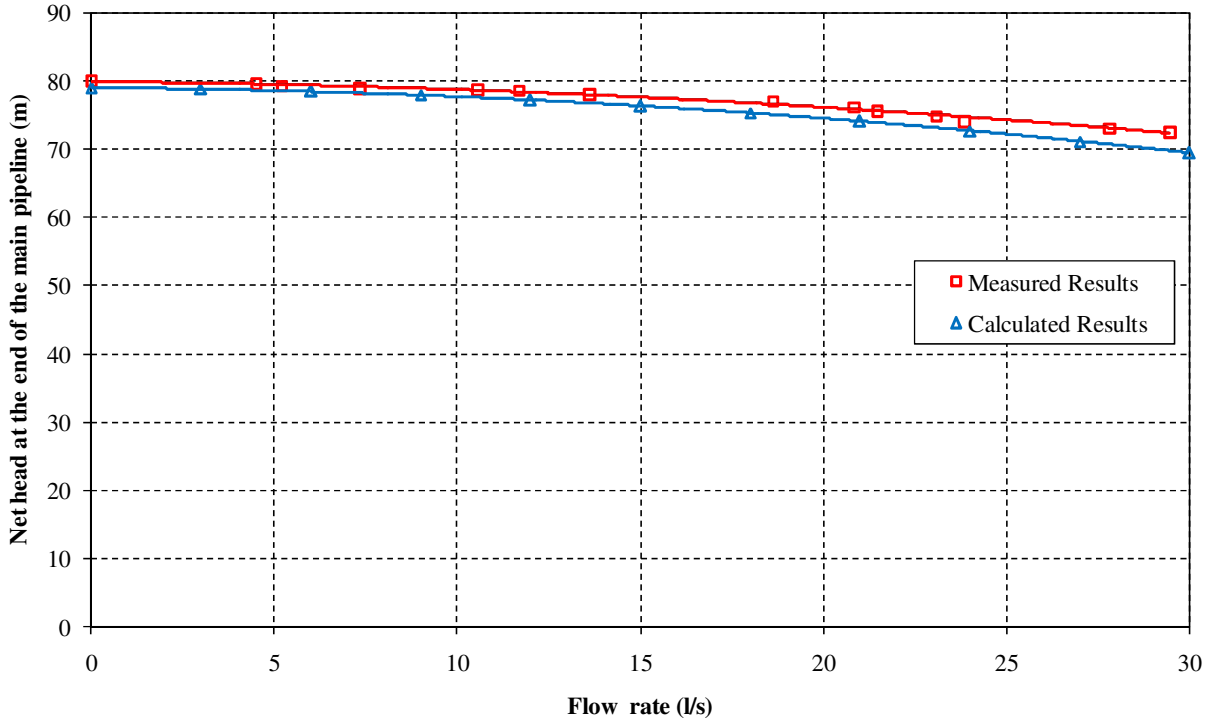


**Figure 32: Measured and calculated net head at the end of the main pipeline.**

### ***PAT Testing***

Testing of the PAT under load and no-load conditions is done with the isolation valve fully open and using the pressure sustaining valve to throttle the head and flow rate to various operating points. Shaft speed and output power is measured by using a torque sensor and a tachometer that are connected between the shafts of the PAT and generator.

The no-load test results of the PAT are shown in Figure 33. It is observed that the actual measured points scatter very much. Hence a curve is fitted to these points, in order to observe the trend of the measured results. The scattering of the measured results is as a result of flow rate measurements that may not be accurate, and also due to the fact that the flow rate, pressure, shaft speed and shaft torque readings are not taken at exactly the same time. In Figure 33, next to each measured no-load operating point, the measured shaft speed is given.

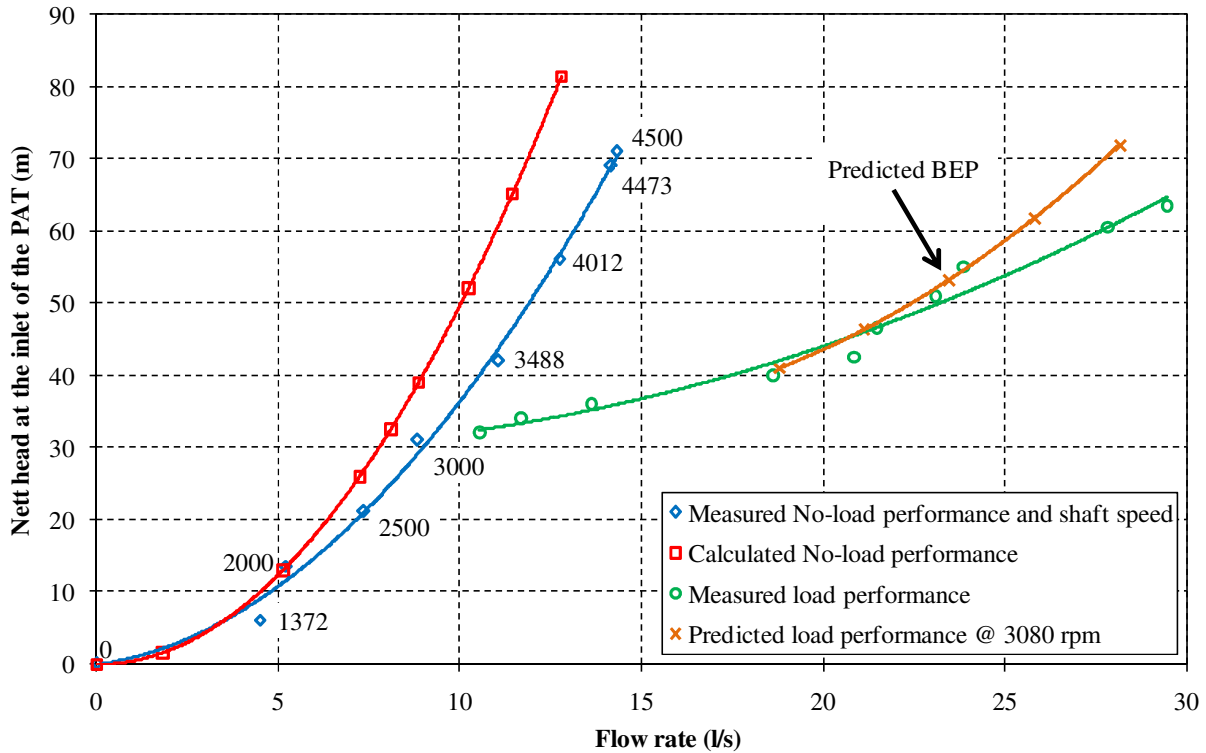


**Figure 33: Predicted and measured no-load and load performance of the PAT.**

It is observed that the difference between the measured and predicted curves increases significantly with increasing flow, hence proving the uncertainty of the accuracy of the predicted performance. With the pressure sustaining valve fully open, it is measured that the runaway head and flow will be 71 m and 14.2 l/s respectively. The maximum no-load speed at this point is measured as 4 500 rpm, which is 13.6 % lower than the 5 211 rpm predicted in section 4.4.2. Runaway results are presented later.

For the PAT load testing, due to the lack of a hydraulic control device inside the PAT, the shaft speed cannot be kept constant at the different operating points. The load test results of the PAT are shown in Table 5, with the head versus flow performance of the PAT under load also shown in Figure 33. It is evident that the seventh and eighth measured load points compare very well with the predicted BEP point of the PAT. From the measured efficiency results in Table 5, it is seen that the actual BEP of the PAT lies at the eighth measured load point. The measured head and flow at this point correlate well with the predicted BEP head and flow given in Table 4. Furthermore, it is observed that the predicted and measured performances only correlate well

near the BEP of the PAT. The complete predicted and measured performance of the PAT is shown in Figure 34.

**Table 5: Actual PAT load test measurements.**

Load Point	Head, $h_t$ (m)	Flow rate, $Q_t$ (l/s)	Speed, $n_t$ (rpm)	Torque, $T$ (N.m)	Power, $P_{shaft}$ (kW)	Efficiency, $\eta_t$ (%)
1	32	10.54	3 000	1.7	0.53	16.14
2	34	11.68	3 012	4.96	1.56	40.16
3	36	13.61	3 022	8.48	2.68	55.83
4	40	18.62	3 034	13.96	4.44	60.72
5	42.5	20.83	3 054	16.54	5.29	60.9
6	46.5	21.46	3 068	21.24	6.82	69.69
7	51	23.08	3 081	24.42	7.88	68.24
8	55	23.83	3 093	29.02	9.4	73.1
9	60.5	27.81	3 108	34.06	11.08	67.16
10	63.5	29.44	3 112	36.98	12.05	65.7

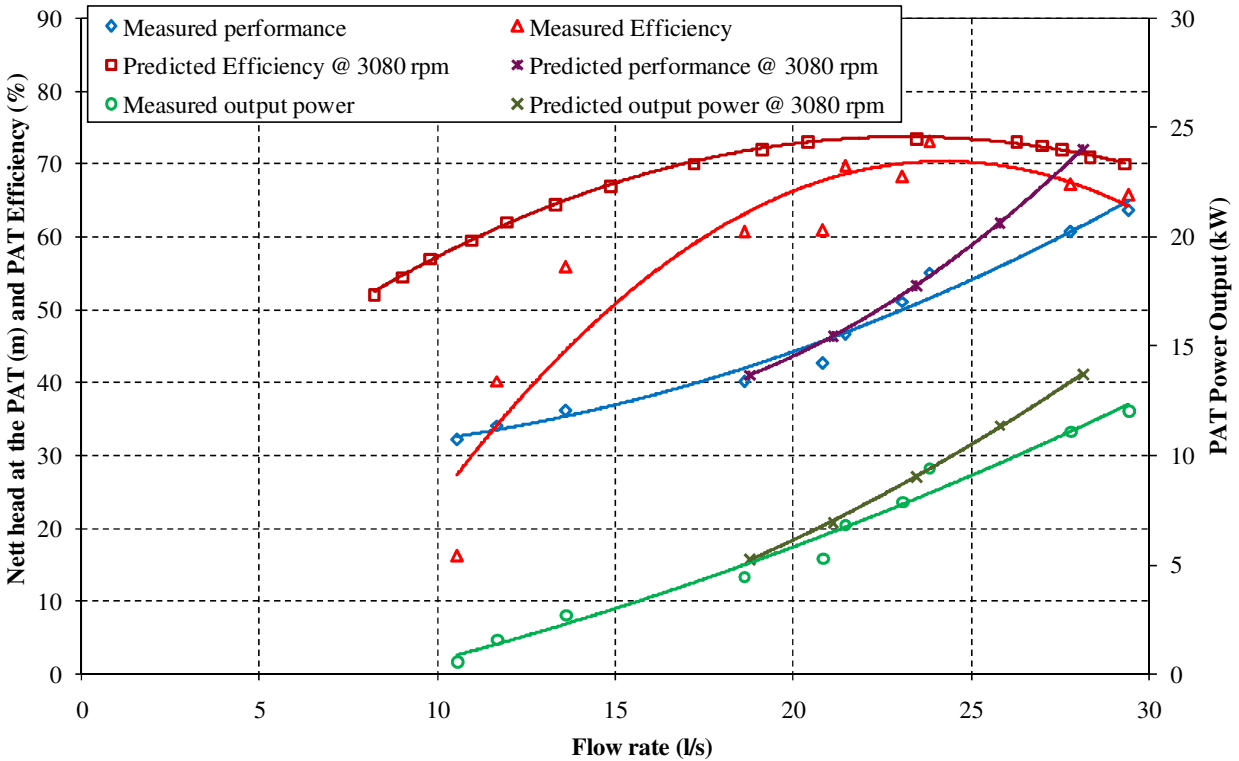


**Figure 34: Predicted and measured performance of the PAT under load.**

The measured peak efficiency of the PAT is 73 %, but this is at a speed of 3 093 rpm and not at 3 080 rpm as predicted. The peak efficiency of the PAT in pump mode is 76.5 % (Figure C.9). If this is compared with the measured peak efficiency of the PAT, the assumption in section 4.2.2 is verified that the peak efficiency of a pump in turbine mode is about 3 % lower than in pump mode. From section 4.2.2 the efficiency of the PAT at flow rates other than the design flow rates was also assumed to be 3 % lower than the available pump mode efficiency at the corresponding flows. From Figure 34, it is found that this is not true since the measured efficiency of the PAT at flow rates away from the BEP flow rate decreases very rapidly.

The relation between the measured and predicted performance at operating conditions away from the BEP cannot really be compared, since limited correction factors are available for predicting PAT performance away from the BEP. However, it seems that the measured and predicted head and flow rate characteristics and power output of the PAT at flow rates lower than the BEP flow rate tend to follow each other. At flow rates higher than 24 l/s the deviation between the two curves increases with increasing flow rate.

With the measured BEP of the PAT very close to the predicted BEP, it can be concluded that the head and flow rate conversion factors proposed by [23] is indeed accurate. Using Equation 4.17, the measured head and flow rate conversion factors is calculated as 1.48 and 1.34 respectively while those used for the prediction is 1.45 and 1.325 respectively.

During testing of the PAT, it is observed that the system takes some time to stabilise as the operating / load points of the PAT are adjusted. The reason for the slight deviation between the measured and predicted BEP could be that the time allowed for the system to stabilise after the operating / load point is adjusted and before readings are taken, is not long enough. The other reason for the deviation that has already been mentioned is that the pressure, torque, speed etc. readings for each operating point are not taken at exactly the same time.

### ***Cavitation***

Although no provision is made to observe cavitation at the PAT and the valves accurately, it is detected by its characteristic noise, similar to that of stones passing through a pipe. Cavitation at the isolation and pressure sustaining valve initiates when the operating flow rate decreases below about 17 l/s. It is detected that cavitation initiates at the PAT at a flow rate of about 29 l/s. For flows beyond this, the cavitation becomes critical due to the fact that for

increasing head and flow rate, the  $NPSH_R$  increases faster than the NPSH that is available. Hence, the PAT should only be operated at flow rates where no cavitation at the valves or at the PAT exists. For safe hydraulic system operation, the system should be operated between flow rates of 18 l/s and 29 l/s.

**Electrical power output**

The power output of the generator, together with its efficiency is shown in Figure 35. Also shown is the combined PAT and generator efficiency, with the actual measured shaft speed at each of these points. From Figure 35 it is seen that the generator delivers its rated output power of 9.2 kW with an efficiency of 84.5 % at a flow of about 26 l/s and a slip speed of about 100 rpm. Laboratory test results of the induction generator showed that its rated output power is delivered at a slip speed of 90 rpm with an efficiency of 85.2 %. The slight deviation between the efficiency and speed of the generator for the two tests is once again due to the fact that the speed, torque and power readings at Waterval are not taken at exactly the same time. The dip in the efficiency profile of the generator at a flow of 18.5 l/s is as a result of input and output power readings that are not taken at exactly the same time.

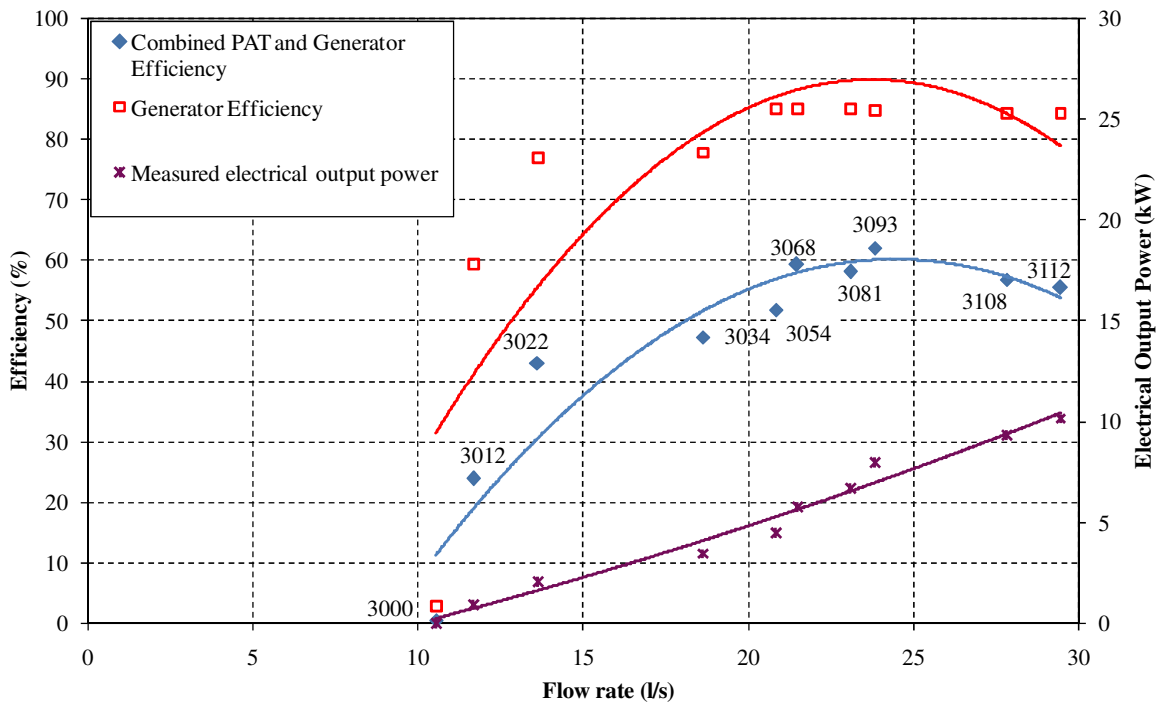


Figure 35: Combined efficiency curves and measured electrical power output for different operating points.

It is also seen that the electrical power output of the generator is about 8 kW when the flow rate through the PAT is 24 l/s. This is only 1.2 % less than the predicted electrical output power in section 5.1.

From these performance curves it is clear that, depending on the amount of water that is available in the Assegaaios River, and considering the above mentioned safe hydraulic operating region of the valves and the PAT, the MHPS can be operated to have a continuous generated electrical power output of between 5 - 9.2 kW, with the combined water to electricity conversion efficiency exceeding 55 %.

***Runaway test results***

The PAT is tested for runaway at various operating / load points as given in Table 6. The pressure relief valve is not set to open only at pressures beyond the maximum of what the main pipeline is rated for, but it is rather adjusted to open at lower pressures according to the operating point of the PAT, in order to avoid excessive water hammer in the pipeline. The results in Table 6 only gives the steady state runaway points after the pressure sustaining valve has throttled to its preset downstream operating pressure. The maximum transient runaway pressure and speed occurred at the last operating point where the head and flow rate through the turbine was at maximum. Unfortunately, the flow rate through the PAT was not measured for these tests.

**Table 6: Runaway test results.**

Test Point	With Load			With no-load	
	PAT Head, $h_t$ , (m)	Pressure Relief Valve opening pressure, $P_{PRV}$ , (m)	PAT and generator Speed, $n_t$ , (rpm)	PAT Head, $h_t$ , (m)	Speed, $n_t$ , (rpm)
1	44	72	3 053	45	3 499
2	46.5	72	3 054	47	3 628
3	50	71	3 060	50	3 751
4	52	71	3 071	52.5	3 823
5	54.5	71	3 069	54	3 928
6	58	70	3 098	58	4 103
7	61	70	3 103	61	4 210

This maximum transient pressure and speed are found to be 86.5 m and 4 505 rpm respectively. It was observed that the pressure relief valve in the bypass line opened during this test, which significantly decreased the water hammer in the pipeline. From these steady state runaway results it can be seen that the steady state runaway speed at a operating pressure of 55.35 m is about 3 950 rpm and not 4 553 rpm as calculated in section 4.5.

***MHPS Performance***

As mentioned in section 5.3.3, the electrical power that has been generated at Waterval since the MHPS was first started is logged, with two power meters that have a sampling time of 15 minutes. Both of these meters at Waterval are set to log an average value over the sampling time and not instantaneous values at the end of each sampling time. The profile of the active power that is generated from the first of July to the 31<sup>st</sup> of August 2009 is shown in Figure 36. Due to plenty of water available in the river for power generation during this period, the system is operated slightly beyond its maximum capacity from the 10<sup>th</sup> of July 2009, as shown in Figure 36.

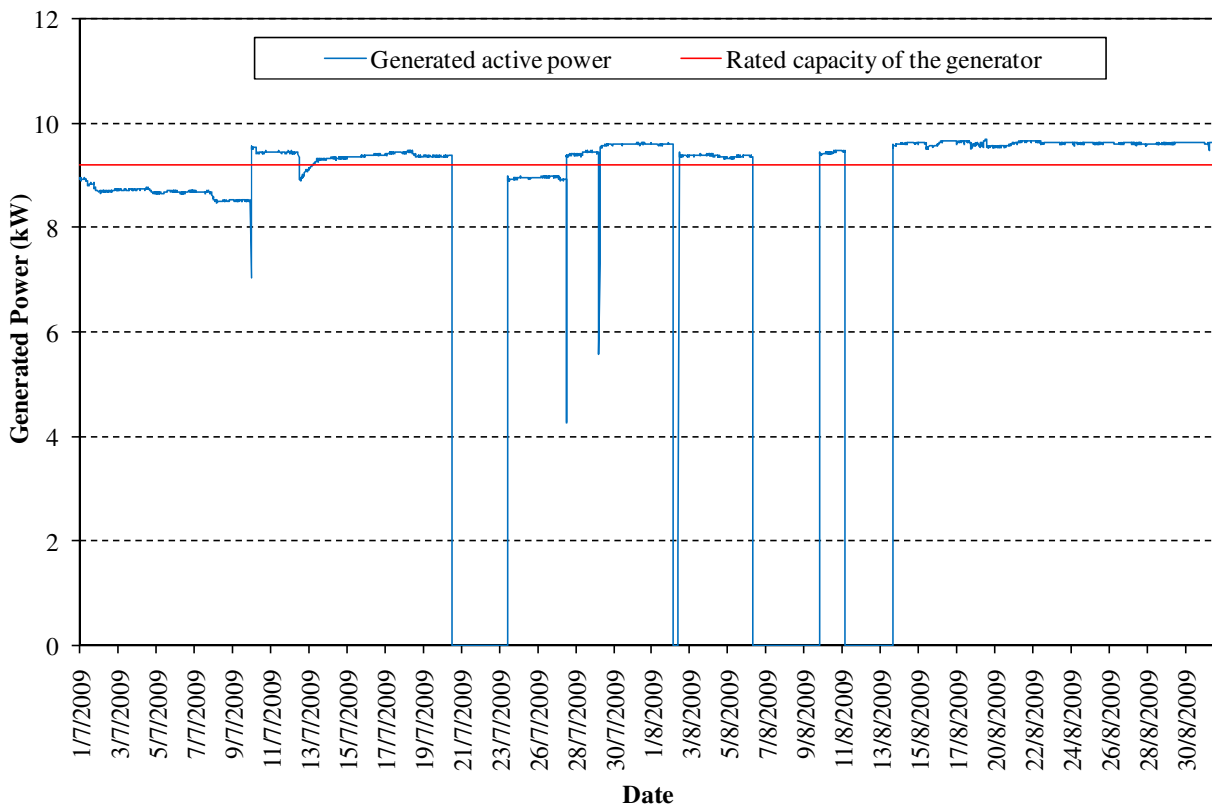


**Figure 36: Waterval MHPS power generating profile.**

The points with a sudden increase in generated power represent the times when the operating point of the MHPS was adjusted. The generated power dips in the profile on the 10<sup>th</sup>, 27<sup>th</sup>, 29<sup>th</sup> of July and on the 2<sup>nd</sup> of August, as shown in Figure 36 are because of a quick shutdown to clean the filters on the pressure relief valve and the pressure sustaining valve. The downtimes between the 21<sup>st</sup> to the 24<sup>th</sup> of July and the 11<sup>th</sup> and 14<sup>th</sup> of August are times when difficulty was experienced with replacing the gland packing on the PAT. Depending on the amount of tourists staying at Waterval over weekends or during certain other periods, the farmer also shuts down the MHPS to have maximum water in the river - this is the reason for the system downtime between the 6<sup>th</sup> and 10<sup>th</sup> of August. From this profile, it is also concluded that the MHPS sustains operating smoothly at its preset operating points. The capacity factor of the MHPS from the first of July to the 31<sup>st</sup> of August 2009 is calculated as 85.7 %.

The power meter that is installed at the PCC has a sample time of 15 minutes and measures and logs the average power demand of the load and the average power that is exported to the grid during times when the generated power capacity exceeds the demand of Waterval. These profiles are shown in Figure 37, for the period extending from the 1<sup>st</sup> of July to the 31<sup>st</sup> of August 2009. From this profile it is clear that with the MHPS installed, the demand of Waterval from Eskom is reduced by an average of about 4 kW. It is also clear that as the load varies, an active power average of about 5 kW is continuously being exported to the grid. Details of the energy scenario at Waterval from the 12<sup>th</sup> of March 2009 when the MHPS was first started to the 31<sup>st</sup> of August when the last measurements is taken, is presented in Figure 38.

The true average power generated by the MHPS can only be calculated when the MHPS has been in operation for at least a year, since it is likely that the generated average power of 8.1 kW as given in Figure 38 will decrease once the operating point of the MHPS is adjusted to accommodate the decrease in available water from the river during summer times. However, when comparing the average power that is generated thus far with the initial calculated potential power in section 2.4, it can be seen that the actual generated power output is higher, which is very satisfying. With the MHPS fully operational and not getting any compensation for energy that is exported to the grid, it can also be seen that the energy demand of Waterval from Eskom has been lowered by 40.6 %.

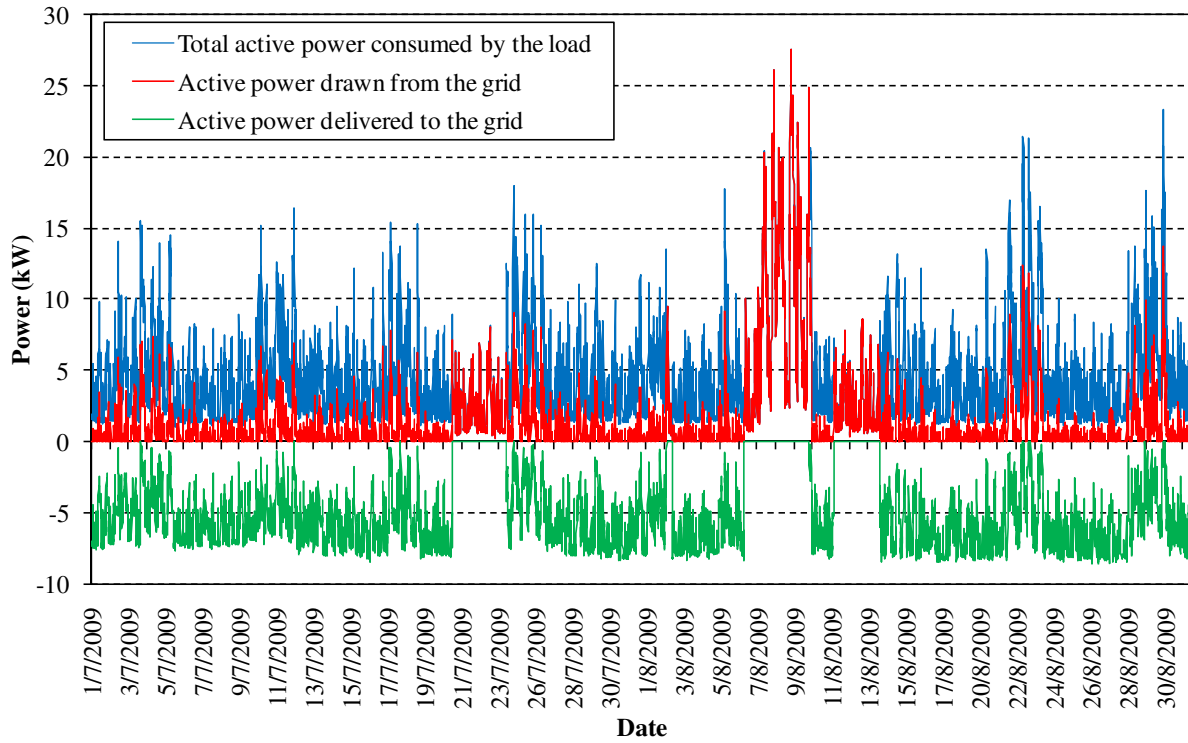


Figure 37: Active power profile at the PCC.

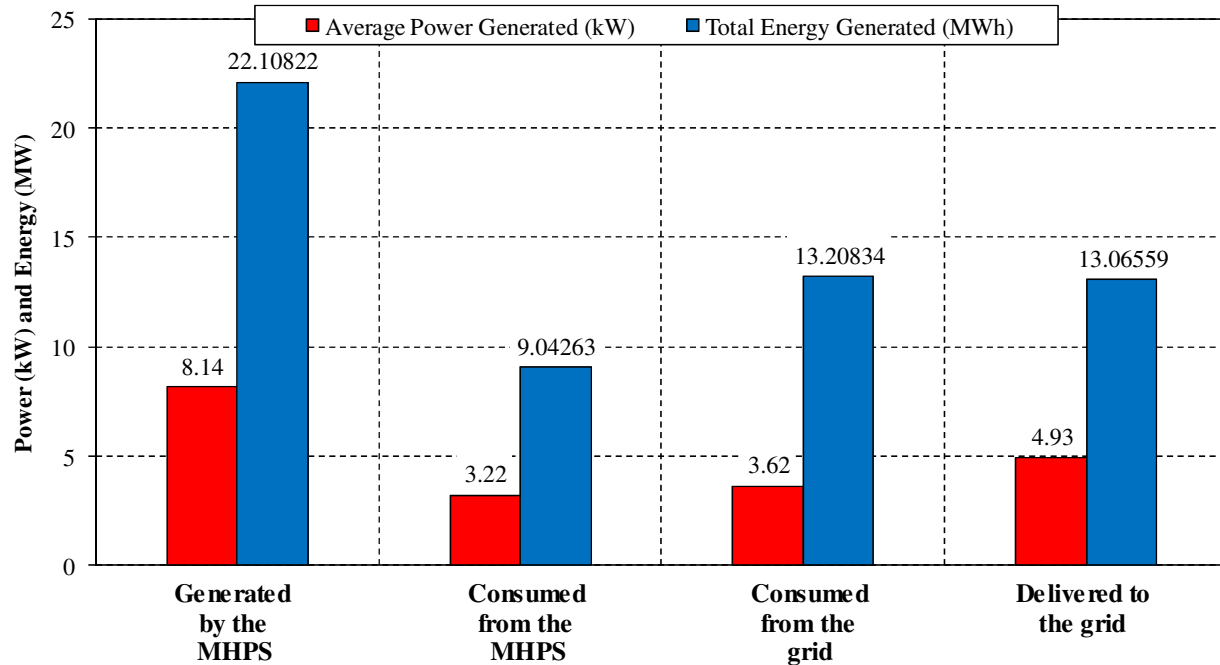


Figure 38: Electrical energy and power details for Waterval from the 12/03/09 – 31/09/09.

Although the demand from Eskom has been lowered, an amount of 13 065.59 kWh's of electrical energy has already been exported to the grid. If the net metering scheme that is previously mentioned, had been implemented by the distributor and credits were obtained for the electrical energy that is exported to the grid, it can be seen that the owner of Waterval would only have had to pay the distributor for 142 kWh's of electrical energy consumed from the grid over a period of 180 days. The compulsory costs mentioned in section 2.4 would also still have to be paid.

From all the above results it is concluded that the system operates very satisfactorily and that the owner definitely benefits from the implementation of the system. It is also evident that the owner will benefit even more once entering into a net metering agreement with the distributor.

### ***Environmental impact mitigation measures results***

All the impact mitigation measures in the EMP for the MHPS at Waterval have been implemented, during the construction and operation phase. The areas that were disturbed during the time of construction recovered well. Photos of some of these locations are shown in Appendix G. After seven months of operation, it is observed that the reduced flow in the river does not affect the environment at all. It is also concluded that the presence of the powerhouse and the above-ground part of the pipeline does not affect the fauna in the environment as they are still very regularly seen on the farm. Hence it can be concluded that the environmental impacts associated with a MHPS are very little, if the necessary mitigation measures are implemented.

## 7. Economics of MHP Systems in South Africa

Before a MHPS can be implemented, its economic feasibility needs to be investigated. A grid-connected MHPS investment involves various costs and compensation benefits over the lifetime of the project. Compensation benefits depend on the interconnection agreement between the distributor and the owner of the MHPS as discussed in the previous two chapters. The economic feasibility of a MHPS relates to a comparison of the costs to the benefits involved, in order to make an informed decision on whether to invest in a MHPS or not.

At the beginning of this chapter there is a discussion on the costs involved over the life cycle of a grid-connected MHPS, where after a discussion on the savings is presented. The methodologies used to analyse the economic feasibility together with the results for the MHPS at Waterval are then presented. The chapter concludes with a discussion on the economic sensitivity of this MHPS system.

### 7.1 MHPS Costs and Savings

#### 7.1.1 Costs

The costs of a MHPS are purely a function of the site characteristics and the size of the proposed system. The involved costs can be divided into the following different phases:

- ***Pre-feasibility study phase*** – This phase involves the costs for doing the preliminary site studies, calculating the potential power that can be generated and obtaining a rough estimated cost of the system, in order to determine whether it is feasible to implement such a system. If costs are involved for obtaining the necessary authorisation of a MHPS, it is also included in this phase.
- ***MHPS design phase*** – This includes the costs of the actual design of the MHPS. These costs can be very low if the system is designed by the owner himself, but as the size of the system and complexity of the site characteristics increase, the need for expert engineering advice increases. If consulting costs are present, then these costs are also included in this phase.
- ***Installation phase*** – This includes the cost of doing the necessary site preparation, the cost of the MHPS components and the equipment and labour necessary to install the system. Any expert advice which may be necessary on installing the system is also

included and if grid connection costs exist, they are also included in the MHPS installation costs.

- **Operational phase** – This basically includes the costs to monitor the installed system and to do the necessary maintenance.

The only costs considered with regard to the MHPS at Waterval are the installation costs and Operation and Maintenance (O&M) costs. For the Waterval project the pre-feasibility and design costs were zero as this was done by the author himself. All the installation costs of the MHPS are summarised in Table 7.

**Table 7: Installation Costs of the MHPS.**

<b>Activities</b>	<b>Cost (ZAR)</b>
<u>Civil Works</u>	
Weir	
• Components	449.11
• Labour (including site preparation)	3 120.00
Pipeline	
• Pipes and fittings	47 639.26
• Miscellaneous Components and Equipment	14 598.04
• Labour (including site preparation)	7 140.00
Powerhouse and Tailrace dam	
• Components	3 718.53
• Labour (including site preparation)	9 600.00
<u>Mechanical Works</u>	
• PAT	4 330.00
• Hydraulic Valves	21 214.00
• Miscellaneous Components and Equipment	234.02
• Labour	630.00
<u>Electrical Works</u>	
• Generator	2 100.00
• Switchgear	7 869.54
• Power Cable	11 440.00
• Miscellaneous Components and Equipment	877.46
• Labour	650.00
<b>Total</b>	<b>135 609.96</b>

A complete breakdown of the installation cost of all the components is included on the CD that is attached at the back of this thesis. For this economic study, VAT is excluded from all the costs, savings and calculations. Currently no costs exist for connecting the generator of a MHPS to the grid, but once a grid code for these small power generating systems has been developed, a certain cost may exist. The total installation cost of the MHPS is R135 609.96 with the cost of the pipes being the highest. This explains why it is crucial to ensure that the pipeline, with reference to head losses, must be designed properly.

Maintenance work of the MHPS at Waterval is discussed in Appendix E.3, but it is found that little is required. Operation and Maintenance (O&M) costs are discussed in Appendix F.1, with the annual average cost calculated at R349.

### **7.1.2 MHPS Savings**

MHPS savings relate to the energy that is no longer needed from the distributor, as a result of the energy that is generated by the MHPS and delivered to the load and the grid. These savings currently strongly depend on the electricity tariff of the distributor. Once a grid code for MHP systems is introduced, the savings will also depend on the interconnection agreement between the owner of a power generating system and the distributor, as tariffs may be introduced by the distributor that will be payable to the owner of a power generating system for being a net exporter of energy.

For the purpose of this economic study it is assumed that credits are obtained from the distributor for energy delivered to the grid and that credits in excess of the total annual energy consumption of the load are carried over to the next year.

## **7.2 Economic Viability of a MHPS**

In this study, a few methodologies are used to determine the financial viability of a MHPS. These include the easy static method of determining the payback period as well as dynamic methods that allow for the time value of money. All of these economic performance indicators that are based on the MHPS installed at Waterval are represented hereafter. These calculations assume the following:

- A designed life cycle of 20 years.

- A capital investment of R136 000 with average annual O&M costs remaining at a constant amount of R349, in real terms. These costs are based on an average installed hydro power generating capacity of 8 kW having a capacity factor of 90%.
- Economic data and electricity tariffs available at the time of October 2009.

### 7.2.1 Payback Period

This method is simply used to calculate the number of years taken for the savings obtained from a MHPS to offset the invested capital amount and the accumulated O&M costs to date. This period is calculated as follows:

$$PP = \frac{CI}{S - OM} \quad (7.1)$$

where  $PP$  is the payback period in [years],  $CI$  is the capital investment in [ZAR],  $S$  is the cost of the annual energy savings in [ZAR] and  $OM$  is the annual operating and maintenance cost of a MHPS in [ZAR].

Considering a capacity factor of 90 % for an average generating capacity of 8 kW at Waterval, the annual amount of energy that is generated is calculated to be 63 072 kWh, hence the cost of this annual amount of energy is saved if it is assumed that credits are obtained for energy exported to the grid. By using the current rural “Landrate 2” electricity tariff of 46.27 c/kWh, the annual savings is calculated as R 29 183, hence resulting in a PP of 4.66 years.

### 7.2.2 Net Present Value

This parameter indicates the financial viability of a MHPS with the time value of money considered. The Net Present Value (NPV) of a MHPS represents the difference between the Present Values (PV) of future project costs and savings. If the NPV at the end of a project’s life cycle results in a positive value, such an investment is worthwhile, whereas a negative NPV indicates it is not. The NPV is calculated by the summation of the difference between the annual PV discounted costs and savings:

$$PV_{Costs\_i} = \frac{LCC}{(1+r)^i} = \frac{CI}{(1+r)^i} + \frac{OM}{(1+r)^i} \quad (7.2)$$

$$PV_{Savings\_i} = \frac{S}{(1+r)^i} \quad (7.3)$$

$$NPV_i = \sum_{i=0}^N PV_{Savings} - \sum_{i=0}^N PV_{Costs} \tag{7.4}$$

where  $PV_{Costs_i}$  is the PV of the costs of a future year in [ZAR],  $PV_{Savings_i}$  is the PV of the savings of a future year in [ZAR],  $i$  is the relative year,  $LCC$  is the life cycle cost in [ZAR],  $r$  is the discount rate in [%],  $N$  is the period in [years] and  $NPV_i$  is the NPV of the MHPS after a certain number of years in [ZAR].

The discount rate used for calculating the NPV, also known as the real interest rate, is the nominal interest rate minus the inflation rate. The real interest rate is currently 4 %. To calculate a very conservative NPV for the MHPS at Waterval, the savings for the first year are based on current electricity prices. As the electricity tariffs will definitely increase in the next year, the savings for the second year are based on an average real escalation rate of 23.5 %, after which it is assumed that the savings in real terms over the rest of the lifetime of the project will remain the same, i.e. that the real escalation rate of electricity tariffs is 0 %. These assumptions are discussed in Appendix F.2. The calculated NPV of the MHPS over its designed lifetime is presented in Figure 39 and the calculation results are presented in Tables F.2 and F.3.

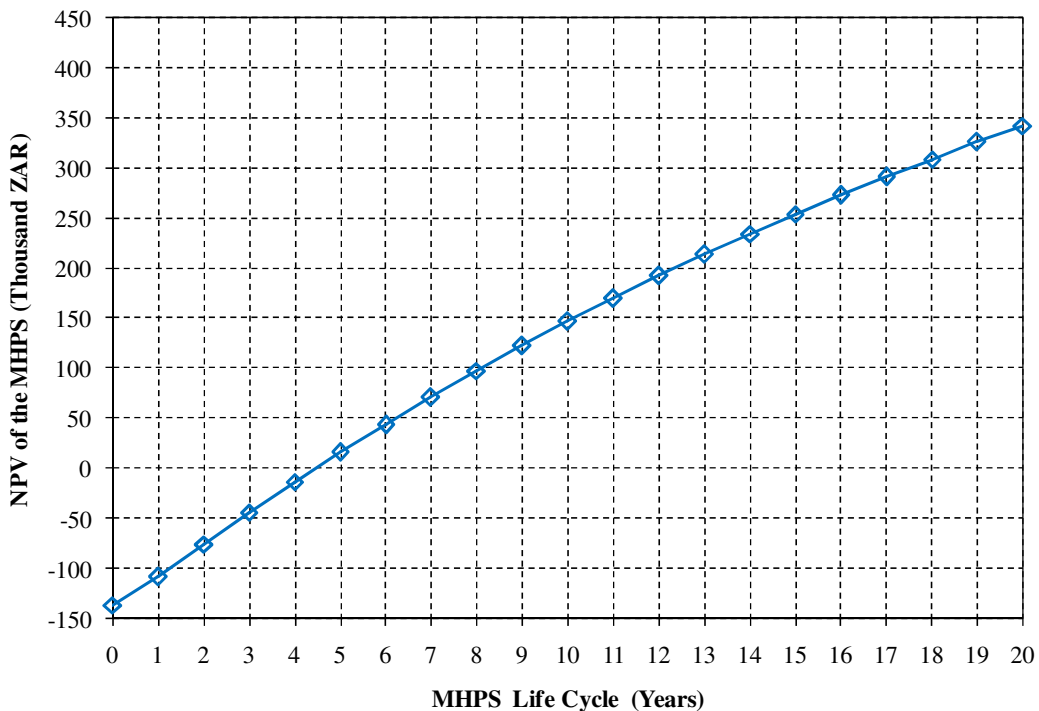


Figure 39: NPV of the MHPS over its lifetime.

From Figure 39, it can be seen that it takes 4 and a half years for the inflated annual savings in electricity to equalise the inflated costs of the MHPS. This short period is mainly due to the fact that the annual savings are largely due to the current high electricity tariffs. With the NPV at the end of 20 years being R342 475, an investment into a MHPS can be considered as desirable.

### 7.2.3 Internal Rate of Return

The Internal Rate of Return (IRR) is a parameter used to determine the profitability of an investment. An investment is considered as profitable if the calculated IRR is above the nominal current interest rate. The IRR is the rate at which the NPV of a project, at the end of its lifetime, equal zero, that is:

$$\sum_{i=0}^N \frac{(S - LCC)}{(1 + IRR)^i} = 0 \quad (7.5)$$

where  $IRR$  is the internal rate of return in [%]. If the same assumptions regarding the electricity escalation rate as in section 7.2.2 are considered, the real IRR of the MHPS is calculated to be 24.9 %. Hence the nominal IRR is 31.3 %. When comparing this to the current nominal interest rate of 10.4 %, it is clearly a very profitable investment

### 7.2.4 Cost of Energy

The cost of the hydro energy that is generated is calculated by dividing the summed life cycle costs of the MHPS by the total amount of energy that is generated over the same period, that is:

$$COE = \frac{\sum_{i=0}^N LCC}{\sum_{i=0}^N E_a} \quad (7.6)$$

where  $COE$  is the cost of the generated energy in [ZAR/kWh] and  $E_a$  is the generated energy over a number of years in [kWh].

The LCC of the MHPS at Waterval is calculated at R142 980 (Table F.3). If it is assumed that the average generating capacity is maintained over the entire lifetime of the MHPS with a capacity factor of 90 %, it is calculated that the energy at Waterval is generated at a cost of 11.30

c/kWh. Hence the hydro energy is generated at a desirable price of four times lower than what is currently charged by the distributor for energy that is consumed from the grid.

### 7.3 Sensitivity Analysis

The accuracy of the above analysed economic indicators largely depends on the accuracy of the assumed time variables used such as interest, inflation and the real escalation rate of electricity tariffs. As mentioned, the performance calculations of the above economic indicators are based on data that is available in October 2009. As future changes in these variables are likely to occur, but are impossible to predict, this section presents an analysis on how the NPV at the end of 20 years of the MHPS varies when varying these time dependent variables.

The results of these calculations are given in Table F.4 and are graphically presented in Figure 40. If the capacity factor of the system drops to below 90 % in the future for reasons such as maintenance, drought, etc., it will have an effect on the NPV of the MHPS, which is also presented in Figure 40. As already explained, note that these results are for varying the real electricity escalation rate from the 3<sup>rd</sup> year onwards, as NPV calculations for the first two years of MHPS operation are based on available data. From this figure it can be concluded that an investment in the MHPS is very desirable, since the NPV of the MHPS remains high when large variations in the time dependent variables are considered.

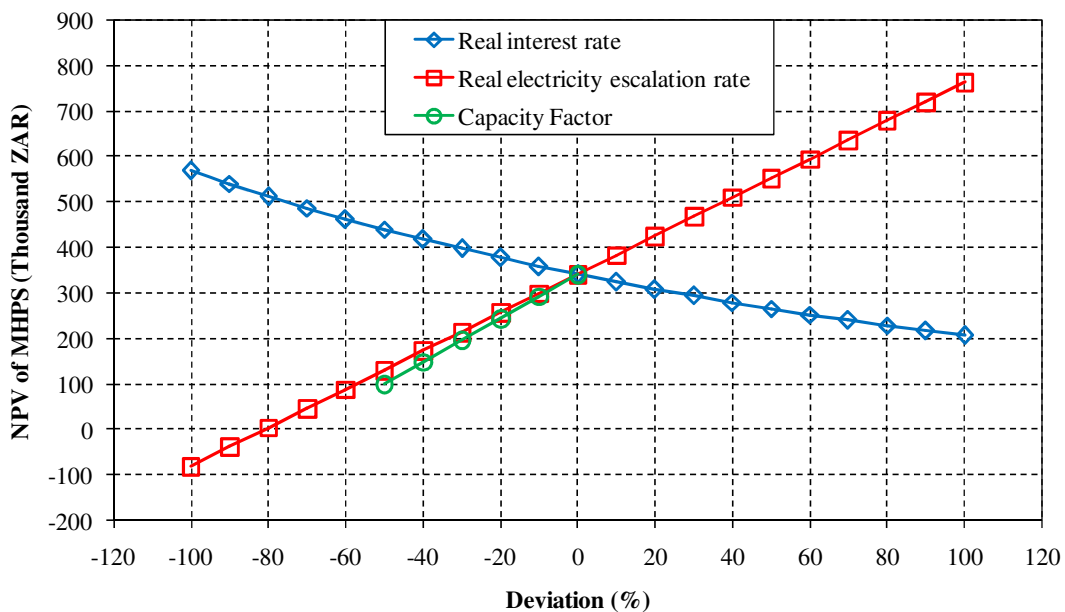


Figure 40: NPV of the MHPS at the end of its lifetime with varying the time dependent variables.

## **8. Conclusion and Recommendations**

This study presents the design of a low cost grid-connected 9.2 kW hydro power system and all the associated aspects of implementing such a system. The whole study is based on a specific site in the Western Cape where the designed system is installed and fully operational.

The process of assessing the available resources prior to designing a micro hydro power system is presented. Some of the activities associated with the implementation of a micro hydro power system, are listed in Regulation 386 of the National Environmental Management Act. It is found that a basic assessment report of the associated impacts of the activities needs to be completed. This document needs to be authorised by the Department of Environmental Affairs and Development Planning prior to installing the hydro power system. From the study that was undertaken for the implementation of the landmark example, it was deduced that the environmental impacts of these activities are of low to medium significance. It was also found that if the applicable mitigation measures are implemented the significance of these impacts are even lower.

The micro hydro power system was designed using only commercially available components. It was found that these components do have a lower efficiency than the conventional custom built components, but their costs are significantly lower. The methods used to design the micro hydro power system and select certain components yielded very good results for operation at the best efficient point of the pump as turbine. The predicted and measured mechanical power output of the pump as turbine at the design flow rate differs with 1.05 %. The measured electrical power output at the design flow rate is 1.2 % less than what was theoretically predicted. It was also found that the efficiency of a pump as turbine drops significantly when it operates at flow rates away from its best efficiency point. This is mainly due to the absence of a hydraulic control device inside the pump as turbine. The problems of water hammer in the pipeline and runaway of the generating set were also addressed. Test results of the incorporated protection measures shows that the micro hydro power system remains operating within safe limits when runaway or water hammer occurs.

All the necessary requirements for connecting a small hydro power system to the grid, utilising an induction generator, are discussed. These requirements are mainly derived from standards used elsewhere in the world as the local distributor currently does not have any grid

connection standard for generation systems with a capacity below 100 kW. The implemented switchgear was tested thoroughly and also yielded good results.

The economic study of the designed and implemented micro hydro power system shows that the initial capital investment is high. However it is shown that the operational and maintenance costs of the implemented system are very low and that the payback time of the system with the time value of money considered, is four and a half years. The results also show that the micro hydro system generates electrical energy at a cost of 11.3 c/kWh, which is much lower than the current tariff of 46.27 c/kWh that is paid by the owner to the distributor for energy that is consumed from the grid. Although the economic feasibility of micro hydro power systems is very site dependent, it seems that investing in a micro hydro power system is very worthwhile.

### **Recommendations**

For future work, it is recommended that the pump as turbine performance when the impeller has been trimmed to match a required operating point should be investigated further. This was completely unclear in this study and was one of the reasons why the initial required operating point had to be adjusted in order to match a pump as turbine with a full impeller size.

The cage rotor of the induction machine is optimally designed for motor use. In an attempt to increase overall system efficiency, it is recommended that further studies must be conducted on redesigning the cage rotor solely for optimal performance in generator mode. If then mass produced, these machines will provide a low cost efficient option for use in micro hydro power generation systems.

## References

1. Department of Minerals and Energy, “Manual for the hydro power projects development in South Africa”.
2. Douglas Banks and Jason Schaffler, “The potential contribution of renewable energy in South Africa“, February 2006.
3. Department of Minerals and Energy, “White paper on renewable energy”, November 2003.
4. C.Dragu, T. Sels, “Small Hydro Power – State of the art and Applications”.
5. Theodore R. Hazen, “A history of the water wheel”, 2002.
6. Oliver Paish, “Small Hydro Power: Technology and Current Status”, February 2002.
7. M. Godoy Simoes, Sudipta Chakraborty and Robert Wood, “Induction generators for small wind energy systems”, 2006.
8. Dr. Barbara A. Gale, “Proposed conversion of existing irrigation furrow to pipeline system and abstraction weir on the Assegaaibos Rvier, Porterville: Motivational Report”, August 2002.
9. Robert H.J. Sellin, “Flow in Channels”, 1969.
10. A.J. Chadwick and J.C. Morfett, “Hydraulics in Civil Engineering”, 1986.
11. BS ISO 1438:2008, “Hydrometry – Open channel flow measurement using thin-plate weirs”, 2008.
12. BS EN ISO 748:2007, “Hydrometry – Measurement of liquid flow in open channels using current-meters or floats”, 2007.
13. P. Fraenkel, O. Paish, V. Bokalders, A. Harvey, A. Brown, R. Edwards, “Micro-Hydro Power – A guide for development workers”, 1991.
14. “Omgewings Ingenieurswese 442 & 454 Class Notes”, Stellenbosch University, 2006.
15. Government Gazette, “National Water Act”, 1998.
16. European Small Hydropower Association, “Guide on how to develop a small hydropower plant”, 2004.
17. F. Sentürk, “Hydraulics of Dams and Reservoirs”, 1995.
18. American Society of Civil Engineers, Committee on Hydropower Intakes, “Guidelines for design of intakes for hydroelectric plants”, 1995.
19. Alternate Hydro Energy Centre, “Micro Hydro Quality Standard”, 2005.

20. John A. Robertson, John J. Cassidy, M. Hanif Chaudhry, “Hydraulic Engineering”, 1988.
21. Ernest F. Brater, Horace W. King, James E. Lindell, C.Y. Wei, “Handbook of Hydraulics”, 1996.
22. Merle C. Potter, David C. Wiggert, “Mechanics of Fluids”, 2001.
23. J.M. Chapallaz, P. Eichenberger, G. Fischer, “Manual on Pumps Used as Turbines”, 1992.
24. A.T. Sayers, “Hydraulic and Compressible Flow Turbomachines”, 1990.
25. Khin Cho Thin, Mya Mya Khaing, and Khin Maung Aye, “Design and Performance Analyses of centrifugal pump”, 2008.
26. Arthur Williams, “Pumps as Turbines – A User’s Guide”, 2003.
27. Theodore Wildi, “Electrical Machines, Drives and Power Systems”, 2002.
28. Nick Jenkins, Ron Allen, Peter Crossley, Daniel Kirschen and Goran Strbac, “Embedded Generation”, 2000.
29. Eskom Distribution, “Distribution Standard for the Interconnection of Embedded Generators”, 2008.
30. City of Anaheim, Public Utilities Department, Electrical Engineering, “Guidelines for Interconnection of Customer Generators”, 2005.
31. BC Hydro, “Net Metering Interconnection Requirements, 50 kW & Below”, 2003.
32. ENMAX Power Corporation, “Guide for Generator Interconnection to the Wires Owner Distribution System”, 2004.
33. Salt River Project, “Interconnection Guidelines for Distributed Generators”, 2000.
34. “South African National Standard’s Wiring Code (SANS 10142-1:2003)”, 2003.
35. Eskom, 2009.
36. South African Weather Services, 2007.
37. Personal Communication, Mac Jordaan (owner) and George Visser, 2007.

## Appendix A Preliminary Site Studies and Environmental Aspects

### A.1. Assegaibos River Flow Measurements

The actual flow rate measurements of the Assegaibos River at Waterval are presented in this section. Measurements obtained from using a thin-plate weir are presented in Table A.1 and those obtained from using a float are shown in Table A.2. The symbols used in these tables refer to those used in the flow measurement setup illustrations in Figures 7 and 8 in Chapter 2.3.2.

The thin plate weir was not build into the river as it was only a temporary structure. Sand bags were used to support the structure and their purpose was also to provide the necessary seal between the riverbed and the weir plate. There was however a little leakage flow between the weir plate and the riverbed which was very difficult to measure, hence the river flow rate during this time is estimated at about 40 l/s.

The distance over which a float is timed in order to calculate the flow rate of the river was very short. The reason for this is that the characteristics of the river are such that only very short straight parts exist where the float for a specific measuring point across the river remains flowing parallel to the length of the river. This method was carried out where the riverbed is pure smooth rock; hence a velocity correction factor of 0.85 is used from Table 1 in chapter 2.3.2. By multiplying this with the calculated flow in Table A.2, the real flow is calculated as 38.3 l/s.

**Table A.1: Flow rate measurements using the thin-plate weir method.**

Reading Number	Date	Time	Height of the water over the crest, $h_{weir}$ [m]	Flow rate through the weir, $Q$ [l/s]
1	6/03/2009	11h00	0.241	38.9
2	6/03/2009	14h00	0.242	39.3
3	6/03/2009	17h00	0.242	39.3
4	7/03/2009	08h00	0.243	39.7
5	7/03/2009	11h00	0.244	40.2
6	7/03/2009	14h00	0.243	39.7
7	7/03/2009	17h00	0.242	39.3
8	8/03/2009	08h00	0.242	39.3
9	8/03/2009	11h00	0.241	38.9
10	8/03/2009	17h00	0.242	39.3
<b>Average measured flow rate</b>				<b>39.4</b>

**Table A.2: Flow rate measurements using the velocity-area method.**

Measuring Point	Depth, $d_i$ [m]	Length over which float is timed [m]	Time [s]	Velocity of the particle [m/s]
1	0.03	0.6	1.08	0.56
2	0.19	0.6	1.06	0.57
3	0.23	0.6	1.06	0.57
4	0.13	0.6	1.07	0.56
5	0.09	0.6	1.10	0.55
6	0.05	0.6	1.08	0.56
7	0.01	0.6	1.07	0.56
<b>Spacing between measuring points, <math>\Delta B</math> [m]</b>				0.11
<b>Cross Sectional Area, <math>A</math> [m<sup>2</sup>]</b>				0.08
<b>Average Velocity of the flow [m/s]</b>				0.56
<b>Flow rate without velocity correction factor [l/s]</b>				45.05

These two methods to measure the flow rate were carried out at different locations in the river. The two results correlate well and for all the calculations in this study a minimum river flow rate of 40 l/s is used.

## A.2. Environmental Impact Assessment Process

A diagram presenting all the steps of the EIA process with the applicable minimum times that each activity takes is shown in Figure A.1. This is derived from the actual EIA that has been completed for the MHPS at Waterval.

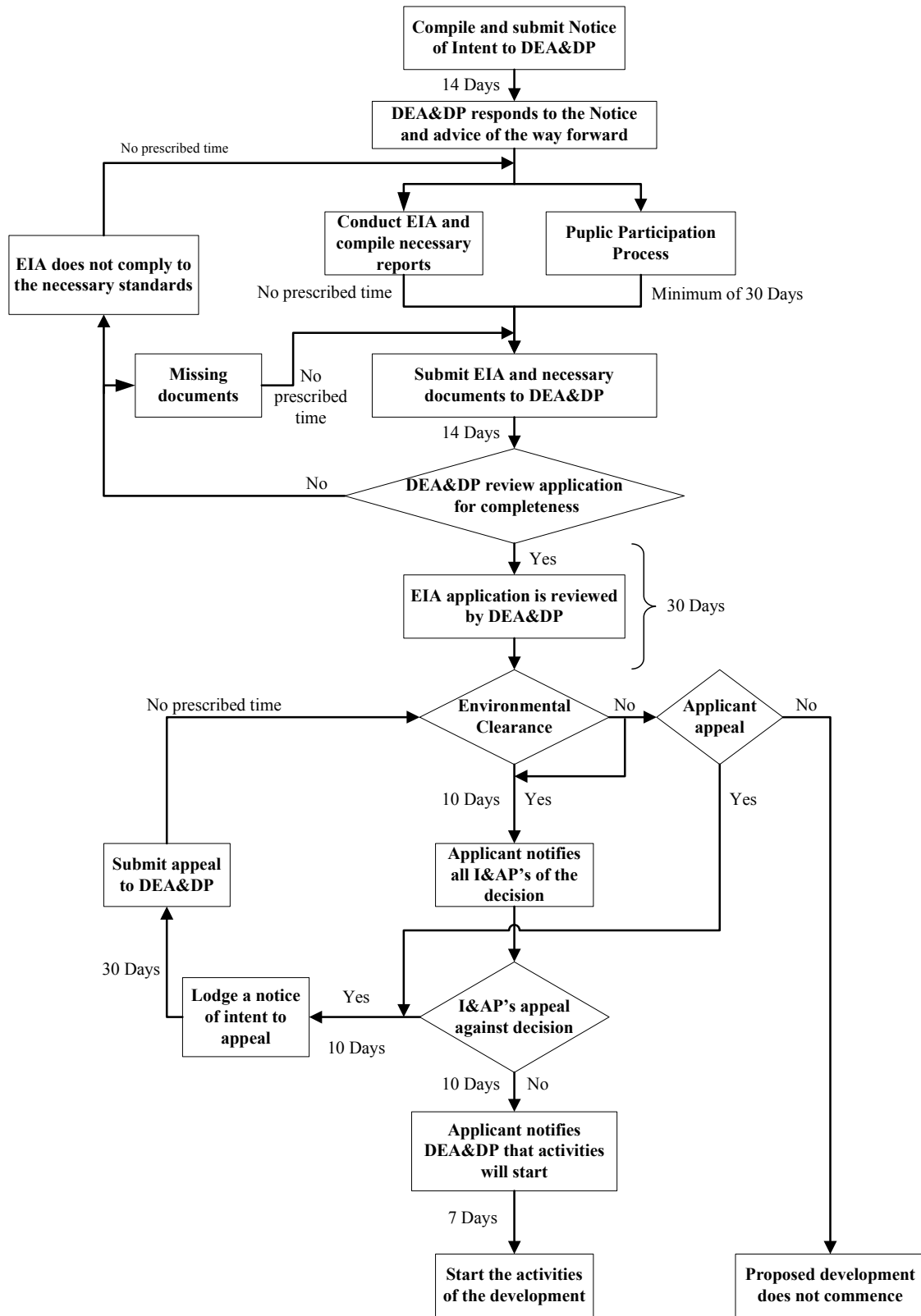


Figure A.1: Flow chart of a Basic Assessment Process and the minimum time the process takes.

## Appendix B Pipeline Design

### B.1. MHPS Design Process

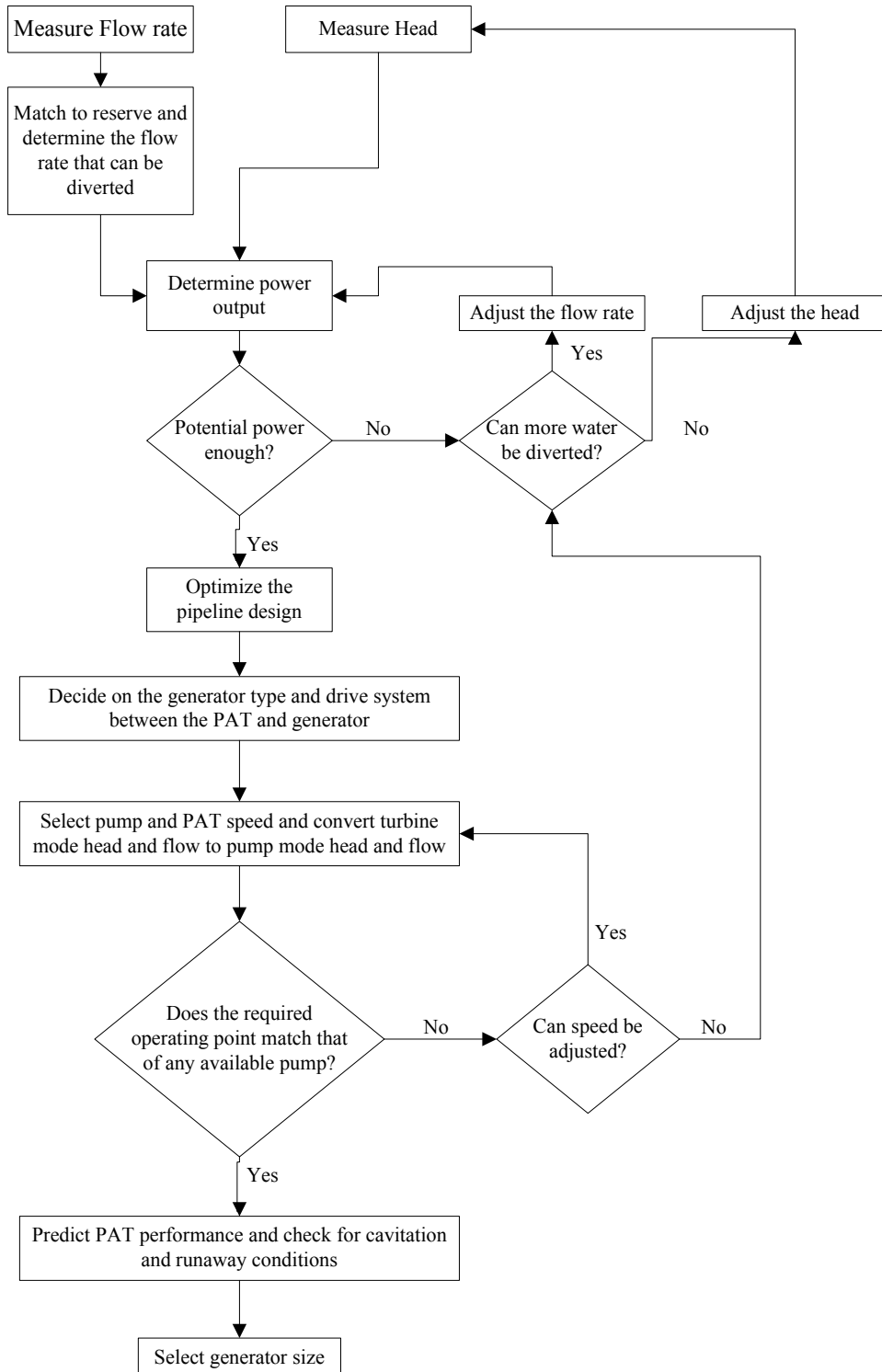


Figure B.1: Diagram of the iterative process used for selecting the appropriate PAT and generator.

## B.2. Pipeline Design Information

General information regarding the pipes considered for the MHPS is presented here. The Hazen Williams loss coefficients for different pipe materials are shown in Table B.1. The wall thickness of different uPVC pipe sizes and the cost of each size are given in Table B.2. Note that the costs presented here are in October 2009.

The minor loss coefficients for the fittings and transitions, which were used for designing the pipeline, are presented in Table B.3. The quantity of fittings used for each of the main pipeline, the manifold line and the draft tube are also shown. The loss coefficient of the Pressure Sustaining Valve is supplied by the manufacturers of this valve. Note that the loss coefficients of this valve and the gate valves are a minimum when they are fully open, but as they close, these coefficients increase to infinity [23].

**Table B.1: Values of the Hazen Williams coefficient [21].**

Type of Pipe	C
New or extremely smooth	140
Very smooth	130
Newly riveted steel	110
Old riveted steel	100
Old cast iron	95
Deteriorated pipes	60 - 80

**Table B.2: uPVC pipe sizes and costs [Petzetakis, 2009].**

Nominal diameter (mm)	Class 9 (Capable of withstanding a pressure of 9 bar)		
	Wall thickness (mm)	Inside diameter (mm)	Cost (ZAR)
110	4.15	101.7	R 55.00 / m
125	4.7	115.6	R 79.00 / m
140	5.2	129.6	R 98.00 / m
160	5.95	148.1	R 117.00 / m
200	7.45	185.1	R 182.00 / m
250	9.2	231.6	R 273.00 / m

**Table B.3: Loss coefficients for fittings used in the whole pipeline [10, 20 - 22].**

Fitting	K-Value	Main Pipeline		Manifold Line		Draft Tube	
		Quantity	Total	Quantity	Total	Quantity	Total
Inward projecting entrance 	0.8	1	0.8				
Top Gate valve (Fully open) Bottom Gate valve (Fully open) 	0.12 0.14	1	0.12	1	0.14		
Pressure sustaining valve (Fully open) 	5.4			1	5.4		
90° Bend 	0.19	3	0.57				
45° Bend 	0.09	24	2.16			1	0.09
Tee (In-line) 	0.4			1	0.4		
Gradual contraction (160 mm – 110 mm) Gradual contraction (110 mm – 50 mm) 	0.055 0.065	1	0.055	1	0.065		
Gradual expansion (65 mm – 110 mm) 	0.04					1	0.04
Outlet 	1						
<b>Sum of K-Values</b>			<b>3.705</b>		<b>6.005</b>		<b>0.13</b>

## Appendix C Turbine Design

### C.1. PAT Selection Diagrams

All the diagrams necessary to select a radial flow PAT and to predict its performance as discussed in Section 4.4 are presented in this section. The pump mode performance diagram of the first considered pump (ETA 50-200) as well as the selected pump (ETA 50-160) is also presented.

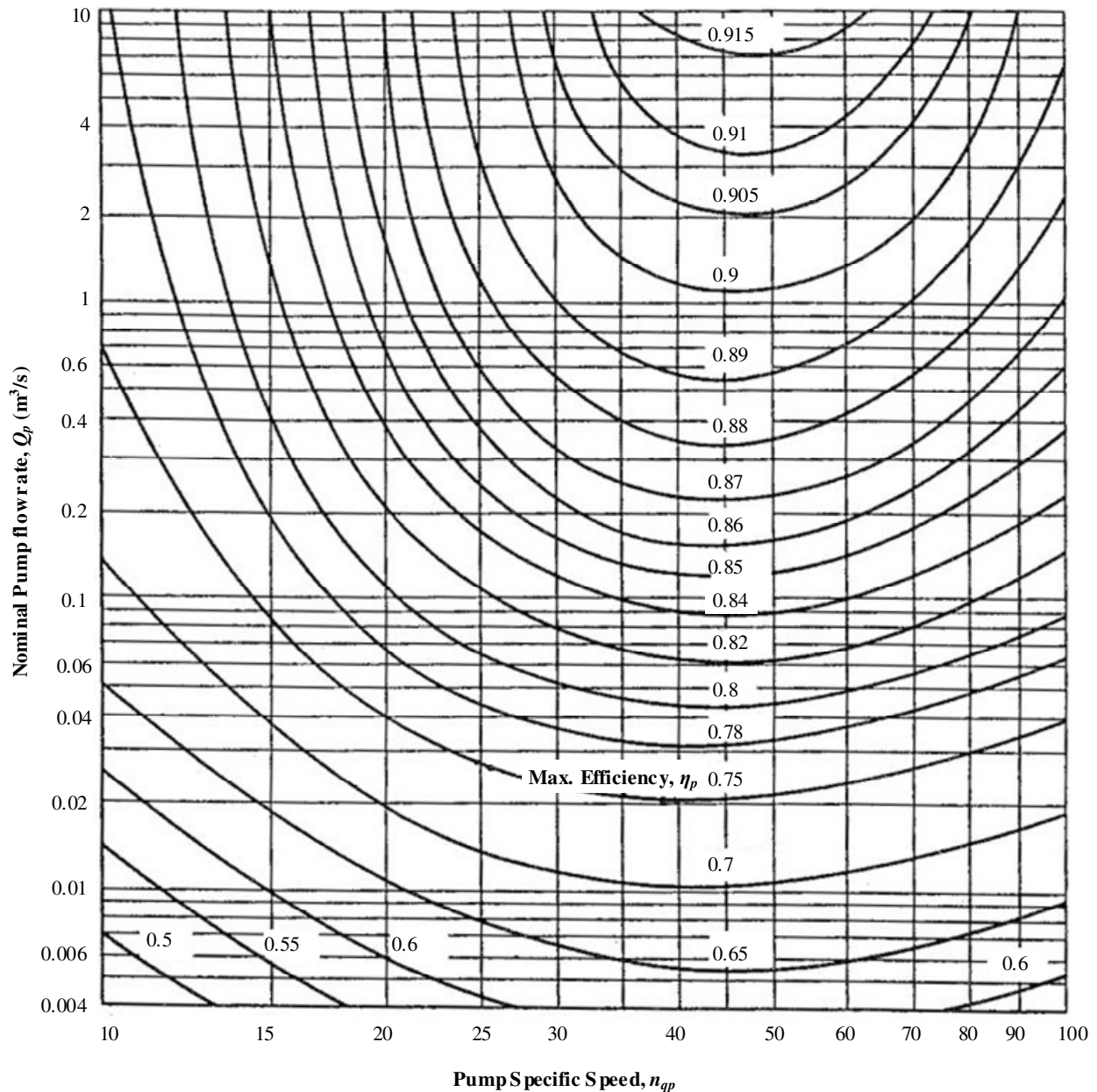


Figure C.1: Maximum pump-mode efficiency as a function of pump-mode specific speed and flow rate [23].

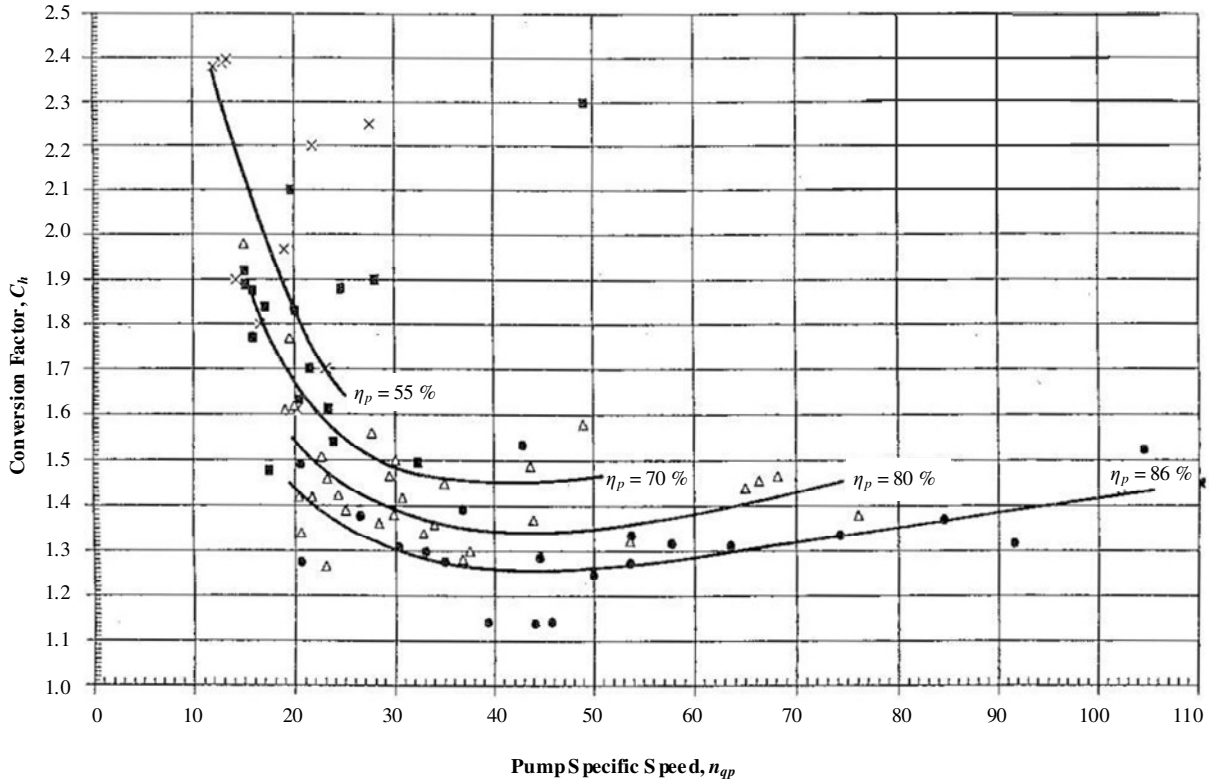


Figure C.2: Head conversion factor [23].

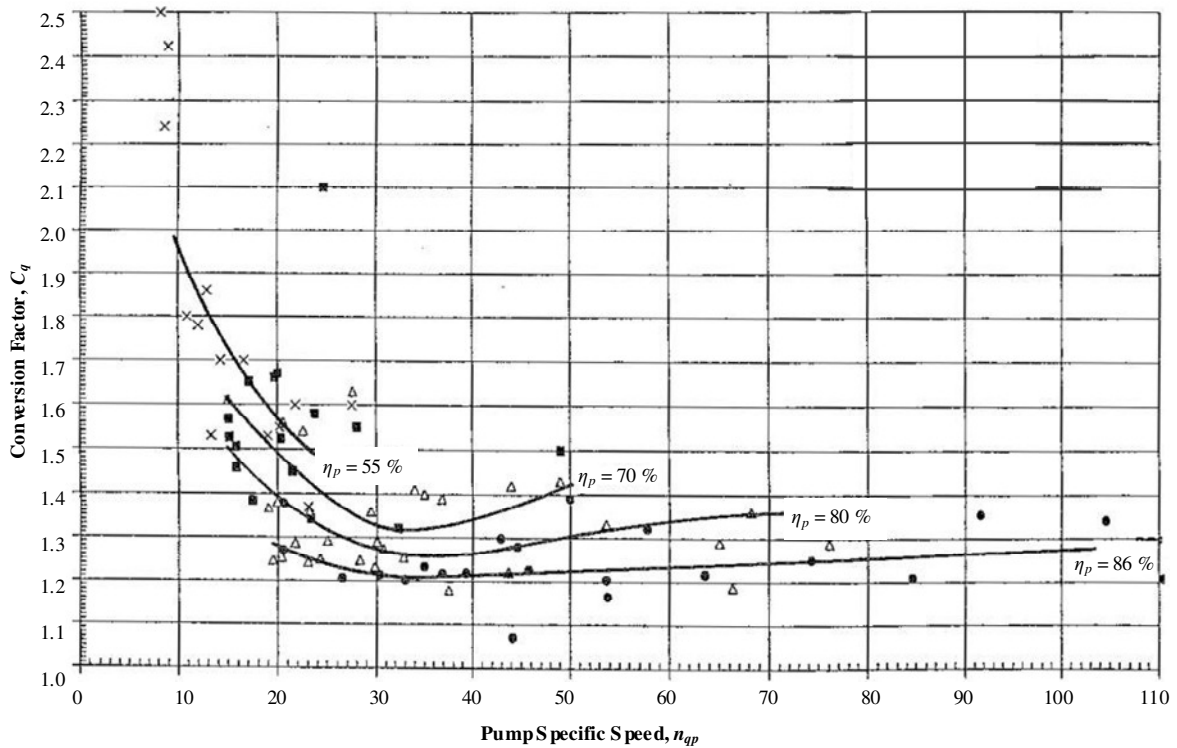


Figure C.3: Flow rate conversion factor [23].

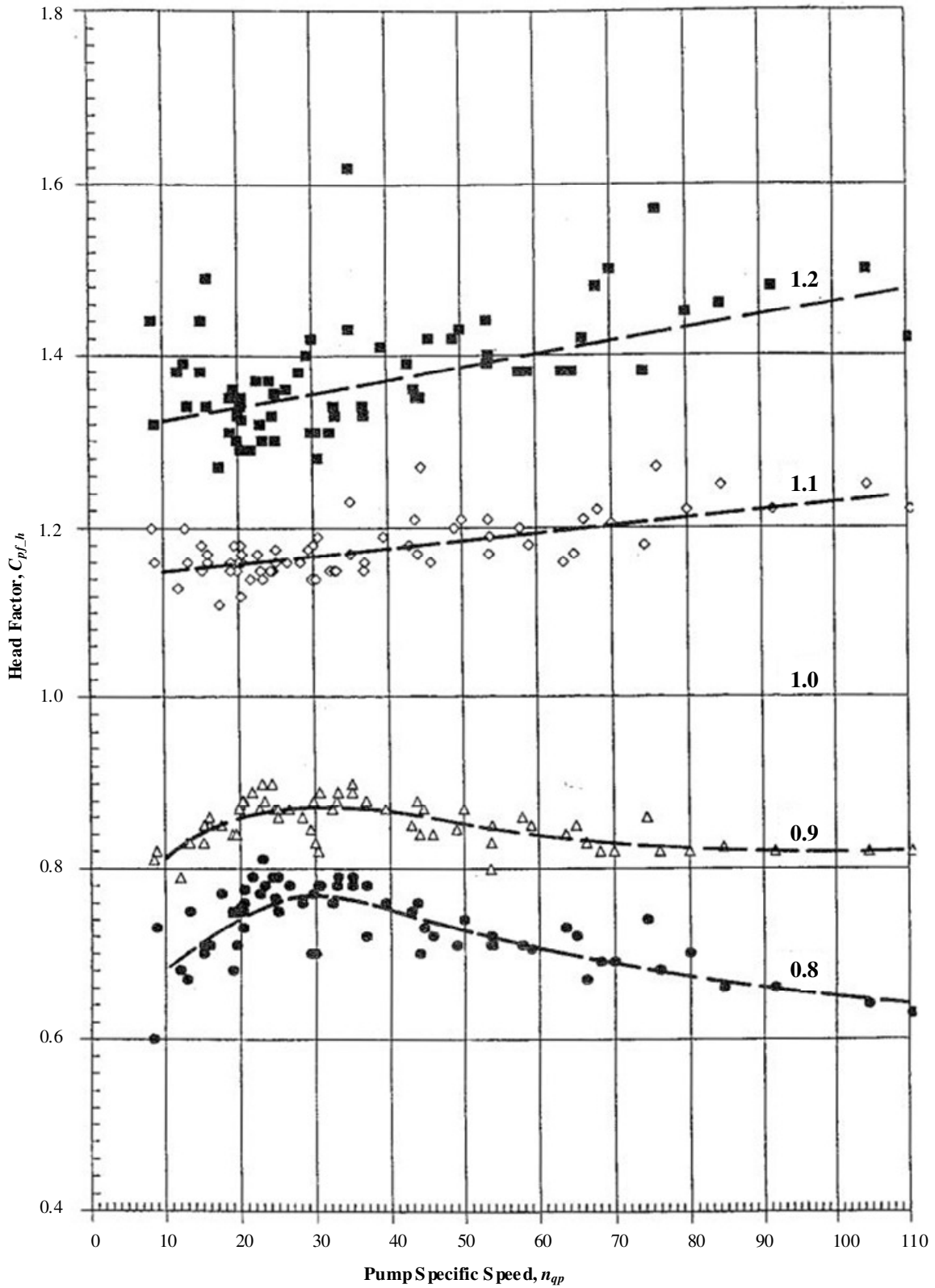


Figure C.4: Head correction factor for PAT performance away from the BEP [23].

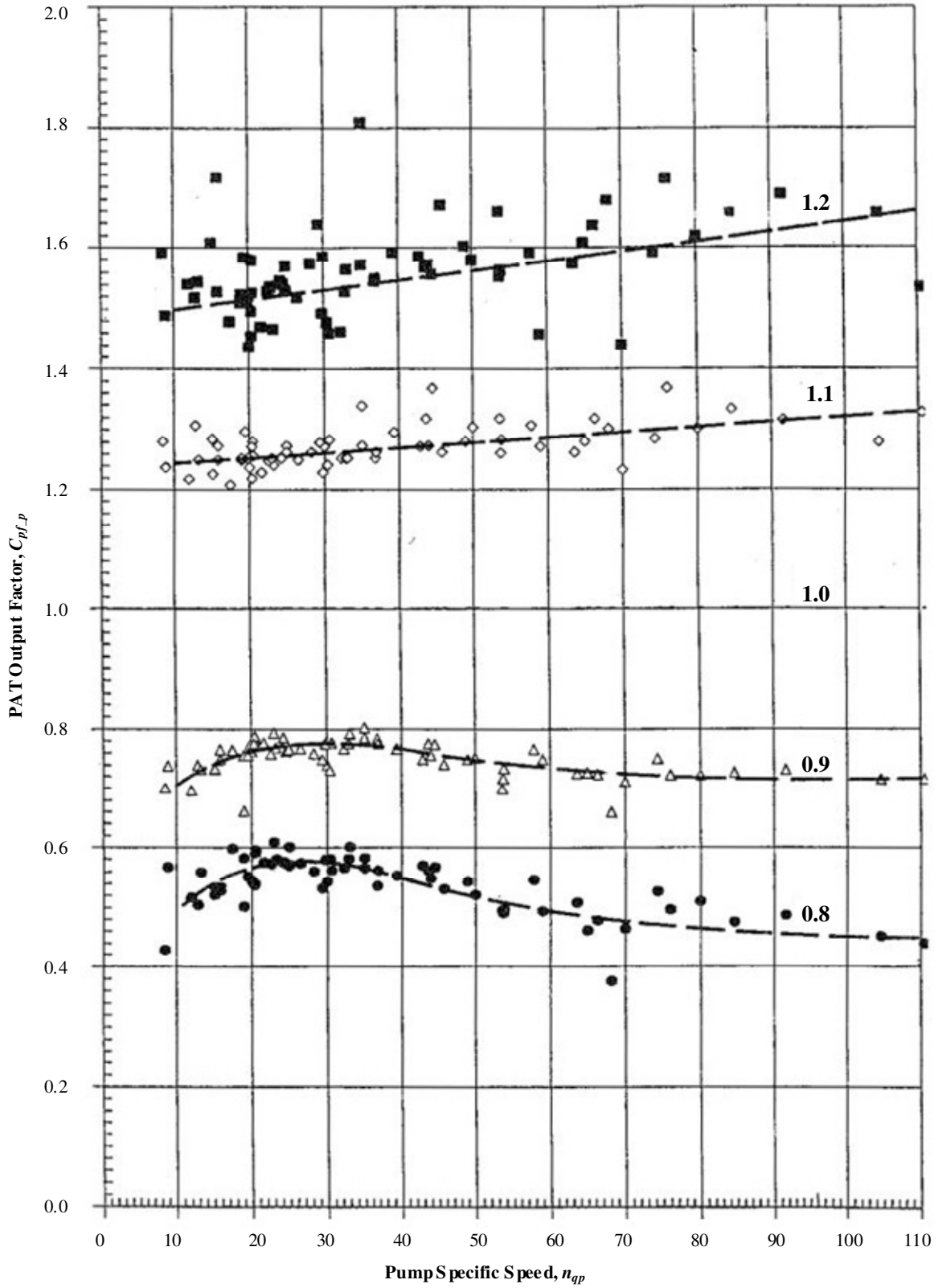


Figure C.5: Power output correction factor for PAT performance away from the BEP [23].

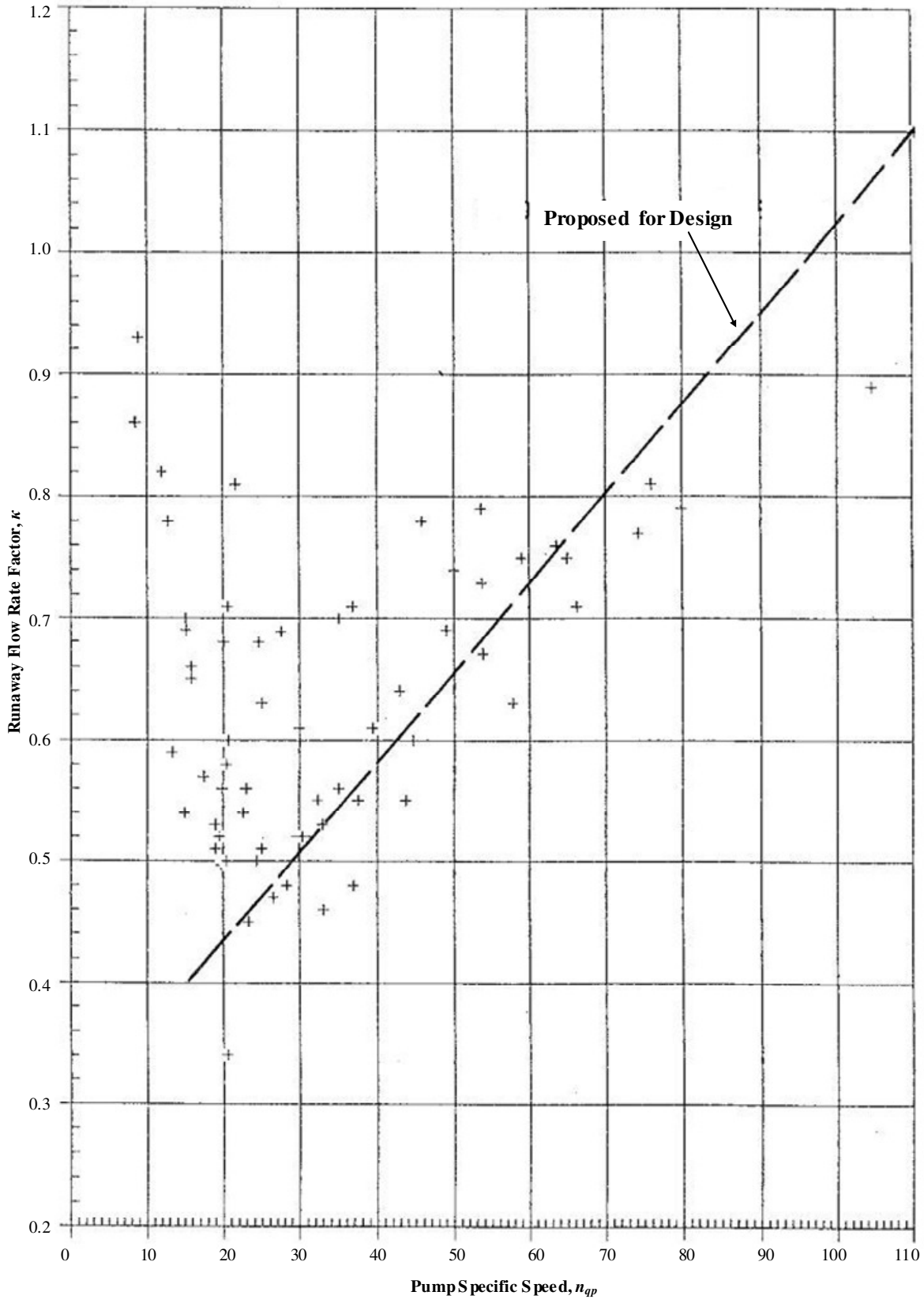
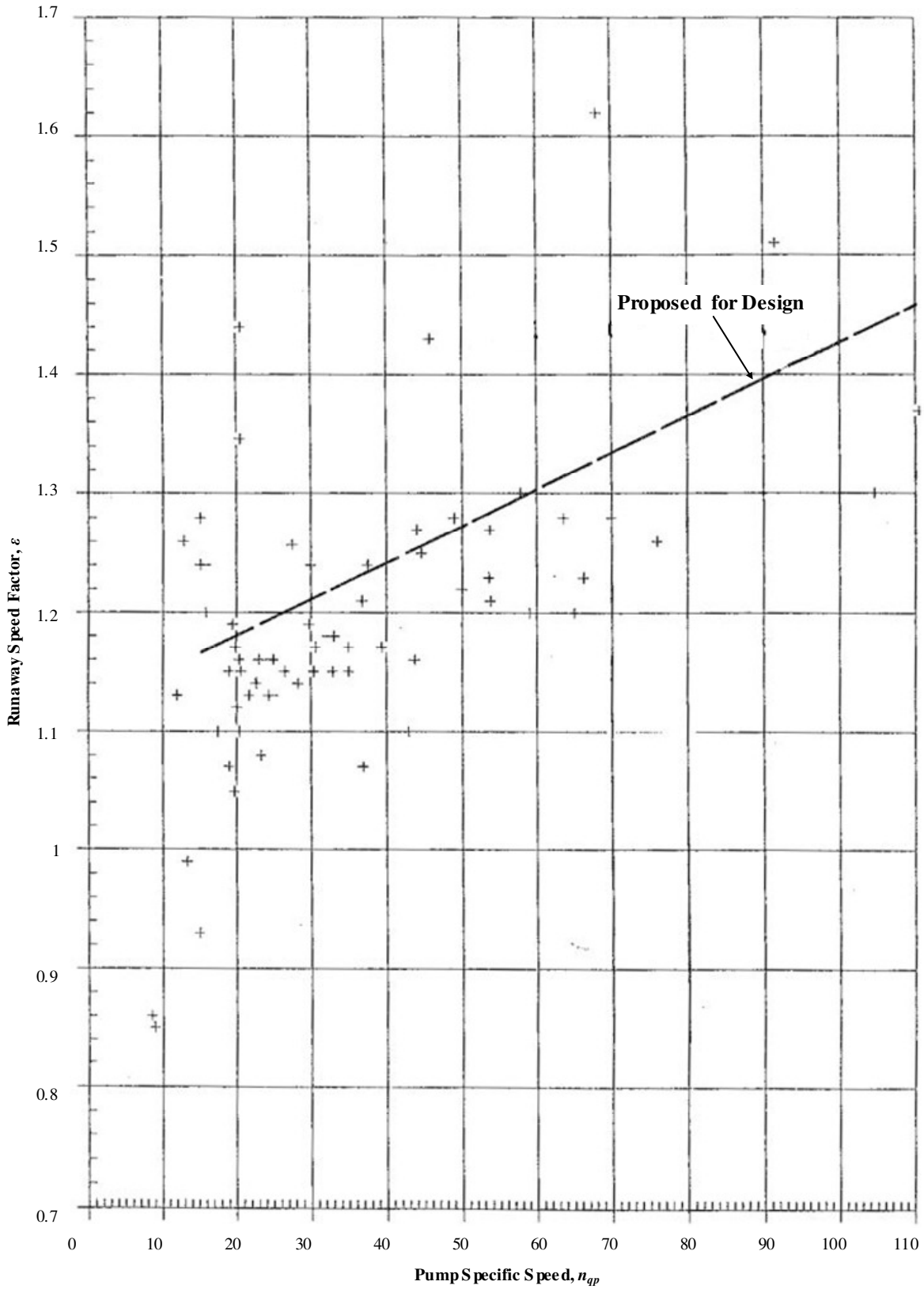


Figure C.6: Pump runaway flow rate at rated pump head [23].



It is evident from this pump performance curve that the impeller of this pump will have to be trimmed to operate at the desired operating point, with the pump then only having an efficiency of 69 %. It is also clear that if this pump is selected, it will not operate slightly beyond the BEP flow rate, hence the turbine mode efficiency can be very low [22].

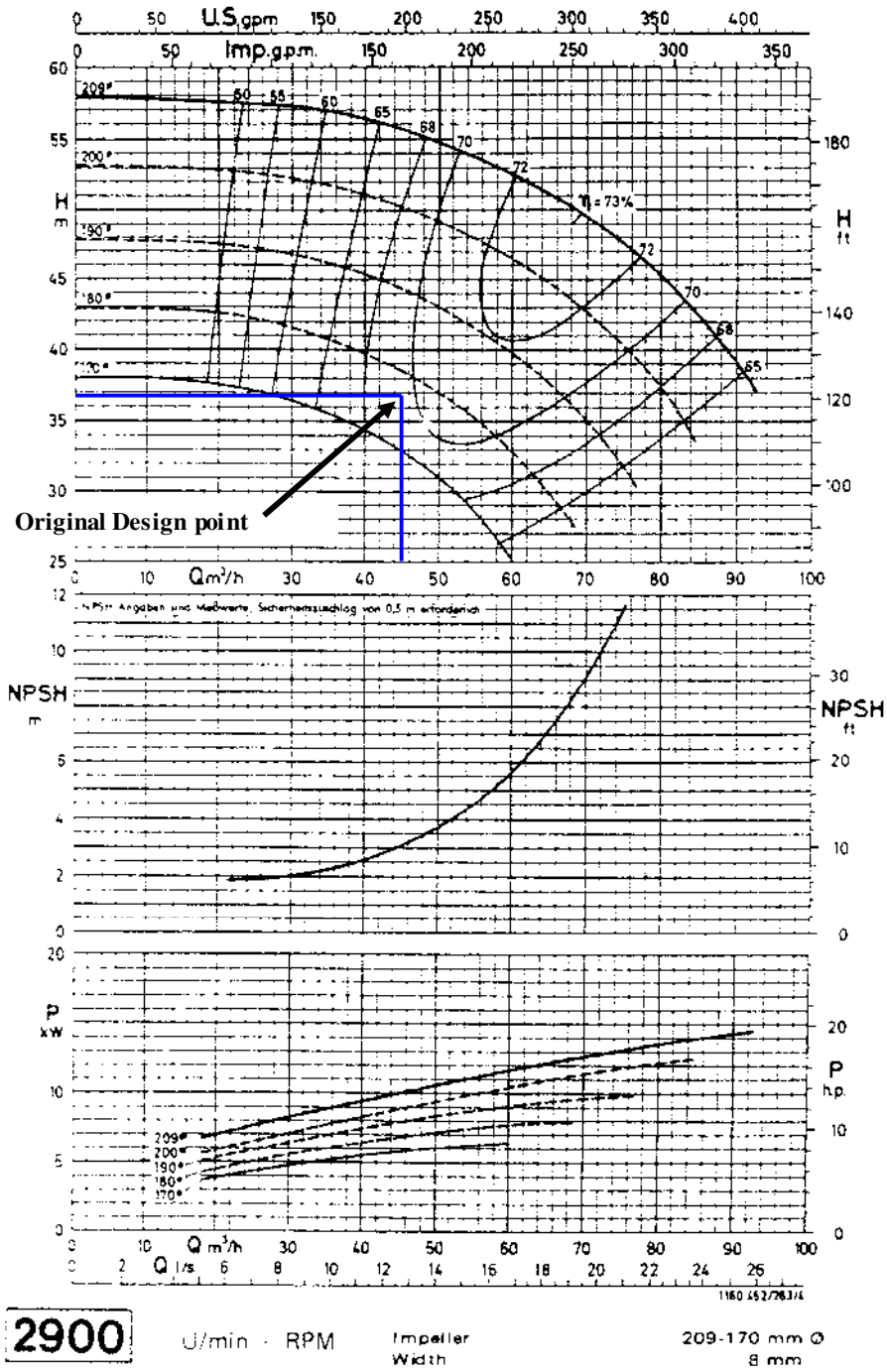


Figure C.8: Pump performance curve of the KSB ETA 50-200 pump.

The model ETA 50-160 pump is the only other option for the MHPS at Waterval. From the performance diagram below, it is clear that the flow rate of the original operating point is still not beyond the BEP flow rate of the machine. As discussed in chapter 4.4.2, the operating point is adjusted as shown.

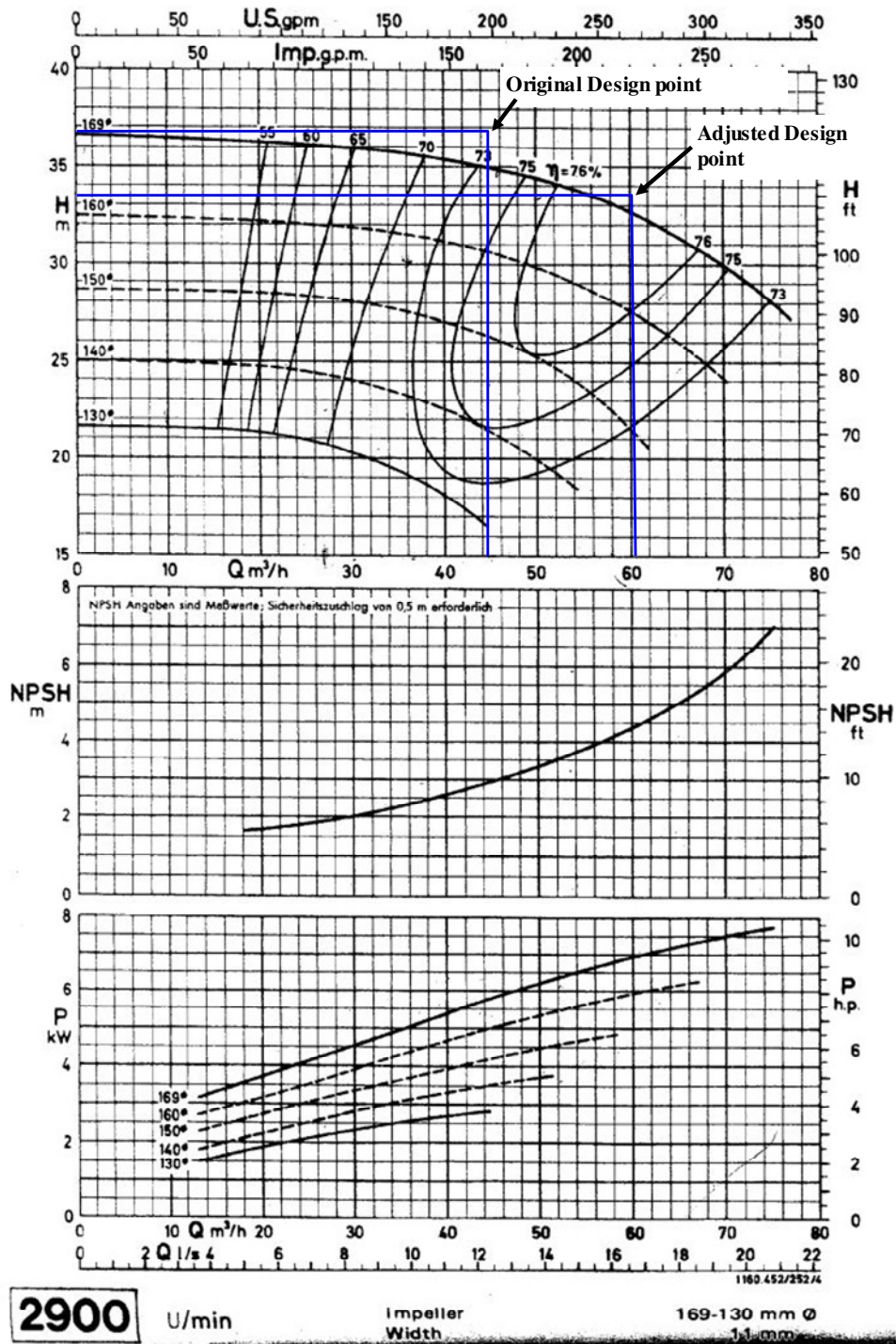


Figure C.9: Pump mode performance diagram of the selected pump (KSB ETA 50-160 pump).

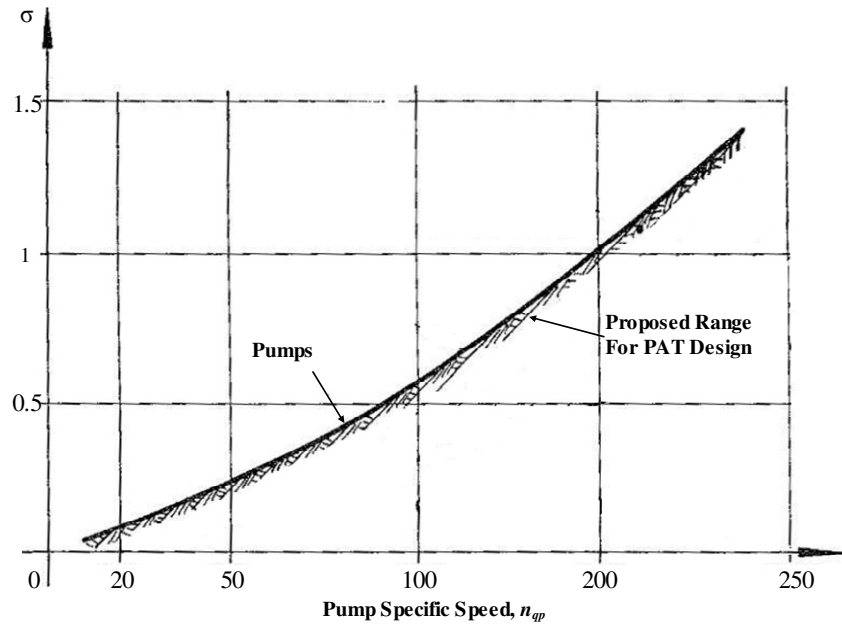


Figure C.10: Thoma number used to analyse cavitation on pumps and PATs [23].

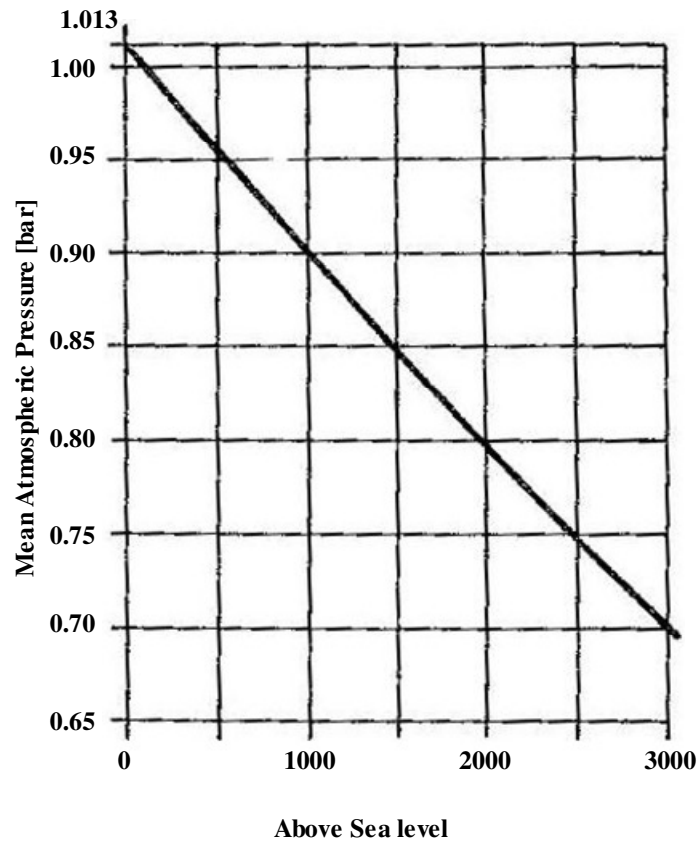


Figure C.11: Atmospheric pressure variation with height above sea level [23].

## C.2. Analytical Results of Selecting the PAT for the MHPS at Waterval

**Table C.1: Analytical results of the PAT selection process for the MHPS at Waterval.**

Parameter	Value
Selected turbine-mode available head, $h_t$	72.02 m
Selected turbine-mode available flow rate, $Q_t$	20 l/s
Selected turbine-mode speed, $n_t$	3 080 rpm
Turbine-mode specific speed, $n_{qt}$ , (Eq. 4.14)	17.62
Pump-mode specific speed, $n_{qp}$ , (Eq. 4.15)	19.80
Rated pump-mode flow rate, $Q_p$ , (Eq. 4.16)	15.4 l/s
Efficiency from Figure C.1	67.5 %
Head conversion factor from Figure C.2, $C_h$	1.72
Flow rate conversion factor from Figure C.3, $C_q$	1.52
Selected pump-mode speed, $n_p$	2 900 rpm
Pump-mode head at rated pump speed, $h_p$ , (Eq. 4.17)	37.15 m
Pump-mode flow rate at rated pump speed, $Q_p$ , (Eq. 4.17)	12.4 l/s
<b>Selected model: KSB ETA 50-160; <math>n_p = 2\ 900</math> rpm</b>	
BEP pump-mode head, $h_{ps}$	32.6 m
BEP pump-mode flow rate, $Q_{ps}$	16.67 l/s
Pump-mode maximum efficiency, $\eta_{ps}$	76.5 %
Pump mode specific speed of selected pump, $n_{qps}$ , (Eq. 4.18)	27.47
Head conversion factor of the selected pump from Figure C.2, $C_{hs}$	1.45
Flow rate conversion factor of the selected pump from Figure C.3, $C_{qs}$	1.325
BEP turbine-mode head of the selected pump, $h_{ts\_BEP}$ , (Eq. 4.19)	52.32 m
BEP turbine-mode flow rate of the selected pump, $Q_{ts\_BEP}$ , (Eq. 4.19)	23.45 l/s
Maximum turbine-mode head of the selected pump, $h_{ts\_max}$ , (Eq. 4.20)	57.55 m
Minimum turbine-mode head of the selected pump, $h_{ts\_min}$ , (Eq. 4.20)	47.09 m
Maximum turbine-mode flow rate of the selected pump, $Q_{ts\_max}$ , (Eq. 4.20)	25.2 l/s
Minimum turbine-mode flow rate of the selected pump, $Q_{ts\_min}$ , (Eq. 4.20)	21.7 l/s
Maximum turbine mode efficiency of the selected pump, $\eta_{ts}$	73.5 %
Maximum turbine mode power of the selected pump, $P_{ts\_max}$ , (Eq. 4.21)	10.46 kW
Minimum turbine mode power of the selected pump, $P_{ts\_min}$ , (Eq. 4.21)	7.36 kW
	<b>Part flow conditions, <math>C_{pf}</math></b>
	<b>0.8      0.9      1      1.1      1.2</b>
Head factor from Figure C.4, $C_{pf\_h}$	0.77      0.87      1      1.16      1.35

PAT output factor from Figure C.5, $C_{pf-p}$	0.58	0.77	1	1.26	1.52				
<b>Maximum values</b>									
Flow rate ( $Q_{ts\_max} \times C_{pf}$ )	20.16	22.7	25.2	27.72	30.24				
Head ( $h_{ts\_max} \times C_{pf-h}$ )	44.32	50.07	57.552	66.76	77.7				
PAT output power ( $P_{ts\_max} \times C_{pf-p}$ )	6.07	8.05	10.46	13.18	15.9				
<b>Minimum values</b>									
Flow rate ( $Q_{ts\_min} \times C_{pf}$ )	17.36	19.53	21.7	23.87	26.04				
Head ( $h_{ts\_min} \times C_{pf-h}$ )	36.25	40.97	47.09	54.62	63.6				
PAT output power ( $P_{ts\_min} \times C_{pf-p}$ )	4.27	5.67	7.36	9.27	11.2				
<b>Runaway conditions</b>									
Runaway flow rate factor, $\kappa$ , from Figure C.6					0.49				
Runaway speed factor, $\varepsilon$ , from Figure C.7					1.205				
<b>Runaway factor of pump mode head, <math>h_{psrf}</math></b>									
Runaway factor of pump mode head, $h_{psrf}$	0	0.05	0.4	0.8	1	1.2	1.6	2	2.5
Runaway head, $h_{tsr}$ , ( $h_{ps} \times h_{rf}$ )	0	1.63	13.0	26.1	32.6	39.1	52.2	55.2	81.5
Runaway flow rate, $Q_{tsr}$ , (Eq. 4.22)	0	1.83	5.2	7.31	8.17	8.95	10.3	10.6	12.9
Runaway head, $h_{tsr}$ , from Figure 23								72.5 m	
Runaway flow rate, $Q_{tsr}$ , from Figure 23								12 l/s	
Runaway speed, $n_{tsr}$ , (Eq. 4.23)								5 211 rpm	

Table C.2: Vapour pressure variation with temperature [23].

Temperature (°C)	Density (kg/m <sup>3</sup> )	Vapour pressure (N/m <sup>2</sup> )
0	999.9	611
5	1000	872
10	999.7	1 228
20	998.2	2 338
30	995.7	4 243
40	992.2	7 376

## Appendix D Electrical Design

### D.1. Voltage Drop Information

Table D.1: Voltage drop of multicore PVC insulated cables [SANS 10142-1:2003].

Conductor cross-sectional area [mm <sup>2</sup> ]	Three / Four core, three phase a.c. copper [mV/A/m]
1.5	29
2.5	18
4	11
6	7.3
10	4.4
16	2.8

### D.2. Electrical Wiring Layout Diagrams

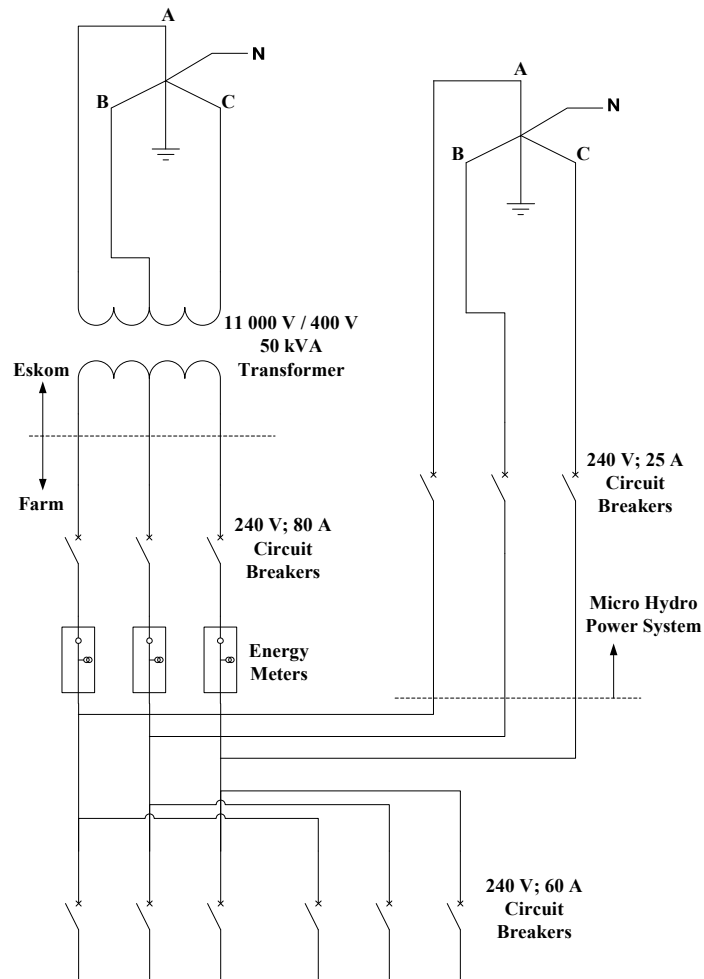


Figure D.1: Electrical wiring diagram of the distribution board at Waterval.

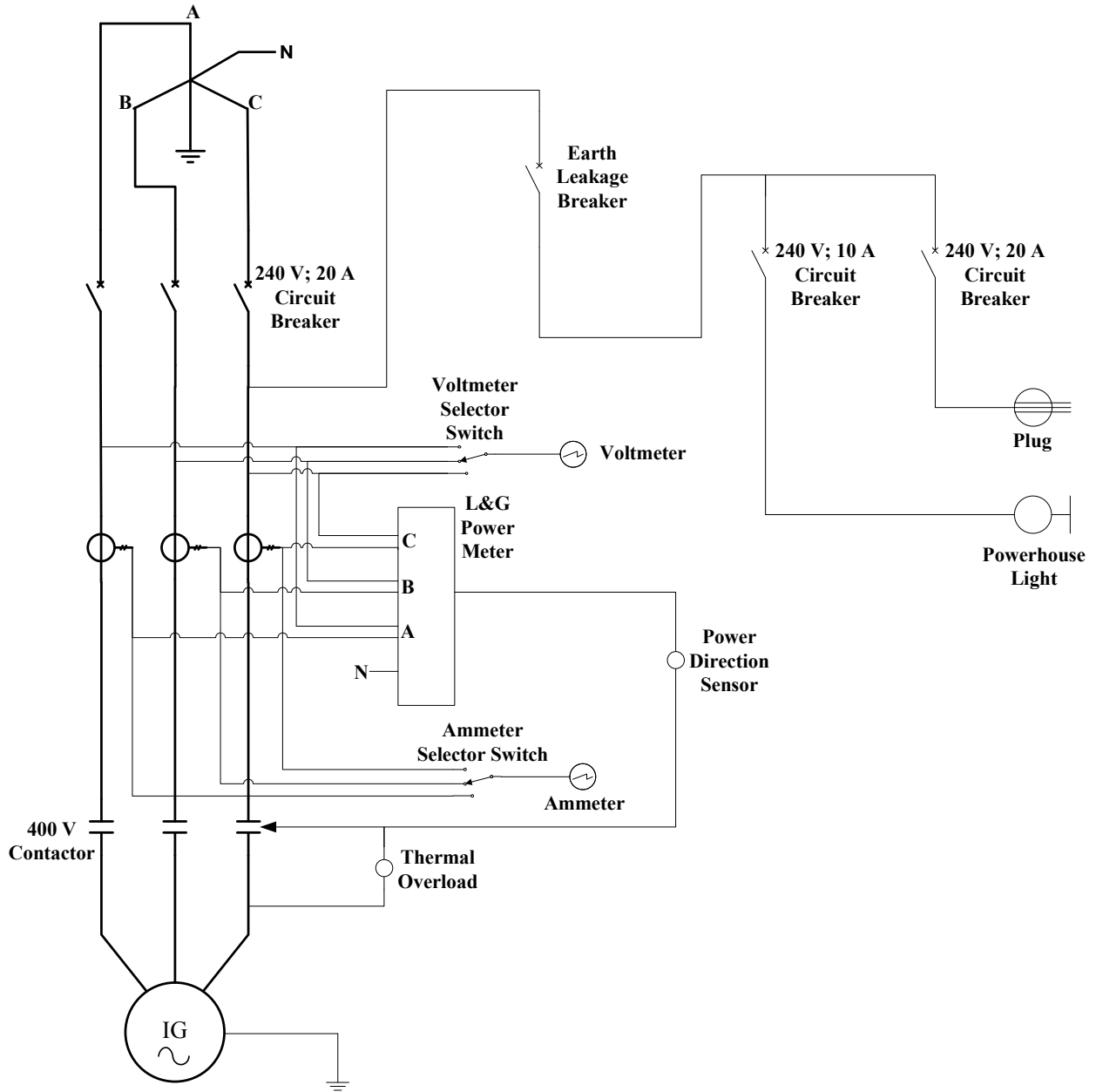


Figure D.2: Electrical wiring diagram of the distribution board in the powerhouse.

## Appendix E Test Results

### E.1. MHPS Layout

An aerial photo of Waterval is shown in Figure E.1. Colour indicators on this figure show the layout of the implemented MHPS.

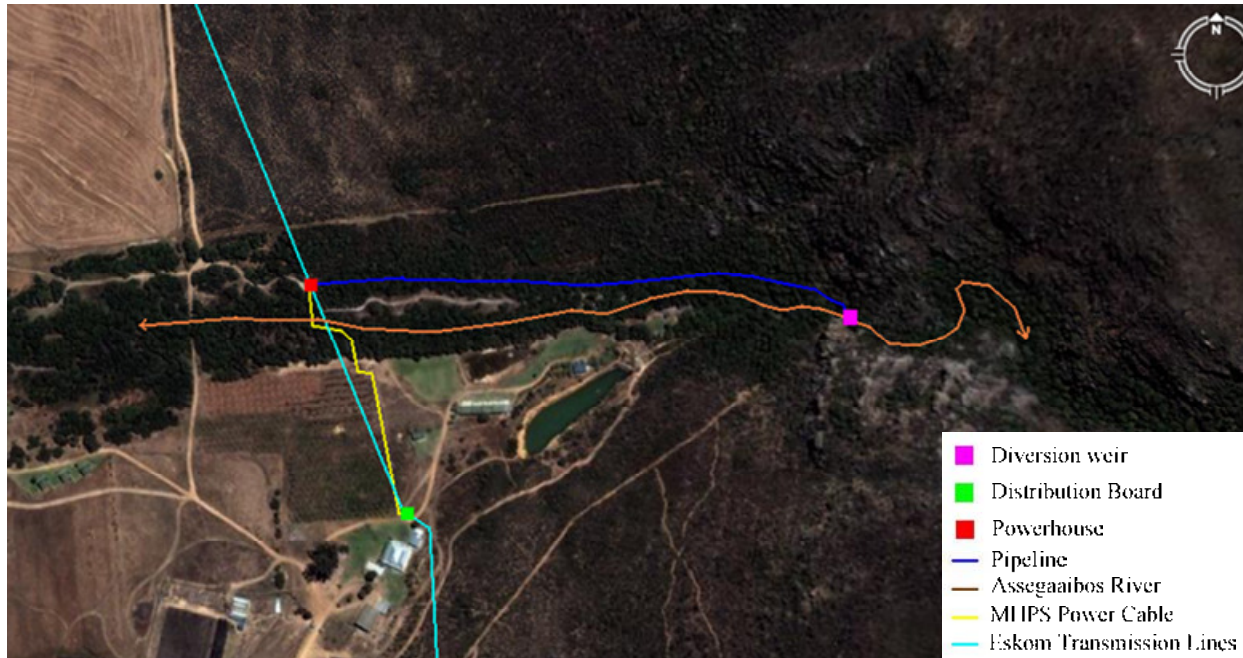


Figure E.1: MHPS layout at Waterval.

### E.2. MHPS Test Results

The test results of the MHPS, for both no-load and full load are presented in table format in Tables E.1 and E.2 hereafter.

Table E.1: PAT No-load Test Results.

No-load Test (20 March 2009)											Height of pressure gaugue considered
Nr.	P <sub>1</sub> (Bar)	P <sub>2</sub> (Bar)	P <sub>PRV</sub> (Bar)	P <sub>PSV</sub> (Bar)	Vol (l)	Time (s)	Q (l/s)	n <sub>s</sub> (rpm)	T <sub>s</sub> (N.m)	P <sub>2</sub> (m)	
1.0	8.0	0.0	0.0	0.0	0.0	0.0	0.0	0.0	0.0	0.1	
2.0	8.0	0.6	1.0	0.6	20.0	4.5	4.5	1372.0	0.4	6.1	
3.0	7.9	1.4	1.8	1.4	16.3	3.1	5.2	2000.0	0.5	13.6	
4.0	7.9	2.1	2.6	2.1	15.7	2.1	7.3	2500.0	0.8	21.1	
5.0	7.9	3.1	3.6	3.1	21.1	2.4	8.8	3000.0	0.9	31.1	
6.0	7.8	4.2	4.7	4.2	28.1	2.5	11.1	3488.0	1.2	42.1	
7.0	7.8	5.6	6.0	5.6	27.6	2.2	12.7	4012.0	1.4	56.1	
8.0	7.8	6.9	7.4	6.9	34.1	2.4	14.1	4473.0	1.6	69.1	
9.0	7.8	7.1	7.4	7.0	26.6	1.9	14.3	4500.0	1.5	71.1	

Table E.2: PAT Load Test Results.

Load Test (20 March 2009)													
Nr.	P <sub>1</sub> (Bar)	P <sub>2</sub> (Bar)	P <sub>PRV</sub> (Bar)	P <sub>PSV</sub> (Bar)	Vol (l)	Time (s)	Q (l/s)	P <sub>PAT</sub> (kW)	n <sub>s</sub> (rpm)	T <sub>s</sub> (N.m)	P <sub>shaft</sub> (kW)	P <sub>G Inst</sub> (kW)	Q <sub>G Inst</sub> (kVAR)
1	8.0						0.0						
2	8.0						4.5						
3	7.9						5.2						
4	7.9						7.3						
5	7.9	3.2	7.5	3.0	19.5	1.9	10.5	3.3	3000.0	1.7	0.5	0.0	3.6
6	7.9	3.4	7.4	3.2	31.5	2.7	11.7	3.9	3012.0	5.0	1.6	0.9	3.8
7	7.8	3.6	7.3	3.4	27.2	2.0	13.6	4.8	3022.0	8.5	2.7	2.1	4.0
8	7.7	4.0	7.3	3.8	48.4	2.6	18.6	7.3	3034.0	14.0	4.4	3.5	4.4
9	7.6	4.3	7.2	4.1	35.0	1.7	20.8	8.7	3054.0	16.5	5.3	4.5	4.8
10	7.6	4.7	7.1	4.5	38.9	1.8	21.5	9.8	3068.0	21.2	6.8	5.8	5.2
11	7.5	5.1	7.0	4.8	40.2	1.7	23.1	11.5	3081.0	24.4	7.9	6.7	5.6
12	7.4	5.5	7.0	5.3	40.8	1.7	23.8	12.9	3093.0	29.0	9.4	8.0	6.5
13	7.3	6.1	6.9	5.9	47.0	1.7	27.8	16.5	3108.0	34.1	11.1	9.4	7.2
14	7.3	6.4	6.9	6.3	53.0	1.8	29.4	18.3	3112.0	37.0	12.1	10.2	7.6

										Pressures with height of gauge considered			
Nr.	PF	S	PF (Calc)	V (V)	I (A)	I (A) (L)	Eff <sub>PAT</sub>	Eff <sub>Gen</sub>	Comb Eff	P <sub>1</sub> (m)	P <sub>2</sub> (m)	P <sub>PRV</sub> (m)	P <sub>PSV</sub> (m)
1										80.1	0.1	0.1	0.1
2										79.7	0.1	0.1	0.1
3										79.3	0.1	0.1	0.1
4										78.9	0.1	0.1	0.1
5	0.0	3.6	0.0	400.0	5.0	5.3	16.1	2.8	0.5	78.7	32.1	74.6	30.1
6	0.2	3.9	0.2	400.0	5.5	5.7	40.2	59.4	23.9	78.6	34.1	74.1	32.1
7	0.5	4.5	0.5	400.0	6.3	6.6	55.8	77.0	43.0	78.1	36.1	73.1	34.2
8	0.6	5.6	0.6	400.0	8.0	8.2	60.7	77.8	47.2	77.1	40.1	72.6	37.6
9	0.7	6.6	0.7	400.0	9.6	9.6	60.9	85.0	51.8	76.2	42.6	72.1	41.1
10	0.7	7.8	0.7	400.0	11.5	11.3	69.7	85.0	59.2	75.6	46.6	71.1	44.9
11	0.8	8.7	0.8	400.0	12.9	12.8	68.2	85.1	58.1	74.9	51.1	70.1	48.1
12	0.8	10.3	0.8	400.0	14.7	14.7	73.1	84.8	62.0	74.1	55.1	70.1	52.6
13	0.8	11.8	0.8	400.0	17.0	16.8	67.2	84.4	56.7	73.1	60.6	69.1	59.1
14	0.8	12.7	0.8	400.0	18.1	18.0	65.7	84.4	55.4	72.6	63.6	69.1	62.6

### E.3. Operational and Maintenance Work

The fully operational MHPS has been monitored for 7 months to determine to what extent maintenance and operational work is required. This required work consists of the following:

- Daily inspection of water levels in the river.
- Daily inspection of the preset operating point of the MHPS.
- Monthly cleaning of the filters on the hydraulic valves.
- Monthly cleaning of the intake.
- Weekly checking of the oil level of the PAT, as it serves as lubrication for the bearings in the PAT.
- Monthly inspection of the above ground part of the pipeline. It should also be inspected after heavy rainfalls as rock slides may occur.

- Replacing the gland packing in the PAT. This is very much dependent on how stiff the packing has been set. If the pump is continuously operated at full load, with its packing stiffness set correctly so that it lets through about two or three drops of water every second, the packing should last for about 4 months.
- Bearings in the generator are self lubricated. Bearings only need to be replaced upon failure. It is impossible to predict the lifetime of the bearings since this depends on various factors such as vibration, temperature, loading etc.

The above work is of such a nature that no technical qualifications are needed to do it. Hence the work can be done by the owner himself or one of his employees and thus there is no need for permanent MHPS operating personnel.

## Appendix F Economic Study of the MHPS

### F.1. O&M Costs

From the information given in Appendix E.3, it is deduced that the only O&M costs involved in the MHPS are the costs of the parts that need to be replaced as well as the lubricating oil that is necessary for the PAT. The MHPS uses one small tub of oil per month and the packing of the PAT is replaced every three to four months. No bearing failures have yet been detected, but a conservative assumption is that the bearings of both the PAT and the generator will have to be replaced every two years. A summary of these costs are presented in Table F.1.

The total O&M costs for two years is R698 and the total O&M cost over the lifetime of 20 years is R6 980. Accordingly, the average annual O&M costs are calculated as R349. It is assumed that the real escalation rate of these O&M costs, for all the future years of the project's lifetime, is 0 %. This means that the difference between the nominal escalation rate of the O&M costs and inflation is zero.

**Table F.1: Summary of the O&M costs of the MHPS at Waterval.**

	Replacement Intervals	Cost [ZAR]	Annual Costs [ZAR]	Additional Costs every second year [ZAR]
Oil	Once every month	14.17	170	
Packing	Once every three months	13.50	54	
Generator Bearings	Once every two years	60.78		61
PAT Bearings	Once every two years	188.12		189
<b>Total annual O&amp;M Costs</b>			<b>224</b>	<b>250</b>

### F.2. Electricity Escalation Rate

The electricity tariff escalation rate assumption for the next 20 years is based on considering the historical relation between the inflation rate and the escalation rate of electricity from 1988 to 2010. These nominal values are presented in Figure F.1. Note that these are all nominal values and that the electricity escalation rate for 2009 represents the actual increase and a projected value for 2010 [35]. The inflation rates for 2009 and 2010 are projected values.

To gain a better understanding of the historical relation between these two variables an index has been developed that is presented in Figure F.2. The index represents compound values

for both the Consumer Price Index (CPI) and the electricity escalation rate, which are then annually increased with the respective values shown in Figure F.1. In the index, it is clearly shown that in real terms, the price of electricity has always been lower than in 1987. Due to the massive price hikes as from 2008, the electricity tariff index has overtaken the CPI and for the first time electricity has become more expensive. To predict the values of future escalation rates is impossible. However, for Eskom to get the necessary funding for new developments to meet an ever increasing electricity demand and to cover O&M costs, it is likely that for the next few years, the escalation rate of electricity tariffs will be greater than or at least equal to inflation. This is proved by the fact that Eskom has recently requested average annual price hikes of 45 % over the next three years, but none of these requested hikes has yet been approved. Taking the index in Figure F.1 and the above discussion into consideration, for the purpose of this study, it is assumed that the tariffs will increase with a nominal average of 31.5 % for 2010. From 2011 and onwards it is assumed that the electricity escalation rate will at least be equal to inflation, hence the real electricity escalation rate being zero.

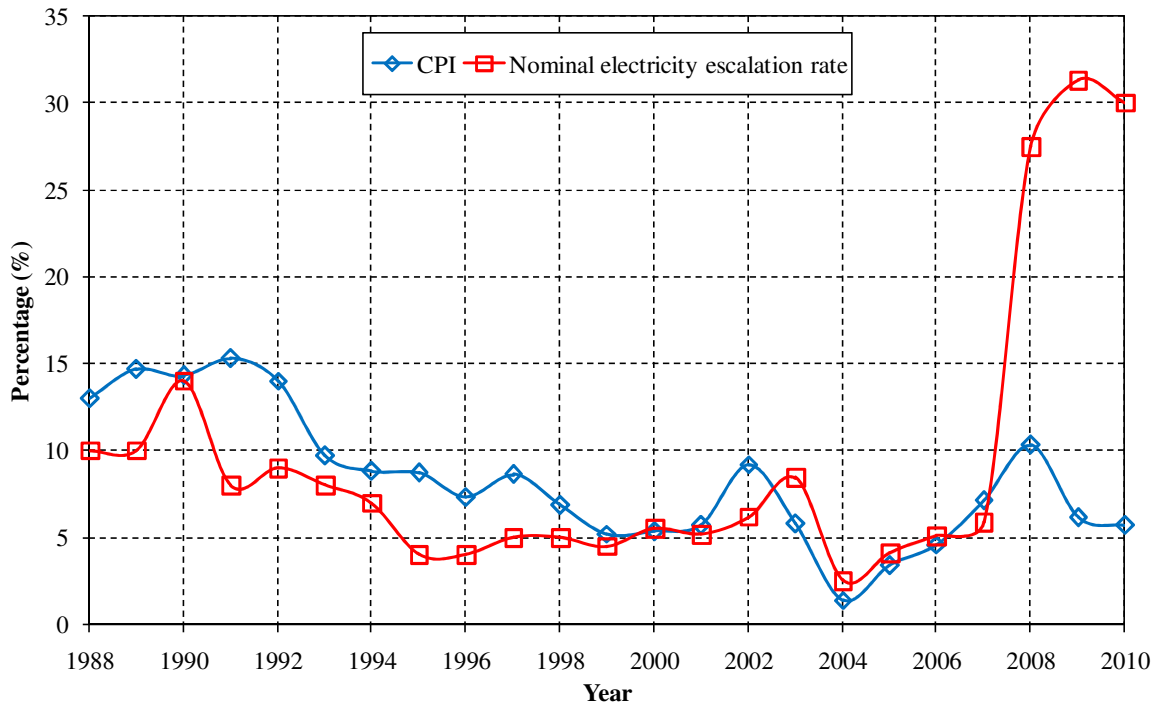


Figure F.1: Inflation and the electricity tariff increases since 1988 [35].

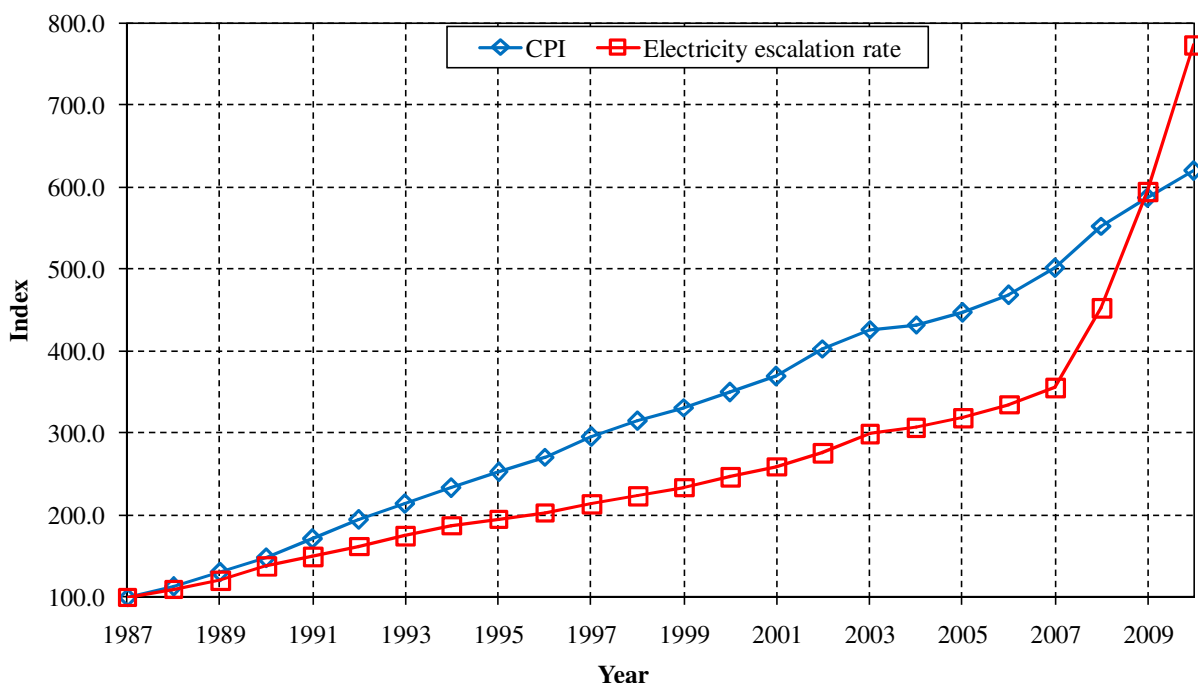


Figure F.2: Index of inflation and electricity tariffs.

### F.3. Results of Economic Performance Parameters

Table F.2: Financial related data used for the calculation of the economic performance indicators.

Annual Energy Consumption	63072
Capital Cost	-136000
Annual O&M Cost	-349
Installed Capacity (kW)	8
Capacity Factor (CF)	0.9
Inflation (%) (p)	6.4
Interest Rate (%) (i)	10.4
Real Interest Rate (%) (r)	4
Electricity Tariff (c/kWh)	46.27
Escalation rate of electricity tariff (%)	0
Current cost of consumed energy	29183.41

Electricity Tariff (c/kWh) (2010)	57.143	From Year 3
Future cost of consumed energy	36041.23	

Electricity Tariff (c/kWh) (2010)	57.143	From Year 4
Future cost of consumed energy	36041.23	

Table F.3: Calculated NPV of the MHPS.

NPV of MHPS										
Year (N)	Investment Cost (IC)	Savings (S)	O&M Cost	Total Annual	PV of TC	NPV of TC	PV of Savings	NPV of S	NPV of Investment	NPV in thousand
0	-136000	0	0	-136000	-136000	-136000	0	0	-136000	-136
1	0	29183	-349	-349	-335.57692	-136335.6	28061	28061	-108275	-108
2	0	36041	-349	-349	-322.67012	-136658.2	33322	61383	-75275	-75
3	0	36041	-349	-349	-310.25973	-136968.5	32041	93424	-43545	-44
4	0	36041	-349	-349	-298.32666	-137266.8	30808	124232	-13035	-13
5	0	36041	-349	-349	-286.85256	-137553.7	29623	153855	16301	16
6	0	36041	-349	-349	-275.81977	-137829.5	28484	182339	44510	45
7	0	36041	-349	-349	-265.21132	-138094.7	27388	209727	71633	72
8	0	36041	-349	-349	-255.01088	-138349.7	26335	236062	97713	98
9	0	36041	-349	-349	-245.20277	-138594.9	25322	261384	122790	123
10	0	36041	-349	-349	-235.77189	-138830.7	24348	285733	146902	147
11	0	36041	-349	-349	-226.70375	-139057.4	23412	309144	170087	170
12	0	36041	-349	-349	-217.98437	-139275.4	22511	331656	192380	192
13	0	36041	-349	-349	-209.60036	-139485	21645	353301	213816	214
14	0	36041	-349	-349	-201.5388	-139686.5	20813	374114	234427	234
15	0	36041	-349	-349	-193.78731	-139880.3	20012	394126	254246	254
16	0	36041	-349	-349	-186.33395	-140066.7	19243	413369	273302	273
17	0	36041	-349	-349	-179.16726	-140245.8	18503	431872	291626	292
18	0	36041	-349	-349	-172.27621	-140418.1	17791	449663	309245	309
19	0	36041	-349	-349	-165.65021	-140583.7	17107	466769	326186	326
20	0	36041	-349	-349	-159.27904	-140743	16449	483218	342475	342
<b>Total Life Cycle Cost</b>				-142980						

Table F.4: Calculated NPV of the MHPS with varying time dependent variables.

NPV of MHPS with deviation of interest rates, electricity escalation rates and capacity factor									
% Dev in interest, r	NPV of the MHPS	Thousands	% Dev in Elec cost	NPV of the MHPS	Thousands	% Dev in C.F.	NPV of the MHPS	Thousands	
-100	570982	571	-100	-79360	-79	-50	100866	101	
-90	541888	542	-90	-37176	-37	-40	149188	149	
-80	514436	514	-80	5008	5	-30	197510	198	
-70	488518	489	-70	47192	47	-20	245831	246	
-60	464035	464	-60	89376	89	-10	294153	294	
-50	440892	441	-50	131559	132	0	342475	342	
-40	419003	419	-40	173743	174				
-30	398289	398	-30	215927	216				
-20	378674	379	-20	258111	258				
-10	360090	360	-10	300295	300				
0	342472	342	0	342479	342				
10	325760	326	10	384662	385				
20	309898	310	20	426846	427				
30	294835	295	30	469030	469				
40	280522	281	40	511214	511				
50	266915	267	50	553398	553				
60	253970	254	60	595582	596				
70	241650	242	70	637765	638				
80	229917	230	80	679949	680				
90	218737	219	90	722133	722				
100	208079	208	100	764317	764				



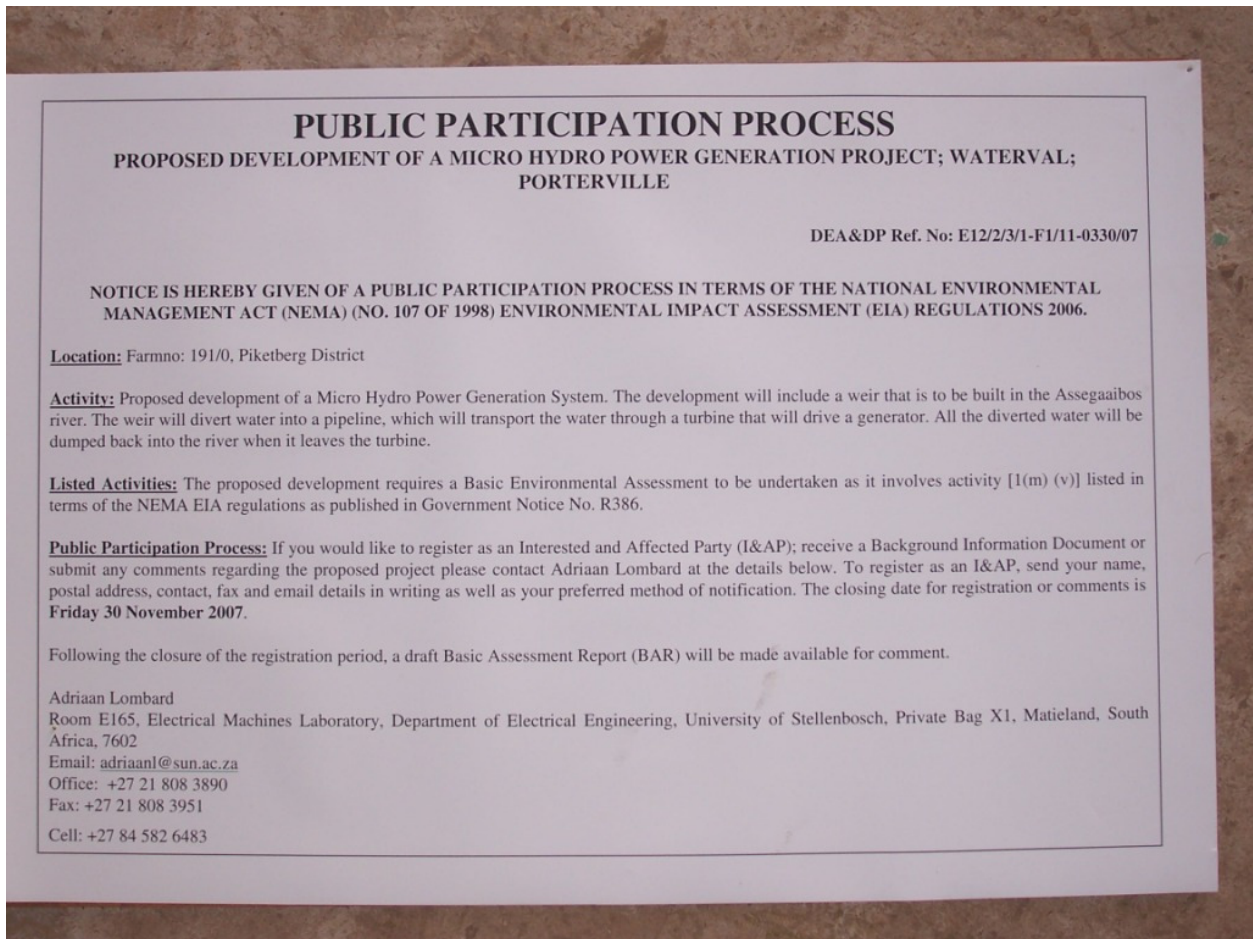


**Figure G.2: Notice of the Public Participation Process that was placed at the entrance to the farm Waterval.**



**Figure G.3: The diversion weir just after construction.**



**Figure G.4: The powerhouse during construction (on the left) and finished (on the right).**



**Figure G.5: The powerhouse from the front where the main pipeline enters.**



**Figure G.6: The underground part of the main pipeline during construction.**



**Figure G.7: Part of the above-ground pipeline during construction.**



**Figure G.8: Part of the above-ground pipeline and also showing the saddles holding the pipes to the concrete blocks.**



**Figure G.9: Part of the above ground pipeline with the constructions that holds the pipes to the boulders.**



**Figure G.10: The isolation valve and pipeline constructed into the diversion weir, with the trash rack located behind the diversion weir.**



Figure G.11: Power cable trench with the cable lying in it.

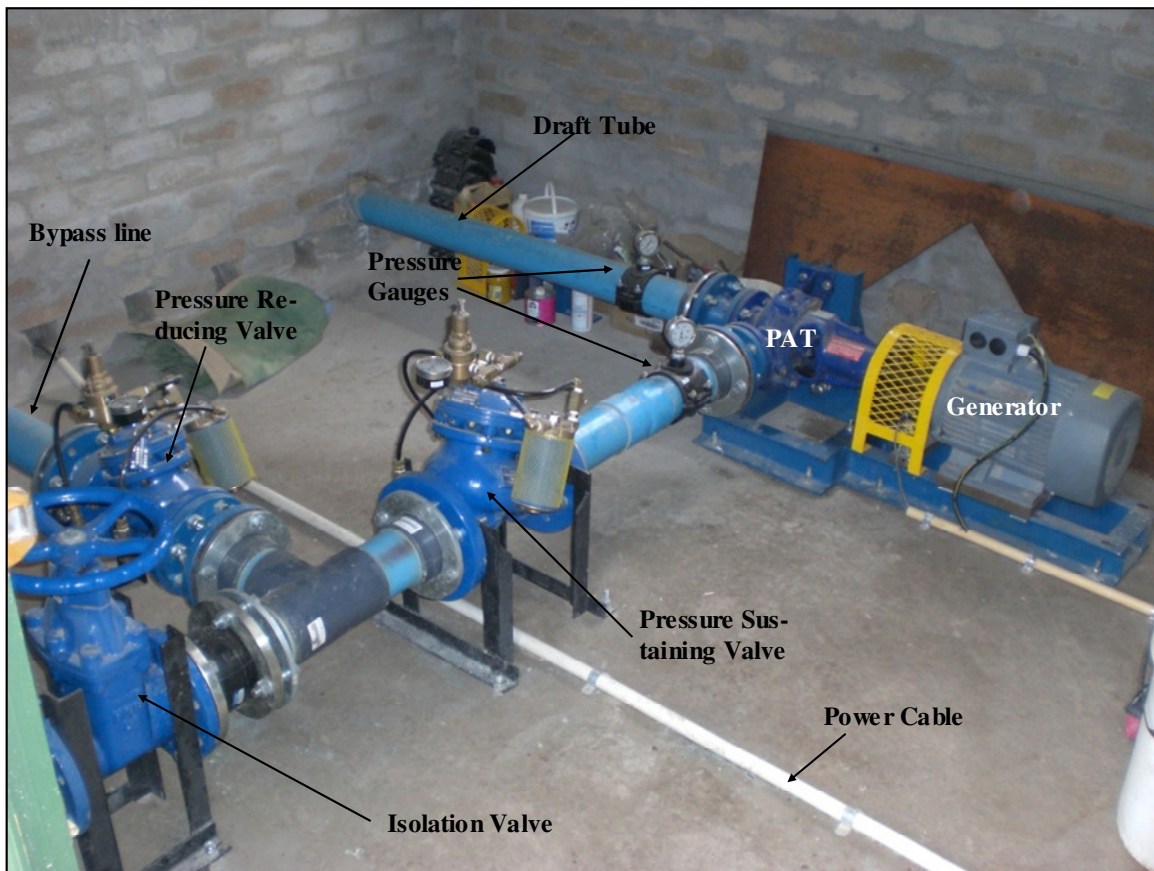
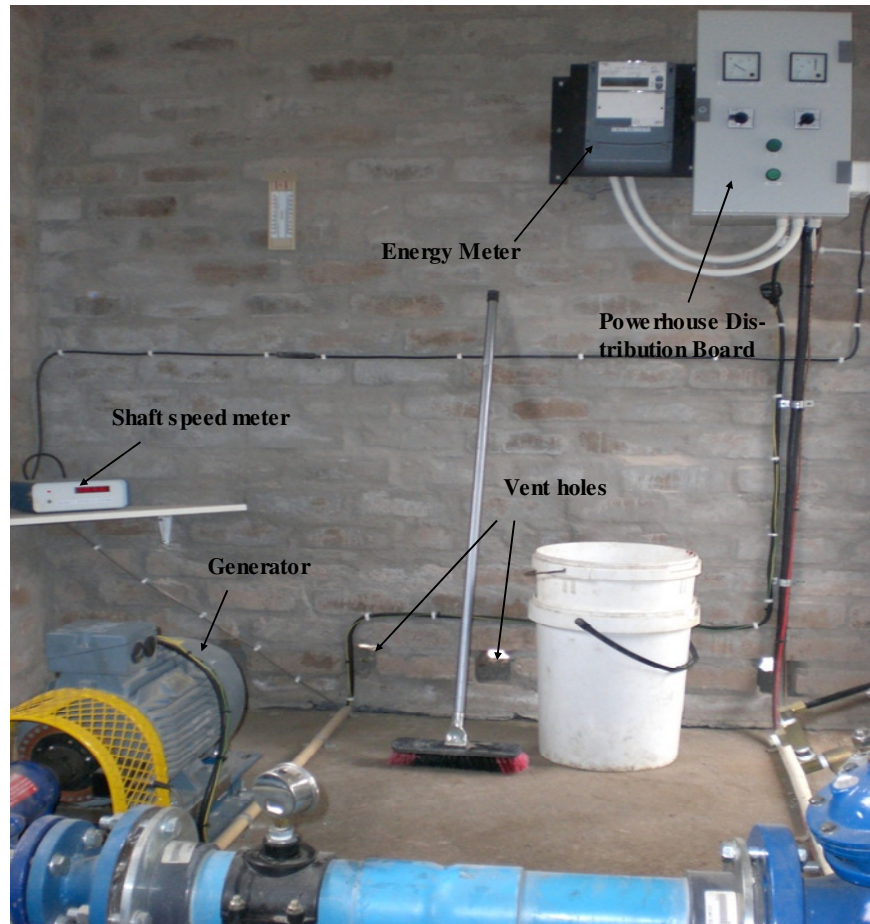


Figure G.12: Inside the powerhouse and showing hydraulic equipment.



**Figure G.13: Inside the powerhouse and showing the electric equipment.**



**Figure G.14: Tailrace dam with the bypass line in the lower right corner and the draft tube in the middle.**



**Figure G.15: Outlet where water is released back into the Assegaaibos River.**



**Figure G.16: Main distribution board where the MHPS is connected to the load and grid.**



**Figure G.17: The underground part of the pipeline, just after it was buried (on the left) and after a year (on the right).**



**Figure G.18: The above-ground part of the pipeline, just after installation (on the left) and after a year (on the right)**